



**Morphological Imaging of the Canine Thyroid Gland with
an Application towards Hypothyroid Dogs**

Olivier Taeymans

Thesis submitted in fulfillment of the requirements for the Degree of
Doctor of Veterinary Sciences (PhD)
2008

Promotor: Prof. Dr. J.H. Saunders
Co-promotor: Prof. Dr. H. van Bree

Department of Medical Imaging
Faculty of Veterinary Medicine
Ghent University

To my beloved wife, and son Matthieu.

Knowledge makes humble, ignorance makes proud...

TABLE OF CONTENTS

TABLE OF CONTENTS

LIST OF ABBREVIATIONS	9
GENERAL INTRODUCTION	13
SCIENTIFIC AIMS	19
CHAPTER 1: REVIEW OF THE LITERATURE: THYROID IMAGING IN THE DOG: CURRENT STATUS AND FUTURE DIRECTIONS	
Summary	26
Introduction	27
Radiography	29
Scintigraphy	32
Ultrasonography	40
Computed Tomography	45
Magnetic Resonance Imaging	49
Conclusions	52
References	53
CHAPTER 2: INTRA- AND INTEROBSERVER VARIABILITY OF ULTRASONOGRAPHIC MEASUREMENTS OF THE THYROID GLAND IN HEALTHY BEAGLES	
Summary	72
Introduction	73
Materials and Methods	73
Results	78
Discussion	80
References	84

TABLE OF CONTENTS

CHAPTER 3: PRE AND POST-TREATMENT ULTRASONOGRAPHY IN HYPOTHYROID DOGS

Summary	90
Introduction	92
Materials and Methods	94
Results	99
Discussion	107
References	113

CHAPTER 4: COMPUTED TOMOGRAPHIC FEATURES OF THE NORMAL CANINE THYROID GLAND

Summary	120
Introduction	121
Materials and Methods	122
Results	125
Discussion	132
References	137

CHAPTER 5: HIGH-FIELD MRI OF THE NORMAL CANINE THYROID GLAND

Summary	146
Introduction	147
Materials and Methods	148
Results	152
Discussion	162
References	166

TABLE OF CONTENTS

GENERAL DISCUSSION	171
References	182
SUMMARY	193
SAMENVATTING	199
DANKWOORD	205
CURRICULUM VITAE	211

LIST OF ABBREVIATIONS

LIST OF ABBREVIATIONS

2D: two-dimensional

3D: three-dimensional

$^{99m}\text{TcO}_4^-$: pertechnetate

$\text{BW}^{0.75}$: metabolic weight

C2: second cervical vertebra

C2/3: intervertebral disc space between C2 and third cervical vertebra

CEUS: contrast-enhanced ultrasonography

CI: confidence interval

CSF: cerebrospinal fluid

CT: computed tomography

DORS: dorsal

FDG: fluorodeoxyglucose

FNA: fine-needle aspirate

FSE T1: fast spin echo T1-weighted image

FSE T1+C: post-contrast fast spin echo T1-weighted image

FSE T2: fast spin echo T2-weighted image

FT4: free thyroxine

GE: gradient echo

HU: Hounsfield unit

IV: intravenous

MHz: megahertz

MIP: maximum intensity projection

MRI: magnetic resonance imaging

LIST OF ABBREVIATIONS

NSAID: non-steroidal anti-inflammatory drug
PD: proton density weighted image
PET: positron emission tomography
rhTSH: recombinant human TSH
ROI: region of interest
RX: radiography
SAG: sagittal
SD: standard deviation
SPECT: single photon emission computed tomography
T1W: T1-weighted image
T2W: T2-weighted image
TgAA: thyroglobulin autoantibodies
TRH: thyrotropin releasing hormone
TS: transverse
TSH: thyroid stimulating hormone, thyrotropin
TT4: total thyroxine
US: ultrasonography
WL: window level
WW: window width

GENERAL INTRODUCTION

GENERAL INTRODUCTION

The two most common thyroid gland pathologies in the adult dog are acquired hypothyroidism and neoplasia.¹ Acquired hypothyroidism is the most common endocrine disorder in the dog, but at the same time is the most over-diagnosed one.²⁻⁷ Reasons for the many false positive diagnoses are the wide variety of vague clinical symptoms, the relatively low accuracy of most biochemical thyroid tests, and the multitude of factors (e.g. systemic diseases, drugs, physiologic fluctuations) that may influence the results of these tests.^{1,2,5,8,9} Combining clinical examination and biochemical tests with a cross-sectional imaging modality (e.g. US, CT, MRI) of the diseased thyroid gland may therefore increase the accuracy in the diagnosis of acquired hypothyroidism in the dog.

The second most common, but not less important, thyroid pathology in dogs is neoplasia. Contrary to cats, thyroid neoplasia in dogs are most commonly carcinomas and are usually non-secreting, meaning that they do not result in altered circulating hormone concentrations.^{1,10} Due to the absence of endocrine related symptoms, dogs with thyroid neoplasia are often presented in an advanced stage of the disease, once the tumor size results in a visible mass in the neck area and/or results in mechanical dysfunction of the upper airway and/or upper digestive tract. Such mechanical dysfunctions result in obvious clinical signs of gagging, regurgitation, coughing and dyspnea.² Because of the large presenting size of these masses, grayscale US combined with FNA often yields a relatively quick and straightforward diagnosis.¹¹⁻¹³

GENERAL INTRODUCTION

Ultrasound however has some restrictions for staging and planning the treatment of these locally very invasive tumors. Limitations are related to the inability to image structures covered by air and the narrow field of view associated with the relatively small footprint size of ultrasound probes. By consequence, US is unable to detect intrathoracic invasion of thyroid masses, to diagnose pulmonary metastases, is limited to a lateral approach of the neck to assess local involvement of soft tissues dorsal to the trachea, and has difficulties to define a thyroïdal origin of large masses distorting the anatomy of the neck.¹⁴⁻¹⁶ These limitations could potentially be overcome by using other imaging modalities like CT or MRI, two imaging modalities becoming more accessible in veterinary medicine.

REFERENCES:

1. Feldman EC, Nelson RW. Canine Hypothyroidism. In: Feldman EC, Nelson RW (eds). *Canine and Feline Endocrinology and Reproduction*. St-Louis, MO: Elsevier-Saunders, 2004:86-151.
2. Daminet S. Doctoral Thesis. *Evaluation of Canine Thyroid Function in Physiological and Pathological Conditions*; 2003, Ghent University, Belgium.
3. Ferguson DC. Testing for hypothyroidism in dogs. *Vet Clin North Am*. 2007 Jul;37(4):647-69.
4. Chastain CB. Anti-triiodothyronine antibodies associated with hypothyroidism and lymphocytic thyroiditis in a dog. *J Am Vet Med Assoc*. 1989(194):531-4.
5. Ferguson DC. Update on diagnosis of canine hypothyroidism. *Vet Clin North Am*. 1994 May;24(3):515-39.
6. Scarlett JM. Epidemiology of thyroid diseases of dogs and cats. *Vet Clin North Am*. 1994 May;24(3):477-86.
7. Herrtage ME. Diseases of the endocrine system. In: Dunn J (ed). *Textbook of small animal medicine*. Philadelphia: W.B. Saunders, 1999:534-41.
8. Scott-Moncrieff JC, Guptill-Yoran L. Endocrine disorders. Hypothyroidism. In: Ettinger SJ, Feldman EC (eds). *Textbook of veterinary internal medicine*. 6th ed. St. Louis, MO: Elsevier-Saunders, 2005:1535-43.

GENERAL INTRODUCTION

9. Daminet S, Ferguson DC. Influence of drugs on thyroid function in dogs. *J Vet Intern Med.* 2003 Jul-Aug;17(4):463-72.
10. Mooney CT. Thyroid Neoplasia and Hyperthyroidism in Dogs. In: Ettinger SJ, Feldman EC (eds). *Textbook of Veterinary Internal Medicine.* 6 ed. St-Louis, MO: Elsevier Inc., 2005:1558-60.
11. Wisner ER, Nyland TG. Ultrasonography of the thyroid and parathyroid glands. *Vet Clin North Am.* 1998 Jul;28(4):973-91.
12. Wisner ER, Nyland TG, Mattoon JS. Ultrasonographic examination of cervical masses in the dog and cat. *Vet Rad Ultrasound.* 1994;35:310-5.
13. Hopkins CR, Reading CC. Thyroid and parathyroid imaging. *Semin Ultrasound CT MR.* 1995 Aug;16(4):279-95.
14. Gotway MB, Higgins CB. MR imaging of the thyroid and parathyroid glands. *Magn Reson Imaging Clin North Am.* 2000 Feb;8(1):163-82.
15. Yousem DM, Scheff AM. Thyroid and parathyroid gland pathology. Role of imaging. *Otolaryngol Clin North Am.* 1995 Jun;28(3):621-49.
16. Higgins CB, McNamara MT, Fisher MR, Clark OH. MR imaging of the thyroid. *Am J Roentgenol.* 1986 Dec;147(6):1255-61.

SCIENTIFIC AIMS

Of all currently available imaging modalities, only grayscale US has been used to describe the morphological (contrary to functional) imaging of the canine thyroid gland.¹⁻⁴ The clinical application of US so far was limited to define thyroid origin of cervical masses of unknown etiology, and to accurately guide needle biopsies of thyroid tumors.^{1,2,5} Besides the characteristic appearance, several authors also mentioned the measured size of the normal thyroid gland with US. These measurements were deemed to play a role in the diagnosis of acquired hypothyroidism, as this pathology is known to be associated with a shrinking of the gland.⁶ The usefulness of such measurements however still needs to be defined and not only size measurements, but also other US features could assist in the diagnosis of hypothyroidism and are currently under investigation. The clinical application of CT has been limited to a single case report suggesting its usefulness in the treatment planning of thyroid carcinomas and to the best of our knowledge, MRI applications have never been described.⁷ Studies describing the normal CT and MRI anatomy of the canine thyroid gland, which are needed as a reference to define pathological changes of the gland, are also lacking in the veterinary literature.

The aims of this work were:

- 1) to evaluate the effectiveness of US size measurements of the thyroid gland in the diagnosis of acquired hypothyroidism
- 2) to define US features, other than size measurements, in acquired hypothyroidism
- 3) to describe the normal CT anatomy and
- 4) to describe the normal MRI anatomy of the canine thyroid gland.

REFERENCES:

1. Wisner ER, Nyland TG. Ultrasonography of the thyroid and parathyroid glands. *Vet Clin North Am: Sm Anim Pract.* 1998 Jul;28(4):973-91.
2. Wisner ER, Nyland TG, Mattoon JS. Ultrasonographic examination of cervical masses in the dog and cat. *Vet Rad Ultrasound.* 1994;35:310-5.
3. Nautrup CP, Kästner W, Denkewitz B, Reese S. The neck. In: Cartee RE (ed). *An atlas and textbook of diagnostic ultrasound of the dog and cat.* London: Manson, 2000:109-22.
4. Bromel C, Pollard RE, Kass PH, Samii VF, Davidson AP, Nelson RW. Comparison of ultrasonographic characteristics of the thyroid gland in healthy small-, medium-, and large-breed dogs. *Am J Vet Res.* 2006 Jan;67(1):70-7.
5. Feldman EC, Nelson RW. Canine thyroid tumors and hyperthyroidism. In: Feldman EC, Nelson RW (eds). *Canine and feline endocrinology and reproduction.* St-Louis, MO: Elsevier-Saunders, 2004:219-50.
6. Brömel C, Nelson RW, Pollard RE, Samii VF, Davidson AP, Kass PH. Ultrasonographic evaluation of the thyroid gland in canine breeds predisposed for hypothyroidism. *ESVIM Abstracts. J Vet Intern Med* 2002;16:632.

7. Slensky KA, Volk SW, Schwarz T, Duda L, Mauldin EA, Silverstein D. Acute severe hemorrhage secondary to arterial invasion in a dog with thyroid carcinoma. *J Am Vet Med Assoc.* 2003 Sep 1;223(5):649-53.

REVIEW OF THE LITERATURE

**THYROID IMAGING IN THE DOG: CURRENT
STATUS AND FUTURE DIRECTIONS**

Olivier Taeymans, Kathelijne Peremans, Jimmy H. Saunders

Department of Medical Imaging, Faculty of Veterinary Medicine, Ghent University, Salisburylaan 133, 9820 Merelbeke, Belgium.

Adapted from:

O. Taeymans, K. Peremans, J.H. Saunders. Thyroid Imaging in the Dog: Current Status and Future Directions.

J Vet Intern Med 2007; 21: 673-684.

SUMMARY

This review describes the advantages and disadvantages of radiography, ultrasonography and nuclear medicine in the two most frequent thyroid pathologies of the dog: acquired primary hypothyroidism and thyroid neoplasia. Ultrasonography and scintigraphy remain the two most indicated imaging modalities for these thyroid abnormalities. However, as in human medicine, computed tomography and magnetic resonance imaging also have potential indications. This is especially the case in the evaluation of the extent, local invasiveness and the presence of local or distant metastases of thyroid neoplasia. Based on experience with different imaging modalities in people, we suggest future directions in the imaging of the canine thyroid gland.

INTRODUCTION

The two major pathologies of the thyroid gland in the adult dog are neoplasia and primary hypothyroidism. Clinically detectable neoplasms (which represent mostly carcinomas and less frequently adenomas) usually are non-secreting, resulting in euthyroidism throughout the course of the disease.¹ Two-thirds of the carcinomas are located in 1 thyroid lobe and one-third involve both lobes.¹ Only 10-20% of the detectable carcinomas secrete excessive thyroid hormones and result in clinical signs of hyperthyroidism.^{2,3} Hyperthyroidism is even less frequent in the rare cases of detectable adenomas.³ When almost the entire gland is destroyed by a bilateral carcinoma, signs of hypothyroidism can also be seen. This has been reported to be present in up to 30% of cases of thyroid neoplasia.²

Hypothyroidism in the adult dog is in more than 95% of the cases the result of a primary dysfunction of the thyroid gland, resulting from an immune-mediated lymphocytic thyroiditis or idiopathic atrophy of the gland.^{1,4,5,6} Acquired secondary hypothyroidism (TSH deficiency) is rarely reported and is related to pituitary tumors or pituitary malformations.^{2,7} Tertiary hypothyroidism (TRH deficiency) has not been described in dogs.^{2,7} In the juvenile dog, congenital primary hypothyroidism is only rarely diagnosed and can be the result of dysgenesis of the gland, dyshormonogenesis or iodine deficiency.^{2,7} Congenital secondary hypothyroidism usually is a feature of

panhypopituitarism. An isolated TSH or TRH deficiency in young dogs has only been described in 2 case reports.^{7,8,9}

In the past, imaging of the canine thyroid gland was only applied in cases of cervical masses of unknown origin. More recently scintigraphy and ultrasonography also have been used for the diagnosis of primary hypothyroidism.^{1,7,10,11,12,13,14,15,16} The diagnosis of primary hypothyroidism in the adult dog is challenging due to the combination of vague presenting clinical signs, the relatively low accuracy of most biochemical tests and the potential influence of numerous drugs on thyroid function. Therefore, besides being one of the most common endocrine disorders, it is also one of the most over-diagnosed endocrinopathies in the dog.⁶ Different imaging modalities have the potential to improve the low clinical diagnostic accuracy of canine hypothyroidism.

The purpose of this article is to present the current status and potential evolution, based on experience in human medicine, of the different imaging modalities in thyroid related pathologies of the dog. The thyroid imaging approach in people is based on the preliminary clinical evaluation. It is recommended that lesions smaller than 2 cm be evaluated by US, preferably in combination with US-guided fine needle aspirates FNA providing tissue for cytological examination. CT and MRI are more restricted to specific indications such as the evaluation of the extent of substernal goiters, characterization of large neck masses,

estimation of local invasiveness of thyroid carcinomas and detection of local and distant metastases.¹⁷

RADIOGRAPHY

Because of the absence of enlargement of the gland, conventional radiography is not useful for evaluation of acquired hypothyroidism. In cases of congenital hypothyroidism however, radiographs of the skeleton are indicated. In contrast to pituitary dwarfism, congenital primary hypothyroidism results in a disproportionate dwarfism. Abnormalities that can be detected in the appendicular skeleton are delayed epiphyseal ossification and epiphyseal dysgenesis (i.e. irregularly formed, fragmented or stippled epiphyseal centers), which are most commonly seen in the proximal tibia and in the humeral and femoral condyles (Fig.1).



Fig. 1: Five-months-old dog. There is delayed epiphyseal appearance and retarded epiphyseal growth of the distal humerus, and proximal and distal radius and ulna. Retarded ossification of the carpal bones is evident. Skeletal age is one month. Figure reprinted with permission from the *Vet Rad Ultrasound*, Vol 32, No. 4., 1991, pp 171-177 (courtesy of H.M. Saunders).

The overall length of the long bones is thus reduced. Valgus deformities are common and result from retarded ossification of the carpal and tarsal bones. Thickening of the radial and ulnar cortices with increased medullar opacity and bowing of these bones also can be seen.

Degenerative joint disease may develop at a later stage. Evaluation of the axial skeleton may show short broad skulls with delayed closure of the sutures and retarded vertebral body epiphyseal growth may result in shortened vertebral bodies with scalloped ventral borders (Fig. 2).^{1,18,19}

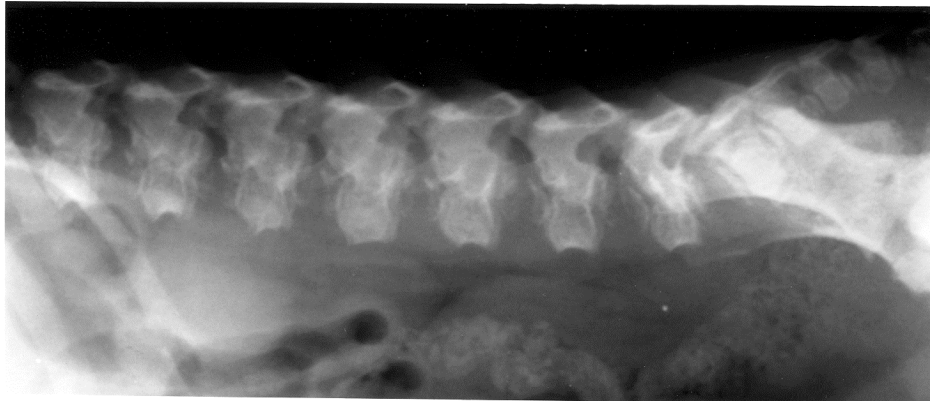


Fig. 2: Five-months-old dog. There is retarded epiphyseal growth, and shortened vertebral bodies. Figure reprinted with permission from the *Vet Rad Ultrasound*, Vol 32, No. 4., 1991, pp 171-177 (courtesy of H.M. Saunders).

In cases of thyroid neoplasia, radiographs of the neck may show a space-occupying mass caudal to the pharynx, sometimes with presence of soft tissue mineralizations.²⁰ The mass, if large enough, may cause an uneven width or deformed laryngeal air space and compress or displace the

trachea ventrally (Fig. 3).^{20,21} Esophageal or tracheal displacement and focal dilatation of the esophagus also may be indicative of tumoral invasion of the esophagus.²⁰ However, neither survey nor contrast radiographs are consistently reliable in diagnosing esophageal neoplasia.²⁰ Metastatic involvement of the retropharyngeal lymph nodes may cause ventral displacement of the pharynx, decreased size of the pharyngeal air space, and loss of the facial planes in the retropharyngeal area.²¹

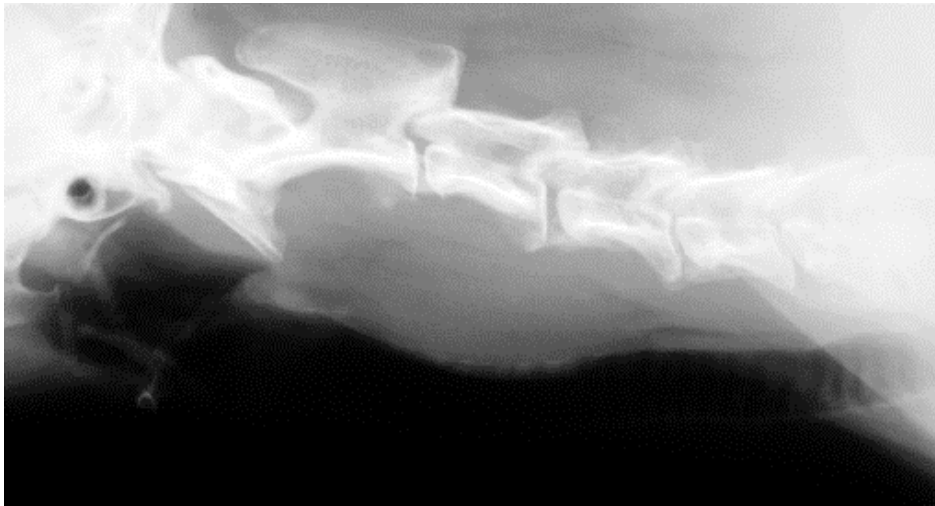


Fig. 3: Lateral radiograph of the cervical area in a skeletally mature dog. Cranial is left on the image. An ill-defined and homogeneous soft tissue mass, with loss of the normal facial planes, is visible just ventral to C3 and C4. This mass results in a focal ventral deviation of the trachea.

Distant metastasis have been estimated to be present in 27-63% of dogs affected with thyroid carcinoma at the time of clinical admission.^{2,22,23,24}

These findings suggest that these dogs are at high risk for development of early pulmonary metastasis. Radiography is more sensitive than scintigraphy for the detection of pulmonary metastasis and should therefore always be performed in cases of thyroid carcinoma.^{3,25} Finally, neoplastic transformation of ectopic thyroid tissue should be included in the differential diagnosis of a cranial mediastinal mass visible on thoracic radiographs.^{20,21}

SCINTIGRAPHY

Nuclear medicine is mainly applied in the diagnosis and treatment of hyperthyroid cats. A review of the literature about the imaging of the thyroid gland in the cat is beyond the scope of this review. As opposed to cats, scintigraphy of the neck area is performed much less frequently in dogs. The two main indications for scintigraphy of the neck area in dogs are cases of cervical neoplasms and canine hypothyroidism; the latter being even less frequently evaluated. The normal canine thyroid lobes after $^{99m}\text{TcO}_4^-$ injection appear as 2 uniformly intense, symmetric ovals in the mid-cervical area (Fig. 4). These ovals have smooth and regular margins and are slightly smaller than the parotid salivary glands, which also concentrate pertechnetate.^{10,11,12,25,26} In normal thyroid glands the ratio of uptake between these two glands is 1:1, although a higher thyroid/salivary gland ratio (T/S ratio) has been reported as well.^{10,13,27,28} It also has been proven that this ratio is dependent on the timing of the scan and that this ratio shows a larger variability in dogs compared to

cats.^{26,28} By using the T/S ratio, a visual estimate of thyroid activity (“trapping”) can be established.

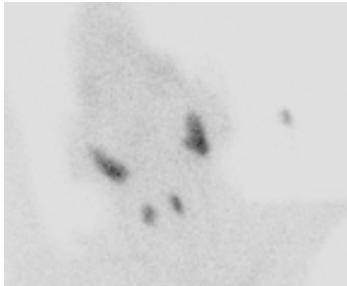


Fig. 4: Ventral planar scintigraphic image of the head and neck obtained after injection of pertechnetate in a dog without thyroidal dysfunction. Rostral is on top of the image. Radionuclide uptake is similar in the parotid salivary glands and both lobes of the thyroid gland. Both thyroid lobes appear as 2 uniformly intense, symmetric ovals in the mid-cervical area and are smaller than the more rostrally located parotid salivary glands.

Unlike ^{99m}Tc , ^{123}I and ^{131}I also are incorporated in thyroglobulin (“organification”) allowing for determination of “true” uptake, which could be more reflective of thyroid physiology.^{10,11,13,29} This explains the disparity between pertechnetate and radioiodine scans seen in some human patients with thyroid neoplasia.^{30,31,32,33} ^{123}I , a cyclotron product, however is much more expensive and therefore not routinely used in veterinary medicine.^{10,11,13,27,34} ^{131}I , used for radiotherapy due to its decay by β^- -transition, also emits γ -radiation. This emission enables scintigraphic imaging, but the high energy of the γ -rays (364 keV) is suboptimal for conventional gamma camera imaging and requires the

use of high-energy collimators. These features, combined with a relatively high radioactive burden to the patient and environment due to the β^- -transition and a long physical half-life of 8.06 days, make the tracer unfavorable for routine diagnostic imaging of thyroid diseases.^{10,11,13,27,35} The preferred radionuclide for anatomic thyroid evaluation is $^{99m}\text{TcO}_4^-$ used in combination with pinhole collimation because this tracer is easily obtainable from an “in-house” molybdenum generator and is relatively inexpensive.³⁰

The scintigraphic appearance of thyroid neoplasia can be unilateral or bilateral. The tumors are of various sizes with irregular areas of pertechnetate uptake and usually show heterogeneous distributions of radioactivity (Fig. 5).^{11,25,27,36}

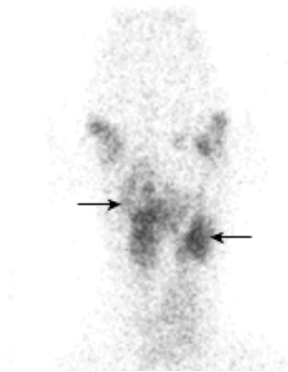


Fig. 5: Ventral planar scintigraphic image of the neck obtained after injection of pertechnetate in a dog with a bilateral thyroid adenocarcinoma. Rostral is on top of the image. Both thyroid lobes (arrows) are enlarged and there is a heterogeneous and irregular distribution of radionuclide uptake in both lobes.

Both diffuse increased or decreased uptake patterns also have been described (Fig. 6).²⁶

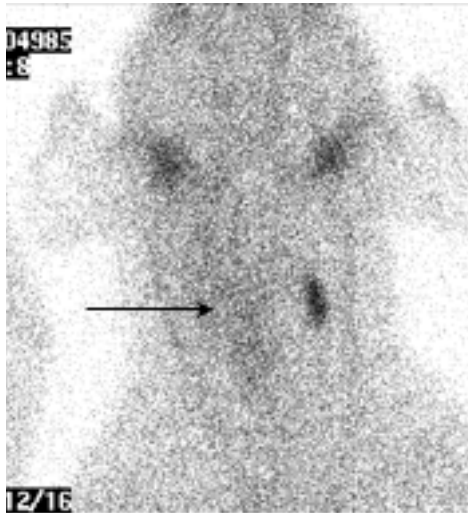


Fig. 6: Ventral planar scintigraphic image of the neck obtained after injection of pertechnetate in a dog with a unilateral adenocarcinoma. Rostral is on top of the image. Diffuse decreased radionuclide uptake is visible in the enlarged right thyroid lobe (arrow). The left lobe is of normal size and shows a normal pattern of radionuclide uptake.

If the tumor is secreting excessive amounts of thyroid hormones, moderate to extensive areas of increased, usually uniform, tracer uptake will be detected and the contralateral lobe will exhibit suppressed uptake because of negative feedback on the pituitary gland.^{2,26,37,38,39} Unfortunately, increased uptake of radionuclide does not always correlate with increased production of thyroid hormones by the tumor. For instance, if the thyroid tumor destroys enough of the thyroid gland

(usually more than 75%) to cause subnormal thyroxine concentration, the pituitary gland will increase its TSH release and the remaining normal tissue will be stimulated.^{2,26} The non-secreting thyroid neoplasm then will show decreased uptake and the remaining normal tissue will have increased uptake.²⁶ The pattern of uptake does not predict the histological type of tumor either, although it seems that tumors with well-delineated homogeneous uptake tend to be more easily resectable than tumors with heterogeneous poorly circumscribed uptake.²⁵ Local and distant metastases potentially can be detected.^{10,26,27} However, false negatives occur until a total or near total thyroidectomy (including remaining normal thyroid tissue) has been performed because an unfavorable tracer competition exists between normal tissue and distant metastases.^{10,26,27,40} For this reason, thyroid scintigraphy is considered a relatively specific tool for identification of metastasis, but is not considered sensitive.^{2,3} Scintigraphic visualization of metastases in the presence of intact thyroid tissue, indicates a high trapping ability of iodine in the tumor tissue, and therefore may be considered as a predictive factor of radioiodine therapy effectiveness.^{3,40} Non-thyroidal masses, esophageal activity from swallowed saliva, breast tissue, thymus and skin contamination also may cause abnormal focal pertechnetate accumulations, resulting in false positive results.^{26,41} For detection of metastasis of thyroid carcinoma in people, radioiodine is more sensitive than pertechnetate.^{40,42} Conflicting results however also have been reported.⁴⁰ The use of tracers such as ^{99m}Tc-sestamibi, ²⁰¹Tl, and

^{99m}Tc -tetrofosmin or use of SPECT instead of planar imaging could increase the sensitivity of scintigraphy in the detection of metastases (Fig. 7).⁴³

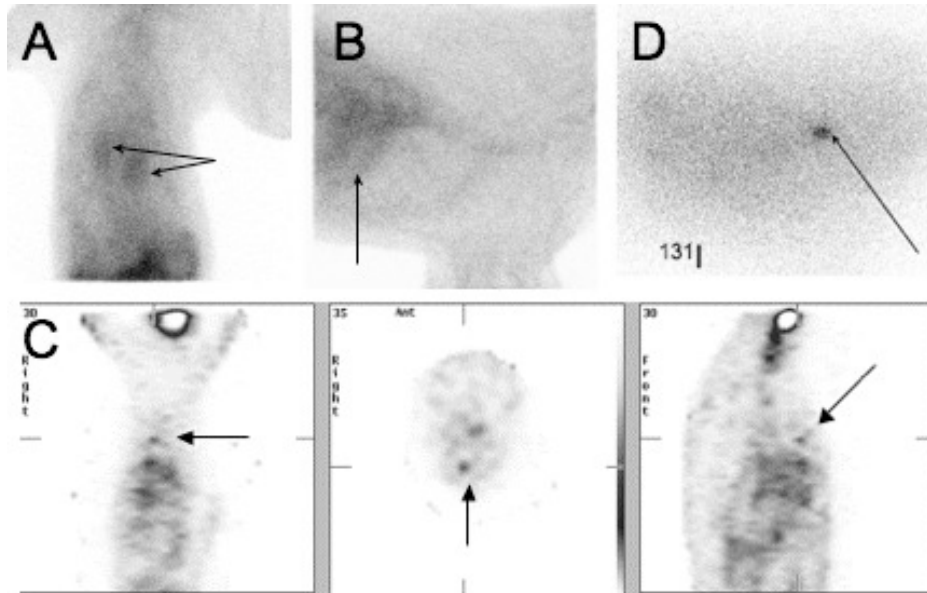


Fig. 7: Same dog as in Fig. 5. Ventral (fig.7a) and lateral (fig.7b) planar scintigraphic images of the thorax obtained after injection with pertechnetate, showing no abnormalities. Cranial is on top of the ventral acquisition and on the right of the lateral acquisition. Normal uptake in the myocardium is visible on both planes (arrows). Subsequent dorsal, transverse and sagittal SPECT acquisitions in the same dog (fig. 7c) showed a focal area of uptake (arrows) in the right cranioventral thorax corresponding to a nodular interstitial lesion seen on radiographs (not included). A focal area of radionuclide uptake (arrow) is visible at the same location on a lateral planar image obtained 24 hours after injection with ^{131}I (fig. 7d), confirming the suspicion of a focal distant metastasis in this dog (cranial is right on the image).

Besides the evaluation of known thyroid neoplasms, scintigraphy may be indicated to determine whether large cervical masses arise from the thyroid gland or from other tissues. When the mass arises from tissues other than the thyroid, both thyroid lobes should be visible exhibiting a normal pattern. Often the normal thyroid gland will be displaced by the non-thyroidal mass.^{26,27}

Few studies describe the use of scintigraphy for evaluation of thyroid function in dogs.⁷ It has been reported that scintigrams typically show decreased or even absent uptake of pertechnetate in primary hypothyroidism and that the gland also may appear smaller than normal if there is some uptake by the gland (Fig. 8).^{1,7,10,11,12,26}



Fig. 8: Ventral planar scintigraphic image of the neck obtained after injection of pertechnetate in a primary hypothyroid dog. Rostral is on top of the image. There is normal uptake of radionuclide in the parotid salivary glands and absence of uptake in both thyroid lobes. The small area of high radioactivity in the lower left corner of the image represents remnants of pertechnetate in the cephalic catheter, glimmering through a lead shield.

In 1 study of hypothyroid dogs there was an absence of uptake in 9 and a T/S ratio of 1.08 ± 0.56 (mean \pm SD) in 27 of 36 cases. The mean T/S ratio of 22 control dogs in this study was 2.01 ± 0.55 .¹³ On the contrary, dogs with non-thyroidal illness (“euthyroid sick syndrome”) or dogs receiving certain medications, both resulting in decreased serum thyroid hormone concentrations, show normal or increased thyroïdal uptake. This should make it possible to differentiate euthyroid sick syndrome from true hypothyroidism.^{1,10,12,27} However, increased uptake also has been documented in a hypothyroid dog with thyroiditis, and so false negatives are possible.⁵ Dietary iodine intake also could result in false positives in the diagnosis of primary hypothyroidism.⁴⁴ Therefore, further evaluation of scintigraphic findings in canine primary hypothyroidism is necessary.⁷ This is further supported by the fact that thyroiditis in humans can mimic other thyroid abnormalities, and the pattern of uptake can be dependent on the stage of the disease.^{29,45,46,47,48} Hashimoto thyroiditis, which closely resembles canine lymphocytic thyroiditis (with the exception of the presence of goiter), can for example show a heterogeneous or a uniform increase or decrease in uptake.^{46,47,48,49,50} Additionally, an extensive list of differential diagnoses for diffusely decreased uptake have been reported in people, including end-stage goiter, Hashimoto thyroiditis, amyloidosis, medications, high-iodine diet, administration of iodinated contrast media, post partum thyroiditis and silent thyroiditis.²⁹ Consequently, it was concluded that

scintigraphy has a low specificity and low sensitivity for detection of acquired primary hypothyroidism.^{35,46} It would therefore be advisable to be cautious in the scintigraphic interpretation of primary hypothyroidism in dogs, until additional studies on this subject have been performed.

Thyroid scintigraphy can be used to differentiate primary from secondary and tertiary acquired hypothyroidism in dogs. Repeat scintigrams after administration of TSH for 3 consecutive days in dogs with secondary and tertiary hypothyroidism result in normal thyroid images, whereas those of dogs with primary hypothyroidism will remain unchanged.^{7,8,26,27,38} Scintigraphy also can be used to differentiate dysgenesis and dyshormonogenesis in congenital primary hypothyroidism. Iodination defects seen in dyshormonogenesis result in enlarged thyroid lobes with normal or increased uptake. On the other hand, young dogs with dysgenesis of the thyroid gland have minimal uptake.^{7,10,11,27}

ULTRASONOGRAPHY

Because of its superficial location of approximately 1.5-2 cm below the surface of the skin, high frequency transducers of at least 10 MHz can be used to examine the thyroid gland. This results in a high spatial resolution of the image, which makes US a very well suited imaging modality for the examination of the morphology of the thyroid gland. Other advantages of US are its widespread availability, its low cost, the absence of ionizing radiation, the short duration of the examination and

the fact that sedation or anesthesia is rarely required. The advent of high-resolution US and FNA have decreased the indications for radionuclide thyroid scanning in people.³⁰

The normal thyroid gland appears as a homogeneous, well-delineated structure with a hyperechoic capsule.^{51,52,53} Its parenchyma is most often hyperechoic compared to the surrounding musculature and its size is correlated with the size of the dog.^{51,52,54} Each lobe has a more or less triangular shape on a transverse plane and a fusiform shape, with a rounded cranial end and a pointed caudal end on a longitudinal plane (Fig. 9).^{51,52,53}

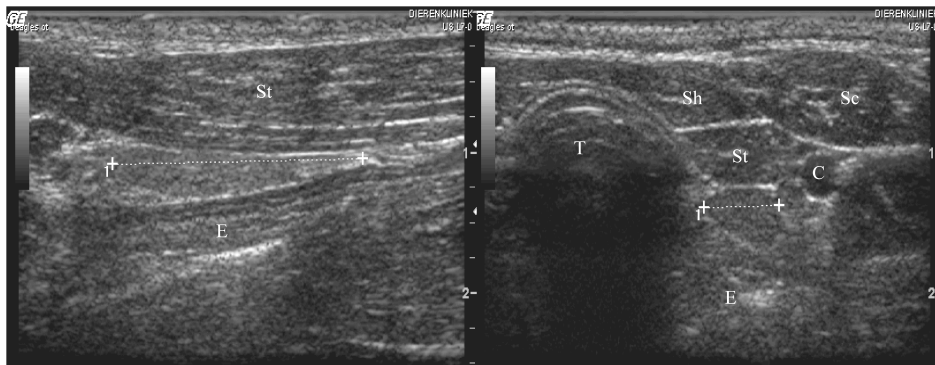


Fig. 9: Longitudinal (left) and transverse (right) ultrasound images of a normal left thyroid lobe obtained with a matrix linear transducer at 12 MHz. Cranial is left on the longitudinal image and medial is left on the transverse image. The linear scale on the right side of each image is in centimeters. The thyroid lobe is indicated by electronic calipers. (C=common carotid artery; E=esophagus; Sc=sternocephalic muscle; Sh=sternohyoid muscle; St=sternothyroid muscle; T=trachea)

Landmarks used for the identification of both thyroid lobes are the medially located trachea, the laterally located common carotid arteries, the ventrally located sternothyroid muscles and the dorsally located esophagus for the left lobe.^{51,52}

Initially, the main indication for US of the canine thyroid gland was a cervical mass of unknown origin for which a thyroid carcinoma was in the list of differential diagnoses. Thyroid carcinomas appear as large non-homogeneous masses, sometimes containing multiple cysts, and with variable delineation.^{52,55} Particularly in poorly delineated neoplasms, invasion of surrounding structures such as the esophagus, fascial sheaths and the cervical vasculature can be detected.⁵² This information is very useful in determining whether surgical treatment is a plausible therapeutic option.⁵² The echogenicity of the carcinomatous gland often is reduced, without presence of distal enhancement.⁵⁵ Presence of hyperechoic foci representing calcification or dense connective tissue can be found.⁵⁵ The masses are highly vascular on power or color-Doppler, and a large arterial vascular plexus often is distributed in and around the thyroid mass.⁵² Development of arteriovenous malformations either on initial presentation or after surgical intervention is reported.⁵² It is sometimes difficult to document the thyroidal origin of the mass when its size is such that the normal anatomy of the cervical area is disrupted.^{2,52,55} There is however a clear distinction between thyroid and parathyroid hyperplasia or neoplasia. The parathyroid glands are much smaller (maximum 20 mm), are

characterized by a round or oval shape, are well delineated and are anechoic to hypoechoic to the normal surrounding thyroid parenchyma.⁵² Unless concurrent regional lymphadenopathy and local invasiveness can be detected, differentiation between benign and malignant thyroid masses cannot be made.^{52,53} Determination of the vascularization and perfusion of thyroid masses by use of contrast enhanced US may be beneficial in this regard.^{56,57,58,59} The 2 most common sites for thyroid carcinoma metastasis are the lungs and retropharyngeal lymph nodes.^{2,3} Other less frequent sites are liver, kidneys, adrenals, spleen, prostate, brain, spinal cord, bone and bone marrow.² Based on clinical and hematologic abnormalities, a suspicion of intra-abdominal metastasis may be raised. In such cases, abdominal US is indicated.^{2,3} Contrast enhanced US also may be helpful to differentiate benign from malignant lesions detected in abdominal organs. So far, its clinical intra-abdominal use in veterinary medicine is only reported for the liver and spleen.^{60,61,62}

More recently, US of the thyroid gland also has been used as a diagnostic aid in the diagnosis of primary hypothyroidism and in the differentiation between “euthyroid sick syndrome” vs. primary hypothyroidism. Reported US features in cases of primary hypothyroidism are hypoechoic parenchyma compared to the overlying sternothyroid muscle, non-homogeneous parenchyma, an irregular outline of the lobe, decreased size of the lobe and a more rounded shape of the lobe on transverse images (Fig. 10).^{14,15,16,63} One or several of

these changes may be present at the same time in the same lobe and the US characteristics also may differ between the 2 lobes.^{14,15,16,63}

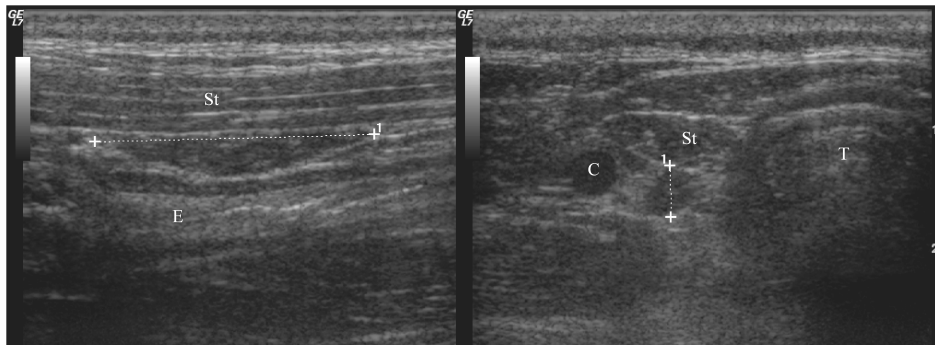


Fig. 10: Longitudinal image of the left lobe (left side of the image) and transverse image of the right lobe (right side of the image) in a primary hypothyroid Border Collie obtained with a matrix linear transducer at 12 MHz. Both lobes are hypoechoic compared to the overlying sternothyroid muscles and show an inhomogeneous parenchyma. The gland has an irregular capsule on the longitudinal image and has a rounded shape on the transverse image. The size of both lobes was reduced. (C=common carotid artery; E=esophagus; St=sternothyroid muscle; T=trachea)

In dogs with “euthyroid sick syndrome” the appearance of the gland is normal.^{14,63} Similar findings are described in Hashimoto thyroiditis in human patients, in whom US has gained widespread use in a variety of thyroid diseases.^{64,65,66,67,68,69,70,71,72,73} An increasing number of abnormalities detected in the same gland results in a higher sensitivity for diagnosing hypothyroidism in dogs.^{16,63} A sensitivity of 98% for hypothyroidism was reported using a combination of size and

echogenicity of the gland.⁶³ Care should be taken however when measuring the gland because a relatively high inter-observer variability has been demonstrated for these measurements.⁷⁴ When comparing different dogs or when performing a follow-up of the size of the gland over time, it is advisable that the same observer performs the measurements. Using the height and volume of the gland results in the lowest intra- and inter-observer variability when evaluating the size of the gland.⁷⁴

When a cranial mediastinal mass is suspected on radiography (e.g. neoplastic transformation of ectopic thyroid tissue), US of the chest is indicated because pleural or mediastinal fluid and accumulation of mediastinal fat may mimic the appearance of an ill-defined mass on radiography.^{75,76} Concurrent pleural fluid also may mask a mediastinal mass on radiographs.^{75,76} An additional advantage of US is that it accurately can guide FNA or biopsies of the mass.⁷⁶

COMPUTED TOMOGRAPHY

To the best of our knowledge, the normal appearance of the thyroid gland on CT has not been described in dogs. In humans and in cats, the thyroid gland has been described as a hyperattenuating structure compared to the surrounding tissues, with an attenuation value of approximately 80-100 HU in people and with a mean attenuation value of 123.2 HU in cats.^{46,77,78,79} The reason for the high attenuation value of the gland is related to its natural high iodine content, which is an element

with a high atomic number (53) compared to most other elements in the body.^{80,81,82,83,84} The IV injection of iodinated contrast material usually increases the attenuation of the gland diffusely.^{46,85} Injection of iodinated contrast media influences the results of nuclear imaging for a period of 6 to 8 weeks.^{17,26,46,86} After IV contrast injection the mean attenuation values in cats were 132.1 HU and 168.5 HU, when scanned after a delay period and immediately after injection, respectively.⁷⁷ If visibility of the normal thyroid gland is as obvious in dogs as in cats and people, CT of the thyroid in dogs could be helpful in differentiating a cervical mass of unknown origin from thyroid neoplasia (Fig 11).

In humans, CT of the thyroid mainly is indicated in cases of neoplasia. This technique is helpful in the determination of local invasiveness of the tumor, the detection of distant metastasis to the lymph nodes and to the lungs, and in the assessment of ectopic thyroid tissue which can be found in the oral cavity, the lateral neck and mediastinum.^{17,30,46,78,79,86} Metastatic lymph nodes may enhance markedly after contrast injection.¹⁷ Other than evaluating the invasiveness of the lesion and detecting lymph node metastasis, CT potentially can also differentiate benign from malignant thyroid diseases by evaluating the change in attenuation after IV contrast injection and the presence and distribution of intraparenchymal calcifications.^{17,18} One report in the veterinary literature has described the usefulness of CT in the evaluation of a thyroid carcinoma invading the carotid artery in a dog.⁸⁷

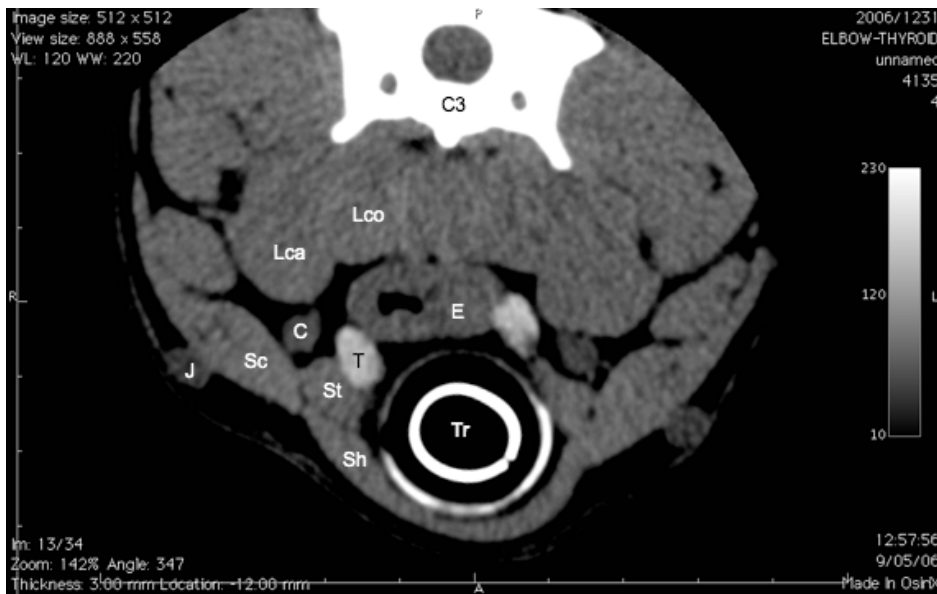


Fig. 11: Pre-contrast transverse CT image at the level of the cranial pole of the thyroid gland in a 2 year old euthyroid Golden Retriever. Both thyroid lobes are directly identified dorsolateral to the trachea and are hyperattenuating compared to the surrounding musculature. (T=right thyroid lobe; C=common carotid artery; E=esophagus; St=sternothyroid muscle; Sc=sternocephalic muscle; Sh=sternohyoid muscle; Lco=longus colli muscle; Lca=longus capitis muscle; J=external jugular vein; Tr=trachea and endotracheal tube; C3=cranial aspect of third cervical vertebra)

CT of the thyroid also yields additional information in different types of thyroiditis and goiter in humans.^{46,78,79,88} Diseased human thyroid tissue is isoattenuating or hypoattenuating to the adjacent musculature using pre-contrast CT.^{78,79,80,82,85} An increase in follicular cells and interstitial tissue, in addition to decreasing iodine concentration in the thyroid follicles, causes decreased HU values in diseased thyroid tissue in

humans.⁸⁰ Similar changes may be seen in hypothyroid dogs, and therefore it is important to know the normal attenuation value of the canine thyroid gland.

Until a few years ago, CT was considered the “gold standard” in detection of pulmonary metastasis in human medicine.⁸⁹ A recent study also demonstrated a significantly higher sensitivity of CT compared to thoracic radiography for detection of pulmonary nodules in dogs.⁹⁰ Today CT still is used as a routine imaging modality for this purpose in people.^{91,92,93} The development of spiral CT in the early 1990s resulted in a higher sensitivity, with an increase of approximately 20%, for meta-analysis because of the ability to perform thin-section imaging with a single breath-hold and thereby preventing misregistration caused by respiratory motion.^{81,92,94,95,96,97} The pitch should be limited to no more than 1.5 at single-row detector CT to avoid obscuring of the nodules due to the effect of greater partial volume averaging.^{98,99} Also, overlapping image reconstruction improves the ability to detect nodules, especially when the size of the nodules is smaller than the slice thickness of the helical CT.^{100,101,102} The advantage of multi-row detector CT is that thin slice thicknesses can be used with a reduced scan time.¹⁰³ Reduction of the slice thickness results in a reduced partial-volume effect.¹⁰³ Another advantage of multi-row detector CT is that thinner sections can be obtained retrospectively from the same raw data, resulting in increased sensitivity.^{103,104,105,106} A major disadvantage of CT is that not all nodules detected are malignant. FDG-PET on the other hand has been shown to

be useful in the detection of malignancy in pulmonary nodules.^{91,92,107,108,109} However, the size threshold for detection of nodules is limited to the PET camera resolution.⁹³ The advent of fusion-imaging modalities (SPECT/CT, PET/CT and PET/MRI) has recently improved the detection of metastatic disease.^{91,110,111} In cases of thyroid carcinoma in particular, integrated ¹³¹I SPECT/CT had additional value in the characterization of equivocal ¹³¹I uptake seen on planar imaging.¹¹²

MAGNETIC RESONANCE IMAGING

To the best of our knowledge, the MRI appearance of the thyroid gland in the dog has not been described. Because of its high soft tissue contrast resolution, MRI has the potential to be useful in the investigation of the thyroid gland (Fig. 12). The normal thyroid gland in people has a slightly higher signal intensity on T1-weighted images, relative to muscle, and high signal intensities on T2-weighted images.^{46,84,113,114,115} After gadolinium administration, the gland enhances diffusely.⁴⁶ In people, both MRI and CT are used for the assessment of enlarged, nodular thyroid glands (goiter), thyroid neoplasms and differentiation of a thyroid mass from an adjacent neck mass.^{17,30,46,116} Both of these modalities help in the identification of cyst formation, hemorrhage, necrosis, calcification, vascular displacement or invasion, metastatic lymph nodes, marginal definition of the lesion and extra-glandular extension of the lesion.^{17,46} MRI is thought to be superior to CT scanning

in detecting early esophageal and tracheal invasion and a recent report demonstrated that MRI accurately demonstrates invasion of the recurrent laryngeal nerve by thyroid carcinomas.^{117,118,119}

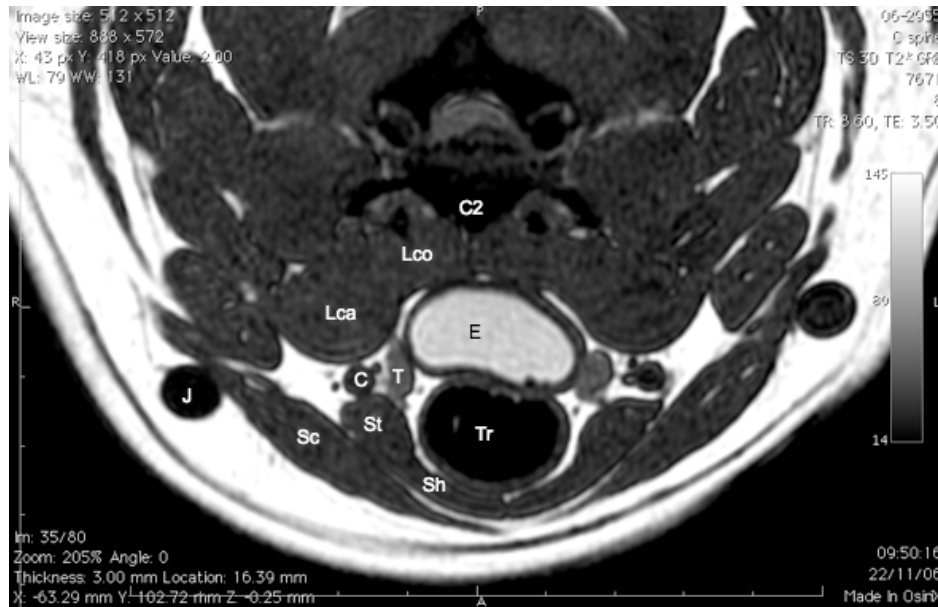


Fig. 12: Transverse T2* weighted gradient echo (3D T2* GE) MRI image of the cranial pole of the thyroid gland in a 5 year old euthyroid Staffordshire Bull Terrier. Both thyroid lobes are directly identified dorsolateral to the trachea and are hyperintense compared to the surrounding musculature. The esophagus is fluid filled. (T=right thyroid lobe; C=common carotid artery; E=esophagus; St=sternothyroid muscle; Sc=sternocephalic muscle; Sh=sternohyoid muscle; Lco=longus colli muscle; Lca=longus capitis muscle; J=external jugular vein; Tr=trachea; C2=caudal aspect of second cervical vertebra) (Courtesy of R. Dennis)

MRI also is especially indicated in mediastinal extension of large goiters.^{17,116} However, as with CT, MRI is not as sensitive as US in

detecting small intraparenchymal nodules in the gland.^{30,120,121} Malignant thyroid lesions are suggested when the margins are ill-defined and there is extraglandular extension, lymph node involvement, and invasion of the surrounding tissues.¹⁷ MRI can also help to grade the malignancy of a thyroid mass. Hemorrhagic necrosis for example is more prevalent in high-grade malignant tumors such as rapidly growing anaplastic carcinomas.¹⁷ Adenomas have low signal intensity on T1-weighted, high signal intensity on T2-weighted images, and enhance after injection of gadolinium.^{17,115}

In cases of Hashimoto thyroiditis, T2-weighted images may show increased signal intensity sometimes with the presence of lower intensity bands, thought to represent fibrosis.^{17,113,114} Signal intensity of these glands varies on T1-weighted images.¹¹⁴

Superior soft tissue contrast, lack of ionizing radiation, lack of streak artifacts, and the ability to demonstrate vascular structures without the need for IV contrast agents are advantages of MRI relative to CT.¹¹⁴ However, because of its relative high cost, MRI is used less frequently than other imaging methods.¹²²

CONCLUSIONS

Different imaging modalities currently are used in human medicine for the diagnosis of thyroid abnormalities with each having advantages and disadvantages. Reports on the clinical use of medical imaging in canine thyroid pathology are sparse. Most of them are related to the use of US and scintigraphy in cases of thyroid carcinomas. Advances in other imaging modalities make them potentially useful as additional tests in the diagnosis of thyroid pathology in veterinary medicine. There still is a large amount of knowledge to be gained from the medical imaging of the canine thyroid gland.

REFERENCES

1. Feldman EC and Nelson RW. Canine Hypothyroidism. In: Feldman EC, Nelson RW, eds. Canine and feline endocrinology and reproduction. St. Louis, MO: Elsevier-Saunders; 2004:86-151.
2. Feldman EC and Nelson RW. Canine thyroid tumors and hyperthyroidism. In: Feldman EC, Nelson RW, eds. Canine and feline endocrinology and reproduction. St. Louis, MO: Elsevier-Saunders; 2004:219-250.
3. Mooney CT. Endocrine disorders. Hyperthyroidism. In: Ettinger SJ, Feldman EC, eds. Textbook of veterinary internal medicine. St. Louis, MO: Elsevier-Saunders; 2005:1544-1558.
4. Chastain CB. Canine hypothyroidism. J Am Vet Med Assoc 1982;181:349-353.
5. Chastain CB, Young DW, Kemppainen RJ. Anti-triiodothyronine antibodies associated with hypothyroidism and lymphocytic thyroiditis in a dog. J Am Vet Med Assoc 1989;194:531-534.
6. Daminet S. Evaluation of canine thyroid function in physiological and pathological conditions. Doctoral Thesis. Ghent University, Belgium, 2003.
7. Scott-Moncrieff JC, Guptill-Yoran L. Endocrine disorders. Hypothyroidism. In: Ettinger SJ, Feldman EC, eds. Textbook of veterinary internal medicine. St. Louis, MO: Elsevier-Saunders; 2005:1535-1543.

8. Greco DS, Feldman FC, Peterson ME, *et al.* Congenital hypothyroid dwarfism in a family of giant schnauzers. *J Vet Intern Med* 1991;5:57-65.
9. Fyfe JC, Kampschmidt K, Van Dang, *et al.* Congenital hypothyroidism with goiter in toy fox terriers. *J Vet Intern Med* 2003;17:50-57.
10. Kintzer PP, Peterson ME. Thyroid scintigraphy in small animals. *Semin Vet Med Surg (Small Anim)* 1991;6:131-139.
11. Kintzer PP, Peterson ME. Nuclear medicine of the thyroid gland. Scintigraphy and radioiodine therapy. *Vet Clin North Am: Small Anim Pract* 1994;24:587-605.
12. Hall IA, Campbell KL, Chambers MD, Davis CN. Effect of trimethoprim/sulfamethoxazole on thyroid function in dogs with pyoderma. *J Am Vet Med Assoc* 1993;202:1959-1962.
13. Balogh L, Thuróczy J, Biksi I, *et al.* Thyroid volumetric measurement and quantitative thyroid scintigraphy in dogs. *Acta Vet Hung* 1998;46:145-156.
14. Brömel C, Pollard RE, Kass PH, *et al.* Ultrasonographic evaluation of the thyroid gland in healthy, hypothyroid, and euthyroid golden retrievers with nonthyroidal illness. *J Vet Intern Med* 2005;19:499-506.
15. Brömel C, Nelson RW, Pollard RE, *et al.* Ultrasonographic evaluation of the thyroid gland in canine breeds predisposed for hypothyroidism. *ESVIM abstracts. J Vet Intern Med* 2002;16:632.

16. Taeymans O, Saunders JH, Daminet S. Ultrasonographic features of the thyroid gland in eight hypothyroid dogs. EAVDI abstract. *Vet Radiol Ultrasound* 2004;45:612.
17. Weber AL, Randolph G, Aksoy FG. The thyroid and parathyroid glands. *Radiol Clin North Am* 2000;38:1105-29.
18. Saunders HM, Jezyk PK. The radiographic appearance of congenital hypothyroidism: skeletal changes with delayed treatment. *Vet Rad Ultrasound* 1991;32:171-177.
19. Wisner ER, Konde LJ. Appendicular skeleton – canine and feline. Diseases of the immature skeleton. In: Thrall DE, ed. *Textbook of veterinary diagnostic radiology*. Philadelphia, PA: Saunders Company; 2002:146-160.
20. Suter PF, Lord PF. Diseases of the nasal cavity, larynx and trachea. In: Suter PF, ed. *Text Atlas, Thoracic Radiography, Thoracic Diseases of the Dog and Cat*. Wettswil, Switzerland: Self-Publishing; 1984:205-252.
21. Kneller SK. Neck and Thorax – Companion animals. The larynx, pharynx, and trachea. In: Thrall DE, ed. *Textbook of veterinary diagnostic radiology*. Philadelphia, PA: Saunders Company; 2002:323-328.
22. Harari J, Patterson JS, Rosenthal RC. Clinical and pathological features of thyroid tumors in 26 dogs. *J Am Vet Med Assoc* 1986;188:1160-1164.

23. Withrow SJ, MacEwen EG. Tumors of the endocrine system. In: Withrow SJ, MacEwen EG, eds. *Small Animal Clinical Oncology*. Philadelphia, PA: WB Saunders; 2001:423.
24. Miles KG, Lattimer JC, Jergens AE, Krause GF. A retrospective evaluation of the radiographic evidence of pulmonary metastatic disease on initial presentation in the dog. *Vet Rad Ultrasound* 1990;31:79-82.
25. Marks SL, Koblik PD, Hornof WJ, Feldman EC. ^{99m}Tc-pertechnetate imaging of thyroid tumors in dogs: 29 cases (1980-1992). *J Am Vet Med Assoc* 1994;204:756-760.
26. Daniel GB, Brawner WR. Thyroid scintigraphy. In: Daniel GB, Berry CR, eds. *Textbook of veterinary nuclear medicine*. North Carolina, NC: American College of Veterinary Radiology; 2006:181-198.
27. Brawner WR. Thyroid and Parathyroid Imaging. In: Berry CR, Daniel GB, eds. *Handbook of Veterinary Nuclear Medicine*. North Carolina, NC: North Carolina State University; 1996:71-79.
28. Adams WH, Daniel GB, Petersen MG, Young K. Quantitative ^{99m}Tc-pertechnetate thyroid scintigraphy in normal beagles. *Vet Rad Ultrasound* 1997;38:323-328.
29. Smith JR, Oates E. Radionuclide imaging of the thyroid gland: patterns, pearls, and pitfalls. *Clin Nucl Med* 2004;29:181-193.
30. Hopkins CR, Reading CC. Thyroid and parathyroid imaging. *Semin Ultrasound CT MR* 1995;16:279-95.

-
31. Arnold JE, Pinsky S. Comparison of $^{99m}\text{TcO}_4$ and ^{123}I for thyroid imaging. *J Nucl Med* 1976;17:261-268.
 32. Dos Remedios LV, Weber PM, Jasko IA. Thyroid scintigraphy in 1000 patients: rational use of $^{99m}\text{TcO}_4$ and ^{123}I compounds. *J Nucl Med* 1971;12:673-678.
 33. Schambaugh GE, Quinn JL, Oyasu R, *et al.* Disparate thyroid imaging: combined studies with sodium pertechnetate $^{99m}\text{TcO}_4$ and radioactive iodine. *J Am Med Assoc* 1974;288:866-869.
 34. Yousem DM, Scheff AM. Thyroid and parathyroid gland pathology. Role of imaging. *Otolaryngol Clin North Am* 1995;28:621-49.
 35. Meller J, Becker W. The continuing importance of thyroid scintigraphy in the era of high-resolution ultrasound. *Eur J Nucl Med Mol Imaging* 2002;29:Suppl 2:S425-S438.
 36. Peterson ME, Kintzer PP, Hurley JR, *et al.* Radioactive iodine treatment of a functional thyroid carcinoma producing hyperthyroidism in a dog. *J Vet Intern Med* 1989;3:20-25.
 37. Rijnberk A. Hyperthyroidism in the dog and its treatment with radioactive iodine. *Tijdschr Diergeneeskd* 1966;91:789.
 38. Rijnberk A. Iodine metabolism and thyroid disease in the dog. Doctoral thesis. University of Utrecht, The Netherlands, 1971.
 39. Rijnberk A, van der Host CJG. Investigations on iodine metabolism of normal and goitrous dogs. *Zentralbl Veterinarmed A* 1969;16:495-508.

40. Boughattas S, Hassine H, Arifa N, *et al.* Preoperative scintigraphic visualization of lymph nodes and pulmonary metastases from papillary thyroid carcinoma. *Ann Nucl Med* 2004;18:59-62.
41. Silberstein EB. The treatment of thyroid malignancies. In: Henkin RE, Boles MA, Dilleha y GL, *et al.*, eds. *Nuclear Medicine*. St. Louis, MO: Mosby; 1996:1557-1567.
42. Campbell CM, Khafagi FA. Insensitivity of Tc-99m pertechnetate for detecting metastases of differentiated thyroid carcinoma. *Clin Nucl Med* 1990;15:1-4.
43. Haugen BR, Lin EC. Isotope imaging for metastatic thyroid cancer. *Endocrinol Metab Clin North Am* 2001;30:469-92.
44. Ferguson DC. Update on diagnosis of canine hypothyroidism. *Vet Clin North Am Small Anim Pract* 1994;24:515-39.
45. Ramtoola S, Maisey MN, Clarke SE, Fogelman I. The thyroid scan in Hashimoto's thyroiditis: the great mimic. *Nucl Med Commun* 1988;9:639-645.
46. Loevner LA. Imaging of the thyroid gland. *Semin Ultrasound CT MR* 1996;17:539-562.
47. Wang PW, Chen HY, Li CH, *et al.* Tc-99m pertechnetate trapping and thyroid function in Hashimoto's thyroiditis. *Clin Nucl Med* 1994;19:177-180.
48. Intenzo CM, Park H, Kim SM, *et al.* Clinical, laboratory, and scintigraphic manifestations of subacute and chronic thyroiditis. *Clin Nucl Med* 1993;18:302-306.

49. Fisher DA, Oddie TH, Johnson DE, Nelson JC. The diagnosis of Hashimoto's thyroiditis. *J Clin Endocrinol Metab* 1975;40:795-801.
50. Alos N, Huot C, Lambert R, Van Vliet G. Thyroid scintigraphy in children and adolescents with Hashimoto disease. *J Pediatr* 1995;127:951-3.
51. Wisner ER, Mattoon JS, Nyland TG, Baker TW. Normal Ultrasonographic anatomy of the canine neck. *Vet Rad Ultrasound* 1991;32:185-190.
52. Wisner ER, Nyland TG. Ultrasonography of the thyroid and parathyroid glands. *Vet Clin North Am Small Anim Pract* 1998;28:973-91.
53. Nautrup CP, Kästner W, Denkewitz B, Reese S. The neck. In: Cartee RE, ed. *An atlas and textbook of diagnostic ultrasonography of the dog and cat*. London, UK: Manson publishing; 2000:109-122.
54. Brömel C, Pollard RE, Kass PH, *et al.* Comparison of ultrasonographic characteristics of the thyroid gland in healthy small, medium, and large breed dogs. *Am J Vet Res* 2006;67:70-77.
55. Wisner ER, Nyland TG, Mattoon JS. Ultrasonographic examination of cervical masses in the dog and cat. *Vet Rad Ultrasound* 1994;35:310-315.

56. Spiezia S, Farina R, Cerbone G, *et al.* Analysis of color Doppler signal intensity variation after Levovist injection: a new approach to the diagnosis of thyroid nodules. *J Ultrasound Med* 2001;20:223-231.
57. Solbiati L, Osti V, Cova L, Tonolini M. Ultrasound of thyroid, parathyroid glands and neck lymph nodes. *Eur Radiol* 2001;11:2411-2424.
58. Calliada F, Pallavicini D, Pasamonti M, *et al.* Topical role and future perspectives of sonographic contrast agents in the differential diagnosis of solid thyroid lesions. *Rays* 2000;25:191-197.
59. Argalia G, De Bernardis S, Mariani D, *et al.* Ultrasonographic contrast agent: evaluation of time-intensity curves in the characterization of solitary thyroid nodules. *Radiol Med* 2002;103:407-413.
60. O'Brien RT, Iani M, Matheson J, Delaney F, Young K. Contrast harmonic ultrasound of spontaneous liver nodules in 32 dogs. *Vet Rad Ultrasound* 2004;45:547-553.
61. Nyman HT, Kristensen AT, Kjelgaard M, McEvoy FJ. Contrast-enhanced ultrasonography in normal canine liver. Evaluation of imaging and safety parameters. *Vet Rad Ultrasound* 2005;46:243-250.

62. Rossi F, Vignoli M, Leone VF, Terragni R. Use of contrast harmonic ultrasound for the characterization of focal lesions of the spleen. IVRA abstract 2006, Vancouver, Canada.
63. Reese S, Breyer U, Deeg C, Kraft W, Kaspers B. Thyroid sonography as an effective tool to discriminate between euthyroid sick and hypothyroid dogs. *J Vet Intern Med* 2005;19:491-498.
64. Pederson OM, Aardal NP, Larssen TB. The value of ultrasonography in predicting autoimmune thyroid disease. *Thyroid* 2000;10:251–259.
65. Lai SM, Chang TC, Chang CC. Sonographic presentation in autoimmune thyroiditis. *J Formos Med Assoc* 1990;89:1057–1062.
66. Vitti P, Lampis M, Piga M. Diagnostic usefulness of thyroid ultrasonography in atrophic thyroiditis. *J Clin Ultrasound* 1994;22:375–379.
67. Marcocci C, Vitti P, Cetani F. Thyroid ultrasonography helps to identify patients with diffuse lymphocytic thyroiditis who are prone to develop hypothyroidism. *J Clin Endocrinol Metab* 1991;71:209–213.
68. Schiemann U, Gellner R, Riemann B. Standardized grey scale ultrasonography in Graves' disease: Correlation to autoimmune activity. *Eur J Endocrinol* 1999;141:332–336.

69. Ying M, Phil M, Brook F. The value of thyroid parenchymal echogenicity as an indicator of pathology using the sterno-mastoid muscle for comparison. *Ultrasound Med Biol* 1998;24:1097–1105.
70. Hayashi N, Tamaki N, Konishi J. Sonography of Hashimoto's thyroiditis. *J Clin Ultrasound*. 1986;14:123–126.
71. Raber W, Gessl A, Nowotny P, Vierhapper H. Thyroid ultrasound versus antithyroid peroxidase antibody determination: A cohort study of four hundred fifty-one subjects. *Thyroid* 2002;12:725-731.
72. Mazziotti G, Sorvillo F, Iori S, *et al*. Gray-scale analysis allows a quantitative evaluation of thyroid echogenicity in the patients with Hashimoto's thyroiditis. *Clin Endocrinol* 2003;59:223-229.
73. Pedersen OM, Aardal NP, Larssen TB, *et al*. The value of ultrasonography in predicting autoimmune thyroid disease. *Thyroid* 2000;10:251-259.
74. Taeymans O, Duchateau L, Schreurs E, *et al*. Intra- and interobserver variability of ultrasonographic measurements of the thyroid gland in healthy beagles. *Vet Rad Ultrasound* 2005;46:139-142.
75. Suter PF, Lord PF. Mediastinal abnormalities. In: Suter PF, ed. *Text Atlas, Thoracic Radiography, Thoracic Diseases of the Dog and Cat*. Wettswil, Switzerland: Self-Publishing; 1984:253-294.

76. Mattoon JS, Nyland TG. Thorax. In: Nyland TG, Mattoon JS, eds. Small animal diagnostic ultrasound. Philadelphia, PA: W.B. Saunders; 2002:325-353.
77. Drost WT, Mattoon JS, Samii VF, *et al.* Computed tomographic densitometry of normal feline thyroid glands. *Vet Rad Ultrasound* 2004;45:112-116.
78. Arger PH, Jennings AS, Gordon LF, *et al.* Computed tomography findings in clinically normal and abnormal thyroid patients. *J Comput Tomogr* 1985;9:111-117.
79. Silverman PM, Newman GE, Korobkin M, *et al.* Computed tomography in the evaluation of thyroid disease. *Am J Roentgenol* 1984;142:897-902.
80. Imanishi Y, Ehara N, Shinagawa T, *et al.* Correlation of CT values, iodine concentration, and histological changes in the thyroid. *J Comput Assist Tomogr* 2000;24:322-326.
81. Nagataki S, Shizume K, Nakao K. Effect of chronic graded doses of iodine on thyroid hormone synthesis. *Endocrinol* 1966;79:667-674.
82. Imanishi Y, Ehara N, Mori J, *et al.* Measurement of thyroid iodine by CT. *J Comput Assist Tomogr* 1991;15:287-90.
83. Curry TS, Dowdey JE, Murry RC. Christensen's Physics of Diagnostic Radiology, 4th ed. Philadelphia, PA: Williams & Wilkins; 1990: 70-98 and 289-322.

84. Cavalieri RR, Blum M. Thyroid imaging. In: De Groot LJ, Jameson LJ (eds): Endocrinology 2001:1399-1408.
85. Sekiya T, Tada S, Kawakami K, *et al.* Clinical application of computed tomography to thyroid disease. *Comput Tomogr* 1979;3:185-93.
86. Hermans J. Les techniques d'imagerie thyroïdienne. *Ann Endocrinol (Paris)* 1995;56:495-506.
87. Slensky KA, Volk SW, Schwarz T, *et al.* Acute severe hemorrhage secondary to arterial invasion in a dog with thyroid carcinoma. *J Am Vet Med Assoc* 2003;223:649-653.
88. Radecki PD, Arger PH, Arenson RI, *et al.* Thyroid imaging: comparison of high-resolution real-time ultrasound and computed tomography. *Radiology* 1984;153:145-147.
89. de Bree R, Deurloo EE, Snow GB, Leemans CR. Screening for distant metastases in patients with neck and head cancer. *Laryngoscope* 2000;110:397-401.
90. Nemanic S, London CA, Wisner ER. Comparison of thoracic radiographs and single breath-hold helical CT for detection of pulmonary nodules in dogs with metastatic neoplasia. *J Vet Intern Med* 2006;20:508-515.
91. Aquino SL. Imaging of metastatic disease to the thorax. *Radiol Clin North Am* 2005;43:481-495.

92. Parsons AM, Detterbeck FC, Parker LA. Accuracy of helical CT in the detection of pulmonary metastases: is intraoperative palpation still necessary? *Ann Thorac Surg* 2004;78:1910-1918.
93. Aquino SL, Kuester LB, Muse VV, Halpern EF, Fischman AJ. Accuracy of transmission CT and FDG-PET in the detection of small pulmonary nodules with integrated PET/CT. *Eur J Nucl Med Mol Imaging*, march 2006.
94. Friese SA, Rieber A, Fleiter T, Brambs HJ, Claussen CD. Pulmonary nodules in spiral volumetric and single slice computed tomography. *Eur J Radiol* 1994;18:48-51.
95. Remy M, Remy J, Giraud F, Marquette CH. Pulmonary nodules: detection with thick-section spiral CT versus conventional CT. *Radiology* 1993;187:513-520.
96. Jablons D, Steinberg SM, Roth J, *et al.* Metastasectomy for soft tissue sarcoma. Further evidence for efficacy and prognostic indicators. *J Thorac Cardiovasc Surg* 1989;97:695-705.
97. Collie DA, Wright AR, Williams JR, *et al.* Comparison of spiral-acquisition computed tomography and conventional computed tomography in the assessment of pulmonary metastatic disease. *Br J Radiol* 1994;67:436-444.
98. Rydberg J, Buckwalter KA, Caldemeyer KS, *et al.* Multisection CT: scanning techniques and clinical applications. *Radiographics* 2000;20:1787-1806.

99. Polacin A, Kalender WA, Marchal G. Evaluation of section sensitivity profiles and image noise in spiral CT. *Radiology* 1992;185:29-35.
100. Klingenbeck K, Schaller S, Flohr T, *et al.* Subsecond multi-slice computed tomography: basics and applications. *Eur J Radiol* 1999;31:110-124.
101. Diederich S, Lentschig MG, Winter F, Roos N, Bongartz G. Detection of pulmonary nodules with overlapping vs non-overlapping image reconstruction at spiral CT. *Eur Radiol* 1999;9:281-286.
102. Diederich S, Semik M, Lentschig MG, *et al.* Helical CT of pulmonary nodules in patients with extrathoracic malignancy: CT-surgical correlation. *Am J Roentgenol* 1999;172:353-360.
103. Kozuka T, Johkoh T, Hamada S, *et al.* Detection of Pulmonary metastases with multi-detector row CT scans of 5mm nominal section thickness: autopsy lung study. *Radiology* 2003;226:231-234.
104. Swensen SJ, Jett JR, Hartman TE, *et al.* Lung cancer screening with CT: Mayo clinic experience. *Radiology* 2003;226:756-761.
105. Diederich S, Thomas M, Semik M, *et al.* Screening for early lung cancer with low-dose spiral computed tomography: results of annual follow-up examinations in asymptomatic smokers. *Eur Radiol* 2004;14:691-702.

106. Libby DM, Smith JP, Altorki NK, *et al.* Managing the small pulmonary nodule discovered by CT. *Chest* 2004;125:1522-1529.
107. Dewan NA, Gupta NC, Redepenning LS, Phalen JJ, Frick MP. Diagnostic efficacy of PET-FDG imaging in solitary pulmonary nodules. Potential role in evaluation and management. *Chest* 1993;104:997-1002.
108. Fisher BM, Mortensen J, Dirksen A, Eigtved A, Hojgaard L. Positron emission tomography of incidentally detected small pulmonary nodules. *Nucl Med Commun* 2004;25:3-9.
109. Gupta NC, Maloof J, Gunel E. Probability of malignancy in solitary pulmonary nodules using fluorine-18-FDG and PET. *J Nucl Med* 1996;37:943-948.
110. Mac Manus MP, Hicks RJ. PET scanning in lung cancer: current status and future directions. *Semin Surg Oncol* 2003;21:149-155.
111. Seemann MD, Meisetschlaeger G, Gaa J, Rummeny EJ. Assessment of the extent of metastases of gastrointestinal carcinoid tumors using whole-body PET, CT, MRI, PET/CT and PET/MRI. *Eur J Med Res* 2006;11:58-65.
112. Tharp K, Israel O, Hausmann J, *et al.* Impact of 131I-SPECT/CT images obtained with an integrated system in the follow-up of patients with thyroid carcinoma. *Eur J Nucl Med Mol Imaging* 2004;31:1435-1442.
113. Noma S, Nishimura K, Togashi K, *et al.* Thyroid gland: MR imaging. *Radiology* 1987;164:495-499.

114. Geftter WB, Spritzer CE, Eisenberg B, *et al.* Thyroid imaging with high-field-strength surface-coil MR. *Radiology* 1987;164:483-490.
115. Higgins CB, McNamara, Fisher MR, Clark OH. MR imaging of the thyroid. *Am J Roentgenol* 1986;147:1255-1261.
116. Gotway MB, Higgins CB. MR imaging of the thyroid and parathyroid glands. *Magn Reson Imaging Clin N Am* 2000;8:163-182.
117. Mancuso AA, Dillon WP. The neck. *Radiol Clin North Am* 1989;27:407-434.
118. Wang J, Takashima S, Takayama F. Tracheal invasion by thyroid carcinoma: prediction using MR imaging. *Am J Roentgenol* 2001;177:929-936.
119. Takashima S, Takayama F, Wang J, Kobayashi S, Kadoya M. Using MR imaging to predict invasion of the recurrent laryngeal nerve by thyroid carcinoma. *Am J Roentgenol* 2003;180:837-842.
120. Gooding GA. Sonography of the thyroid and parathyroid. *Radiol Clin North Am* 1993;31:967-989.
121. Funari M, Campos Z, Gooding AW. MRI and ultrasound detection of asymptomatic thyroid nodules in hyperparathyroidism. *J Comput Assist tomogr* 1992;16:615-619.
122. Reading CC, Gorman CA. Thyroid imaging techniques. *Clin Lab Med* 1993;13:711-724.

**INTRA- AND INTEROBSERVER VARIABILITY OF
ULTRASONOGRAPHIC MEASUREMENTS OF THE
THYROID GLAND IN HEALTHY BEAGLES**

Olivier Taeymans¹, Luc Duchateau², Elke Schreurs¹, Martin Kramer³,
Sylvie Daminet³, Jimmy H. Saunders¹

Department of Medical Imaging¹, Department of Physiology and Biometrics², and Department of Medicine and Clinical Biology of Small Animals³, Faculty of Veterinary Medicine, Ghent University, Salisburylaan 133, 9820 Merelbeke, Belgium.

Adapted from:

Intra- and interobserver variability of ultrasonographic measurements of the thyroid gland in healthy Beagles. O. Taeymans, L. Duchateau, E. Schreurs, M. Kramer, S. Daminet, J.H. Saunders.
Vet Radiol Ultrasound 2005;46,139-142.

SUMMARY

The repeatability of ultrasonographic measurements of the canine thyroid gland was evaluated. The variability of 3 different parameters (the maximal length, width and height) within observer, between observer and between dogs was assessed based on 3 different measurements made by each of 3 observers in 5 healthy beagle dogs. From the 3 parameters, the volume of the gland was estimated using a formula of a rotation ellipse. The height and the volume had the lowest intra- and inter-observer variability, while measurements of the length had the biggest intra- and inter-observer variability. The mean values, with their 90% confidence interval were: height = 0.53 cm [0.33-0.73], length = 2.45 cm [2.04-2.85], width = 0.62 cm [0.46-0.78], volume = 0.38 cm³ [0.20-0.55].

INTRODUCTION

Ultrasonography of the canine thyroid gland is mainly performed when a cervical mass of unknown origin is present.¹ Sonography can also be used to evaluate the size and volume of the human and canine thyroid gland.²⁻⁷ It has been suggested that in Golden Retrievers measurements of the gland could assist in making a diagnosis of hypothyroidism since this is associated with a decreased size of the gland in this breed.^{3,4} However, the repeatability of such measurements and their variability in healthy dogs has not been determined and this is needed before these measurements can be used clinically.

The purpose of the present study was to assess the intra- and inter-observer variability of sonographic measurements of the thyroid gland.

MATERIALS AND METHODS

Five neutered female beagle dogs of 3 years of age with a mean body weight of 12.8 kg were used. The euthyroid status of the dogs was confirmed by a clinical examination, hematology, serum biochemistry, TT₄ serum concentration, TSH serum concentration and the absence of TgAA. Hair overlying the ventral cervical region was clipped in an area from the larynx to the thoracic inlet and coupling gel was applied. The dogs were positioned in dorsal recumbency with the neck in extension. No tranquilization or anesthesia was used.

Three observers trained in sonography of the neck, 2 ECVDI diplomates (JHS and MK) and 1 ECVDI resident (OT), scanned both thyroid lobes of each dog 3 separate times. The thyroid gland was scanned with a multifrequency linear array probe of 7 to 12 MHz.* The 3 observers operated with the same machine settings, using only the highest probe frequency (12 MHz). An area extending from the larynx to the thoracic inlet was scanned with a transducer pressure only enough to provide sufficient contact for adequate image quality. The thyroid gland and its surrounding anatomy were identified according to a previously described technique.⁸ When visible the external parathyroid gland were not included in measurement of length, whereas the embedded internal parathyroid glands were not identified.

The observers were asked to measure the maximal length, width and height of each lobe on a frozen image. The maximum length was measured in a sagittal plane and both the width and height were measured in a transverse plane (Fig. 1-3). The volume of the gland was estimated by use of a formula of a rotation ellipse that is used in humans for evaluation of the thyroid gland: volume = length x width x height x 0.479.⁹

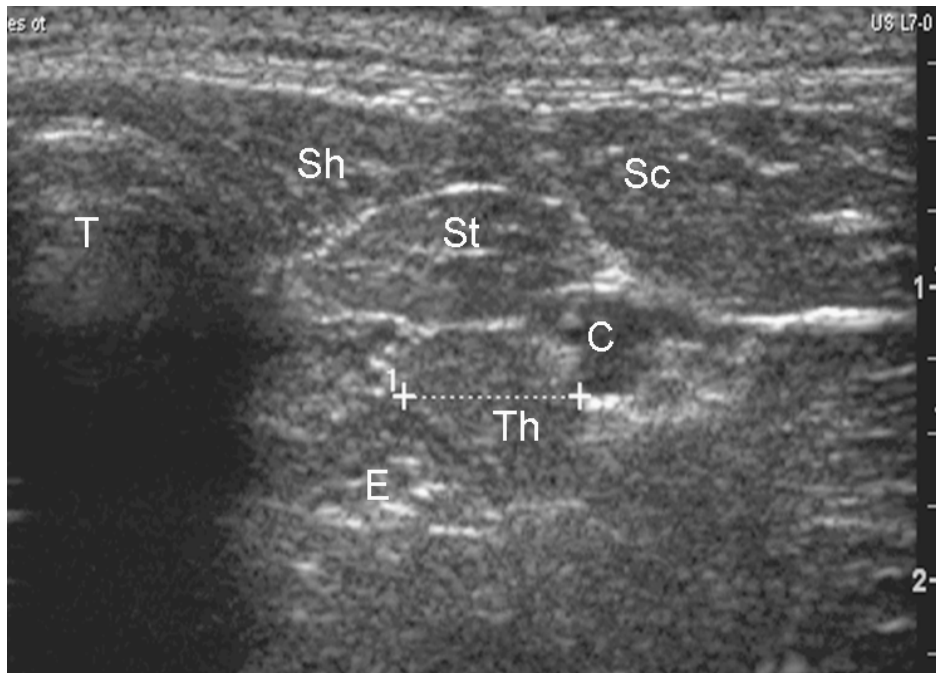


Fig. 1: Transverse US image of the left thyroid lobe (Th). Lateral is right on the image. The scale on the right side of the image is in centimeters. Electronic calipers indicate the maximum width of the thyroid lobe. T = trachea; C = common carotid artery; E = esophagus; Sh = m. sternohyoideus; St = m. sternothyroideus; Sc = m. sternocephalicus

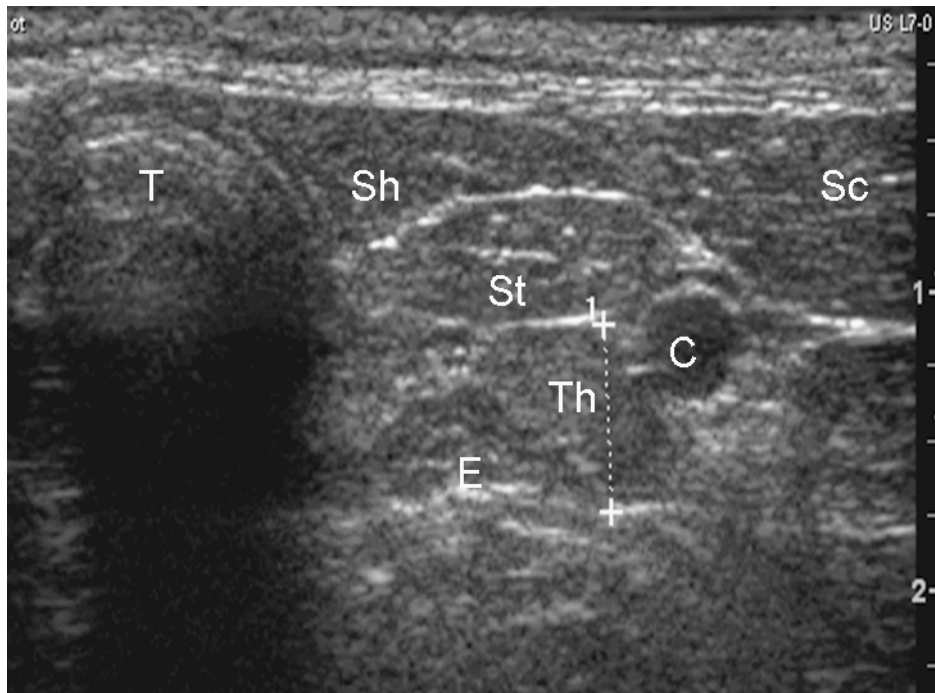


Fig. 2: Transverse US image of the left thyroid lobe (Th). Lateral is right on the image. The scale on the right side of the image is in centimeters. Electronic calipers indicate the maximum height of the thyroid lobe. T = trachea; C = common carotid artery; E = esophagus; Sh = m. sternohyoideus; St = m. sternothyroideus; Sc = m. sternocephalicus

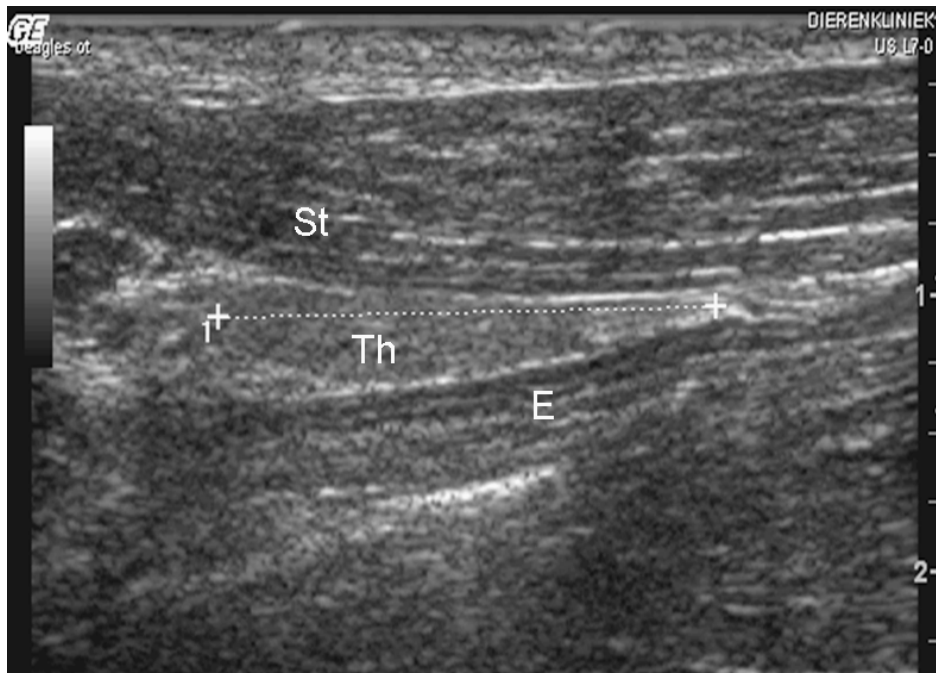


Fig. 3: Longitudinal US image of the left thyroid lobe (Th). Cranial is left on the image. Electronic calipers indicate the maximum length. E = esophagus; St = m. sternothyroideus

A random effects model was fit to the data with dog, observer and measurement within observer as random effects.¹⁰ Within the context of this random effects model, the dog variability (σ_d^2) and inter- and intra-observer variability (σ_i^2 and σ_a^2 respectively) can be estimated based on restricted maximum likelihood techniques¹¹ and these different sources of variability can be compared to each other.¹²

RESULTS

The overall mean [90% CI] was 0.53 [0.33;0.73]cm for height, 2.45 [2.04;2.85]cm for length, 0.62 [0.46;0.78]cm for width resulting a mean volume of 0.38 cm³.

The length measurement had the highest intra- and inter-observer variability ($\hat{\sigma}_a^2=0.0306$ and $\hat{\sigma}_i^2=0.0181$). Based on these variance component estimates, intervals were derived that contain 90% of the measurements of the same dog by the same observer (intra-observer), and 90% of the measurements of the same dog but assessed by different observers (inter-observer) (Fig. 4).

The smallest intra-observer variability was found for height ($\hat{\sigma}_a^2=0.0055$). However, the inter-observer variability for height ($\hat{\sigma}_i^2=0.0065$) had a substantial contribution to the overall variability (Fig 4). The variability when height measurements were made by different observers was 2.2 times the variability when measurements were done by the same observer (Fig. 4). When considering the 5 dogs, the variability increased further, with $\hat{\sigma}_a^2=0.0029$ (Fig. 4).

The intra-observer variability for width ($\hat{\sigma}_a^2=0.0087$) was higher than for height. There was however less variability between observers ($\hat{\sigma}_i^2=0.0001$), and curves for different observers were similar for height and width (Fig. 4).

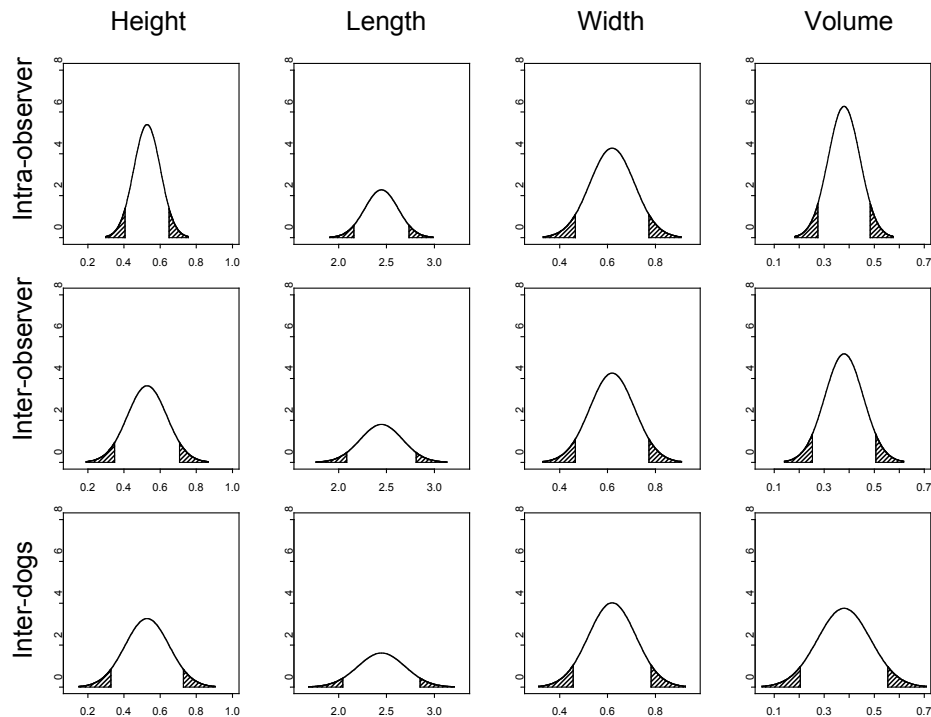


Fig. 4: Intra- and inter- observer variability and dog variability for height, length, width and volume of the thyroid gland. The curves correspond to the density functions of the particular measurement for measurements within an observer on the same dog (first row), for measurements of different observers on the same dog (second row) and measurements of different observers on different dogs (third row), with 90% of the measurements lying in the non-shaded area.

The variability when width measurements were made by different observers was 1.01 times the variability when measurements were done by the same observer.

The highest intra-observer variability was for length ($\hat{\sigma}_a^2=0.0306$). All 3 observers experienced difficulty in identifying the caudal end of the gland when measuring length. The variability when length measurements were made by different observers was 1.59 times the variability when measurements were made by the same observer. The between dog variability ($\hat{\sigma}_d^2=0.0117$) was much more than in the 2 other variables.

The volume of the thyroid gland, based on height, length and width, had the smallest intra-observer variability ($\hat{\sigma}_a^2=0.0041$), and additionally smaller inter-observer variability ($\hat{\sigma}_i^2=0.0019$) than the height, but its between dog variability ($\hat{\sigma}_d^2=0.0053$) was higher than for height and width.

DISCUSSION

In humans it is accepted that the size and volume of the thyroid gland can be measured accurately using sonography.¹³⁻¹⁶ However, the thyroid volume measurements based on US are systematically smaller than measurements based on CT and are less reproducible than with CT and MRI.⁵ Nevertheless sonography seems to be the preferred method in most human centers because of its accessibility, low cost and absence of exposure to ionizing radiation.^{5,13,16}

The reason that variability of the length was largest is a result of the difficulty of identifying the caudal end of the gland. This is probably due to the sharpness of the gland at that level and to the natural variation in the gland shape, with most glands not lying in a perfect longitudinal plane. A second reason for the variability of the length is that because of their small size parathyroid glands are usually not identified on ultrasound examination and thereby might be included in measurement of length.

A possible explanation for the larger difference between intra- and inter-observer variability for height compared to the other variables (Fig. 4) is that observer B measured the height and the width on the same frozen image, whereas observer A and C measured the height and the width at two different locations. Observer B assumed that the maximal width and the maximal height of the gland were located in a same image plane. The fact that his transverse images were frozen at the level of the maximum width of the gland, means that the measurements of the height did not obtain maximal values.

It has been suggested that sonography may represent an interesting tool in the diagnosis and follow-up of dogs with hypothyroidism.³ But whether the gland increases or decreases in size and whether changes in texture occur in hypothyroid dogs is still questionable. In a pilot-study, a significant decrease in size of the thyroid gland in Golden Retrievers with hypothyroidism versus healthy and euthyroid sick Golden

Retrievers was found.⁴ Because of these hypothyroidism related changes of the gland it is important that transducer pressure is kept to a minimum, since too much pressure could result in a distortion of the relational anatomy in this region.

The diagnosis of hypothyroidism can be challenging because of the absence of specific clinical signs, reliable biochemical tests and, because many factors influence the results of these tests.¹⁷⁻²² Due to the difficulty of making a diagnosis of hypothyroidism based on biochemistry alone, it would be useful to see if additional information obtained by US of the gland could improve the diagnostic capabilities. In humans, a combination of biochemistry, scintigraphy, US and US guided aspirations of the gland are used to identify thyroid abnormalities.² The value of US to diagnose hypothyroidism in dogs is unknown. Because of the relative high inter-observer variability in our study, the value of making a diagnosis of hypothyroidism based on US measurements only is questionable. Therefore, both the absolute mean difference in thyroid gland size between healthy and hypothyroid dogs and the inter-observer variability in hypothyroid dogs should be studied further to evaluate the overlap between normal and abnormal values.

Volume measurements of the gland could be beneficial in monitoring response of therapy. Changes in size over time are considered

particularly useful as an objective means of evaluation of therapy in humans.^{13,14,23} For subsequent measurements of the gland, we suggest that the consequent measurements of the gland should be done by the same observer.

As an overall conclusion, it can be stated that height and especially volume seem to be the most promising parameters in evaluating the size of the thyroid gland in dogs. However guidelines should be given to the clinician of how to measure these in a standard way.

*: Logic 7, General Electric Medical Systems, Milwaukee, WI, USA.

REFERENCES

1. Wisner ER, Nyland TG, Mattoon JS. Ultrasonographic examination of cervical masses in the dog and cat. *Vet Radiol Ultrasound* 1994;35:310-315.
2. Barraclough BM, Barraclough BH. Ultrasound of the thyroid and Parathyroid glands. *World J Surg* 2000;24:158-165.
3. Nelson R, Brömel C, Samii V, Pollard R, Davidson A, Kass P. Ultrasonographic Evaluation of the Thyroid Gland in Golden Retrievers. National Parent Club Canine Health Conference, 2001.
4. Brömel C, Nelson RW, Pollard RE, Samii VF, Davidson AP, Kass PH. Ultrasonographic Evaluation of the Thyroid Gland in Canine Breeds Predisposed for Hypothyroidism. *ESVIM Abstracts. J Vet Intern Med* 2002;16:632.
5. Nygaard B, *et al.* Thyroid Volume Measured by Ultrasonography and CT. *Acta Radiol* 2002;43:269-274.
6. Brander A, Viikinkoski P, Tuuhea J, Voutilainen L, Kivisaari L. Clinical versus Ultrasound Examination of the Thyroid Gland in Common Clinical Practice. *J Clin Ultrasound* 1992;20:37-42.
7. Gómez JM, Maravall FJ, Gómez N, Gumà A, Soler J. Determinants of thyroid volume as measured by ultrasonography in healthy adults randomly selected. *Clin Endocrinol* 2000;53:629-634.

-
8. Wisner ER, Nyland TG. Ultrasonography of the Thyroid and the Parathyroid Glands. *Vet Clin North Am: Sm Anim Pract* 1998;28:973-991.
 9. Brunn J, Block U, Ruf G, Bos I, Kunze WP, Scriba PC. Volumetrie der Schilddrüsenlappen mittels RealTime Sonographie. *Dtsch Med Wschr* 1981;106, 1338.
 10. Duchateau L, Janssen P. An example-based tour in linear mixed models. In: Verbeke G, Molenberghs G (eds): *Linear mixed models in practice*. New York: Springer-Verlag, 1997;11-61.
 11. Patterson HD, Thompson RP. Recovery of inter-block information when block sizes are unequal. *Biometrika* 1971;58, 545-554.
 12. Festing MFW, Overend P, Das RG, Borja MC, Berdoy M. The design of animal experiments. *The Royal Statistical Society Medicine Press Limited*, London, 2002; 30-34.
 13. Hermans J. Les techniques d'imagerie thyroïdienne. *Annales d'encrinologie* 1995;56:495-506.
 14. Cavalieri RR, Blum M. Thyroid imaging. In: DeGroot LJ, Jameson JL (eds): *Endocrinology*. Philadelphia: WB Saunders, 2001:1399-1408.
 15. Hegedüs L, *et al.* The Determination of Thyroid Volume by Ultrasound and Its Relationship to Body Weight, Age, and Sex in Normal Subjects. *J Clin Endocrinol Metab* 1983;56:260-263.

-
16. Hegedüs L. Thyroid Ultrasound. *Endocrinol Metab Clin North Am* 2001;30:339-360.
 17. Daminet S, Ferguson DC. Influence of Drugs on Thyroid Function in Dogs. *J Vet Intern Med* 2003;17:463-472.
 18. Peterson ME, Melián C, Nichols R. Measurement of serum total thyroxine, triiodothyronine, free thyroxine, and thyrotropin concentrations for diagnosis of hypothyroidism in dogs. *J Am Vet Med Assoc* 1997;211:1396-1402.
 19. Dixon RM, Mooney CT. Evaluation of serum free thyroxine and thyrotropin concentrations in the diagnosis of canine hypothyroidism. *J Small Anim Pract* 1999; 40:72-78.
 20. Scott-Moncrieff JC, Nelson RW, Bruner JM, *et al.* Comparison of serum concentrations of thyroid-stimulating hormone in healthy dogs, hypothyroid dogs, and euthyroid dogs with concurrent disease. *J Am Vet Med Assoc* 1998;212:387-391.
 21. Surks MI, Stievert R. Drugs and thyroid function. *New Engl J Med* 1995;333:1688-1694.
 22. Davies PH, Franklyn JA. The effects of drugs on tests of thyroid function. *Eur J Clin Pharmacol* 1991;40:439-451.
 23. Gelfland RE. Thyroid. In: Putman CE, Ravin CE (eds). *Textbook of diagnostic imaging*. Philadelphia: WB Saunders, 1994: 1457-1468.

**PRE- AND POST- TREATMENT
ULTRASONOGRAPHY IN HYPOTHYROID DOGS**

Olivier Taeymans¹, Sylvie Daminet², Luc Duchateau³,
Jimmy H. Saunders¹

Department of Medical Imaging¹, Department of Medicine and Clinical
Biology of Small Animals² and, Department of Physiology and
Biometrics³, Faculty of Veterinary Medicine, Ghent University,
Salisburylaan 133, 9820 Merelbeke, Belgium.

Adapted from:

O. Taeymans, S. Daminet, L. Duchateau, J.H. Saunders. Pre- and post-
treatment ultrasonography in hypothyroid dogs.

Vet Radiol Ultrasound 2007; 48: 262-269.

SUMMARY

Primary hypothyroidism is a frequent endocrine disorder in the adult dog. However, false-positive diagnoses are common because of the relatively low accuracy of most commonly used biochemical tests. The purpose of this study was to describe the ultrasonographic features of the thyroid gland in hypothyroid dogs, to calculate the diagnostic sensitivity of gray-scale ultrasound using a combination of clinical symptoms and biochemical thyroid tests as gold standard, and to investigate the evolution of the ultrasonographic features after treatment of hypothyroidism. Eighteen dogs were studied prospectively. All dogs underwent an ultrasound examination at first presentation and 13 underwent one or two additional ultrasound examinations over time. At first presentation, a sensitivity of 76.5% (95% CI [50.0%-93.0%]) for decreased echogenicity, 64.7% (95% CI [38.3%-85.8%]) for inhomogeneity, 70.6% (95% CI [44.0%-89.7%]) for irregular capsule delineation, 64.7% (95% CI [38.3%-85.8%]) for abnormal lobe shape and 47.1% (95% CI [23.0%-72.2%]) for decreased relative thyroid volume was obtained. Combining these five parameters together resulted in an overall sensitivity of 94.1% (95% CI [71.3%-99.9%]) for gray-scale ultrasound in the detection

of acquired hypothyroidism at first presentation. A continuous decrease of thyroid volume was seen over time after treatment, while the other investigated parameters did not change significantly during the follow-up period. None of the thyroid glands were considered normal at the last presentation. Grayscale ultrasound is a sensitive and quick test for the diagnosis of primary hypothyroidism in dogs.

INTRODUCTION

In dogs, acquired primary hypothyroidism is the result of lymphocytic thyroiditis or idiopathic follicular atrophy of the gland.^{1,2,3,4} Whether both conditions are separate entities or if atrophy is the end-result of thyroiditis is not established.³ Primary hypothyroidism is a common endocrinopathy in the dog, but it is also the most overdiagnosed endocrine disorder in this species.^{5,6,7,8,9} Reasons for overdiagnosis are the wide variety of clinical manifestations, the relatively low accuracy of most biochemical tests and the fact that many factors like non-thyroidal diseases, drugs and normal physiologic fluctuations can lower circulating thyroid hormone concentrations.^{3,4,5,7,10} Measurements of FT4 after equilibrium dialysis and TgAA, possibly combined with a TSH-stimulation test, is sometimes required to confirm a suspicion of primary hypothyroidism based on the classic assessment of TT4 and TSH values. However, FT4, TgAA, and TSH quantification is expensive and at least two of them are not commonly available in many countries.⁵ Similar problems in diagnosing thyroid disease also exist in humans.^{11,12} A combination of several diagnostic modalities is therefore used in humans to improve diagnostic accuracy. Biochemistry and nuclear imaging define the function of the thyroid gland, whereas ultrasound defines its structure and volume. An important additional advantage of ultrasound is that it allows guidance of needle aspirates and biopsies.¹³

Chronic autoimmune thyroiditis in humans is characterized by a decrease in echogenicity and size of the gland on ultrasound.^{14,15,16} Ultrasonography is valuable in the evaluation of the thyroid and parathyroid glands in canine patients as well.^{17,18,19,20,21,22,23} The superficial location of these glands allows modern, high frequency ultrasound equipment to give high resolution images of the thyroid gland. The normal gland in the dog has a homogeneous parenchyma, is most frequently hyperechoic compared to the surrounding musculature, is sharply delineated by a smooth hyperechoic capsule and its size is related to the size of the dog. Each lobe has a triangular to polygonal shape in the transverse plane and a fusiform shape, with a rounded cranial end and a pointed caudal end, in a longitudinal plane (Fig.1).^{17,20,21,23}

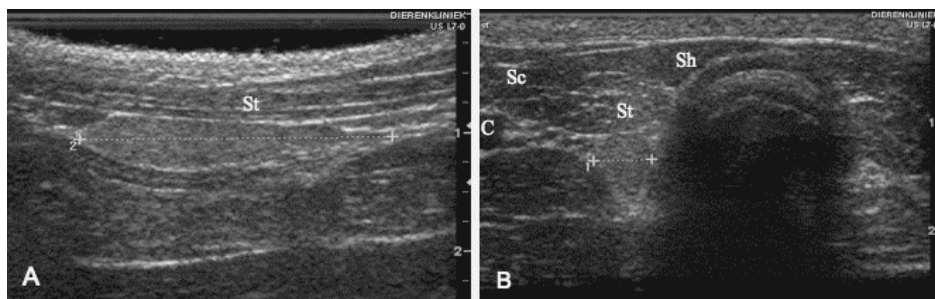


Fig. 1: Longitudinal (A) and transverse (B) US images of a normal thyroid lobe. Cranial is left on the longitudinal image and lateral is left on the transverse image. This lobe was considered homogeneous, hyperechoic compared to the surrounding musculature, having a smooth capsule and a normal triangular shape on transverse section. (C=common carotid artery; Sc=sternocephalic muscle; Sh=sternohyoid muscle; St=sternothyroid muscle; T=trachea)

During the last two decades, ultrasound of the canine thyroid was mainly restricted to the differentiation of non-thyroidal cervical masses from thyroid neoplasms and to define the local invasiveness and vascularity of those tumors.^{18,20,21} Very recently, ultrasound was also applied in the diagnosis of canine primary hypothyroidism and in the differentiation between “euthyroid sick syndrome” from “true” primary hypothyroidism.^{24,25}

The purpose of the present study is to report the ultrasound appearance of the thyroid gland in 18 dogs with confirmed hypothyroidism, to describe the ultrasonographic changes after treatment and to calculate the diagnostic sensitivity of gray-scale ultrasound in this disorder.

MATERIALS AND METHODS

Dogs

Data were collected prospectively from January 2003 to March 2006. Eighteen hypothyroid dogs of eleven different breeds were studied. Mean age at first presentation was 79 months (range: 35 – 129) and mean body weight was 33.1 kg (range: 12 – 60 kg). There were 10 females (6 intact, 4 neutered) and 8 males (4 intact, 4 castrated). The dogs had various clinical symptoms suggestive of acquired hypothyroidism and were examined by the same board-certified internist (S.D.). Criteria to diagnose acquired hypothyroidism were clinical manifestations, and results from biochemical and hematological blood analyses. The positive biochemical tests consisted of either

abnormal TT4 (< 15nmol/L) and TSH serum concentrations (> 0.6 ng/mL) or a positive dynamic function test using rhTSH with TT4 serum concentrations 4 hours after intravenous administration of 90 µg rhTSH, being lower than 40 nmol/L.^{26,27} Further, dogs had to have a positive response to treatment with levothyroxine to be included. Resolution of the clinical signs, together with a normalization of TT4 values, was considered a positive response.

Ultrasound examination

Hair was clipped from the ventral aspect of the neck, in a region from the larynx to 10-15cm more caudally. Dogs were in dorsal recumbency without the use of tranquilization or anesthesia and were restrained manually.

Both thyroid lobes were scanned with a GE Logic 7* machine connected to a multifrequency (7-14 MHz) linear matrix transducer with the frequency set at 12 MHz. The image presets (image depth, number and location of the focal points, focal width, output power and dynamic range) were identical for all patients. The overall gain and the time gain compensation were adjusted for each patient. No standoff pad was used. Each lobe was first observed in a transverse plane. Scanning was started in the midline, just caudal to the larynx, followed by a slow gliding motion of the probe caudally. Minimal transducer pressure was applied to the skin. Landmarks used for the localization of each lobe were the laterally located common carotid arteries, the medially located

trachea, and the ventrally located sternothyroid muscles. An additional landmark for the left lobe was the dorsally located esophagus. The maximum height and the maximum width of each lobe, which were not necessarily located in the same plane, were measured on transverse images by use of electronic calipers with a precision of one tenth of a millimeter. Following this, a longitudinal image of each lobe was obtained either by slowly rotating the probe 90° or by using a longitudinal image of the common carotid artery and the trachea as landmarks, according to a previously described approach.¹⁷ The maximum length of each separate lobe, excluding the cranially located external parathyroid gland if visible, was obtained in this plane. The homogeneity of the gland, its relative overall echogenicity compared to the overlying sternothyroid muscle, and the capsule delineation of the gland were assessed on both the transverse and longitudinal images. A visual interpretation of an equal echogenicity throughout the parenchyma of the lobes was recorded as a homogeneous parenchyma. Any difference in echogenicity throughout the parenchyma resulted in the interpretation of a heterogeneous lobe. To record the relative overall echogenicity of each lobe, scores of 0, 1 and 2 were attributed to hyperechogenicity, isoechogenicity and hypoechogenicity, compared to the overlying sternothyroid muscle respectively. The delineation of each lobe was recorded as being smooth or irregular. The shape of the lobes was assessed only on transverse images, and this at the level of the maximum height of the lobe. Each lobe was recorded as normal in

shape if it had a triangular to polygonal shape. Any variation to this shape, being rounded, ovoid or amorphous in shape, was considered abnormal and recorded as such. All ultrasound examinations were performed by the same board-certified radiologist (O.T.)²²

Data analysis

The maximum width, the maximum height and the maximum length of each lobe were used to calculate the volume of each lobe according to a formula of a rotation ellipse [volume (cm³) = length (cm) x width (cm) x height (cm) x $\pi/6$]. Some lobe measurements were lacking in one dog, preventing volume calculation. This dog was excluded from further analysis. Total thyroid volume was given by the sum of right and left thyroid lobe volumes. Thyroid volume was divided by the BW^{0.75} of the dog to obtain a relative volume of the thyroid gland, as described previously.²⁵ Relative thyroid gland volume was considered small when less than a relative volume of 0.05 mL/kg^{0.75}, a value being advocated as a useful cut-off.²⁵ As a control, we applied this cut-off value onto the measurements performed by the same observer (O.T.) on five healthy Beagles from a previous study.²²

Thirteen out of the 18 dogs had one or two additional ultrasound examinations after the initial diagnosis and thus after treatment. Ten had one revisit and 3 dogs underwent a third ultrasound examination of their thyroid gland. This resulted in 34 ultrasound examinations, including the 18 initial studies. The number of days between each follow-up

examination and the initial ultrasound examination were calculated using a free downloadable software program[†].

Statistical analysis

Sensitivity was calculated as the percentage of the 18 hypothyroid dogs outside the published reference limits. The derivation of the 95 % confidence interval was based on the binomial distribution assumption. Combining all parameters to calculate the overall sensitivity of ultrasonography in the detection of acquired hypothyroidism, dogs were considered abnormal when only one parameter was outside the reference limits. The evolution of the individual lobe relative volume over time was analyzed by a mixed model with dog as random effect using as covariate, either a binary covariate (before or after treatment) or a continuous covariate (time since start of the treatment). For the other four parameters, the first (before treatment) and the last assessment were compared by the Wilcoxon signed rank test with dog as block factor. Finally, the Spearman rank correlation coefficient between the five considered parameters was calculated. All analyses were performed in SAS (Version 9.1) at a significance level of 5%.

RESULTS

All relative thyroid gland volume measurements from the healthy Beagles were above the suggested cut-off value of 0.05 mL/kg^{0.75}, with a mean relative thyroid volume of 0.149 mL/kg^{0.75}. In the hypothyroid dogs, all thyroid lobes were visible and all measurements, with the exception of 2 length measurements and 1 width measurement, could be obtained. The impossibility to obtain these 3 measurements occurred in the same dog, a heavily agitated Riesenschnauzer. It was decided to exclude this dog from further analyses because of these missing data. The 17 other dogs were very- to relatively well compliant and sedation was not required in any of these dogs. Sedation was not required in any of the revisits either. Figures 2 and 3 show examples of the thyroid gland on gray-scale ultrasound in two different hypothyroid dogs.

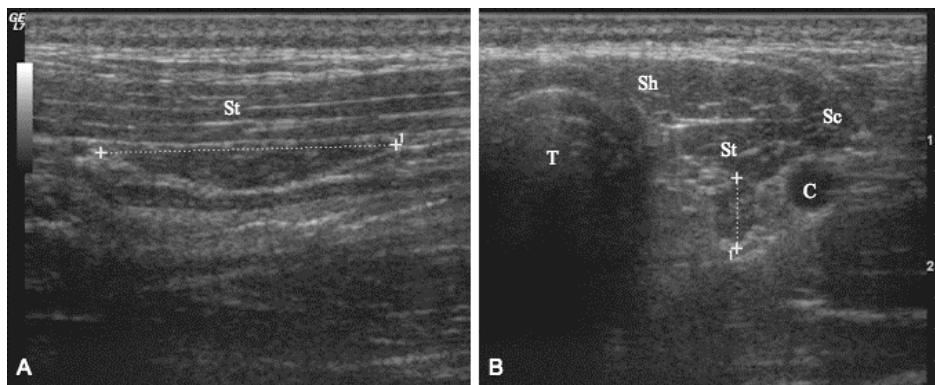


Fig. 2: Longitudinal (A) and transverse (B) US images of a thyroid lobe in a hypothyroid dog at first presentation. The thyroid lobe is indicated by electronic calipers. This lobe was considered heterogeneous, hypoechoic compared to the surrounding musculature, having an irregular capsule and being abnormal in shape on transverse section. The calculated relative thyroid gland volume in this dog was $0.054 \text{ mL/kg}^{0.75}$.

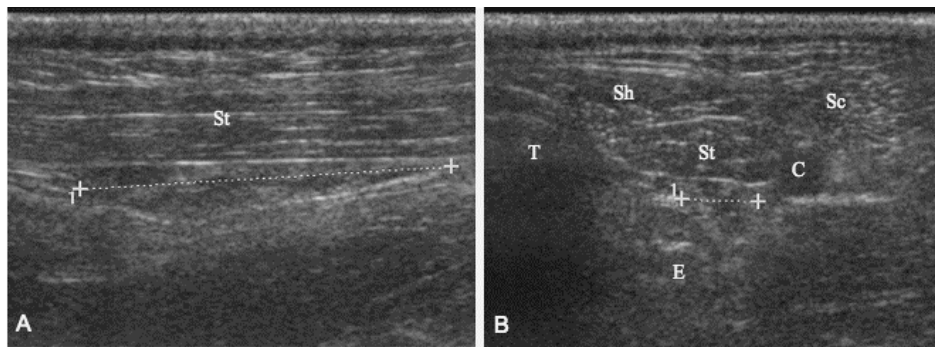


Fig. 3: US images of both thyroid lobes of a hypothyroid dog at first presentation. Fig. 3A is a longitudinal image of the right lobe. Fig. 3B is a transverse image of the left lobe. The thyroid lobes are indicated by electronic calipers. Both lobes in this dog were considered heterogeneous, being isoechoic compared to the surrounding musculature, having a smooth capsule and being normal in shape on transverse section. The calculated relative thyroid gland volume was $0.061 \text{ mL/kg}^{0.75}$.

Results of homogeneity of the lobes, relative echogenicity, capsule delineation and shape of the lobes on transverse sections are summarized in figure 4 for all hypothyroid dogs at first presentation.

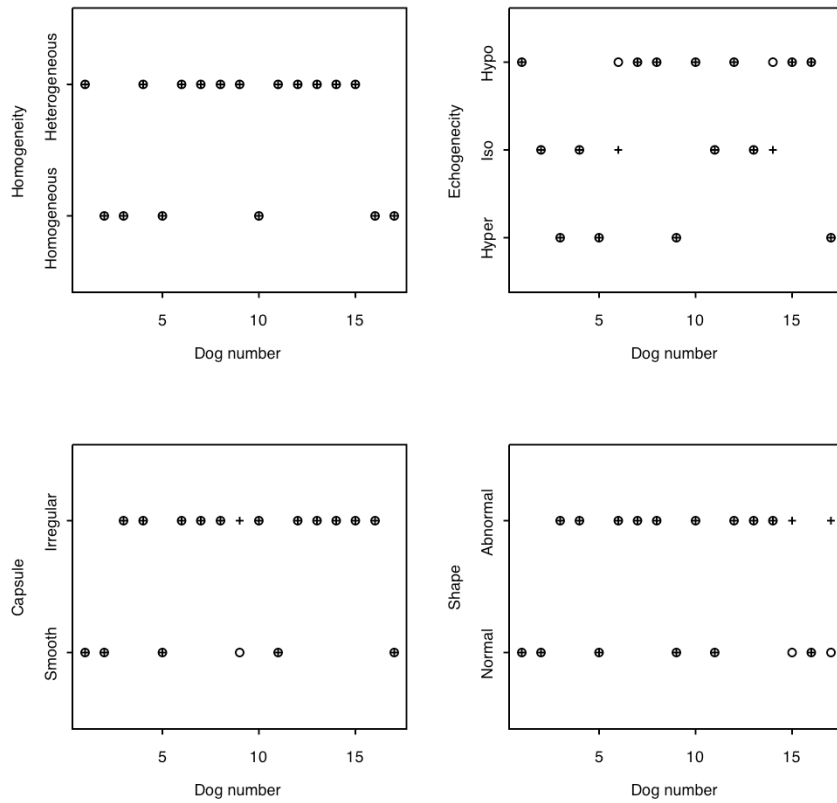


Fig. 4: Graphical representations of homogeneity, relative echogenicity, capsule delineation and shape of both thyroid lobes at the time of first presentation in each dog. A cross represents the right lobe, a circle represents the left lobe. The evaluated parameters are usually the same for both lobes. (hypo=hypoechoic; iso=isoechoic; hyper=hyperechoic)

Findings for each separate parameter, at the exception of the relative volume, for the left and right thyroid lobes were usually the same. For homogeneity, findings for both lobes were identical in all dogs. The capsule delineation was different between the left and right lobe in only one dog. A difference in shape between both lobes was seen in two dogs and a difference in echogenicity between both lobes was equally seen in two dogs. The findings were similar between both thyroid lobes in 63/68 (93%) parameters.

Regarding the individual lobes at first presentation, 22/34 (65%) lobes were heterogeneous, 22/34 (65%) had an irregular capsule, 20/34 (59%) were abnormal in shape and 26/34 (76%) were hypoechoic or isoechoic compared to the sternothyroid muscles. When considering that only one of the two lobes has to be outside the normal limits for the four parameters other than volume, the calculated sensitivity for detecting acquired hypothyroidism at first presentation was 64.7% (95% CI [38.3%-85.8%]) for homogeneity, 70.6% (95% CI [44.0%-89.7%]) for capsule delineation and 64.7% (95% CI [38.3%-85.8%]) for shape. Considering isoechogenicity compared to the surrounding musculature as being abnormal, the sensitivity for echogenicity was 76.5% (95% CI [50.0%-93.0%]). Allowing isoechogenicity as being a normal finding, as was suggested by others²³, the sensitivity for echogenicity decreased to 52.9% (95% CI [27.8%-77.0%]). Results for relative thyroid gland volume at first presentation are graphically represented in figure 5.

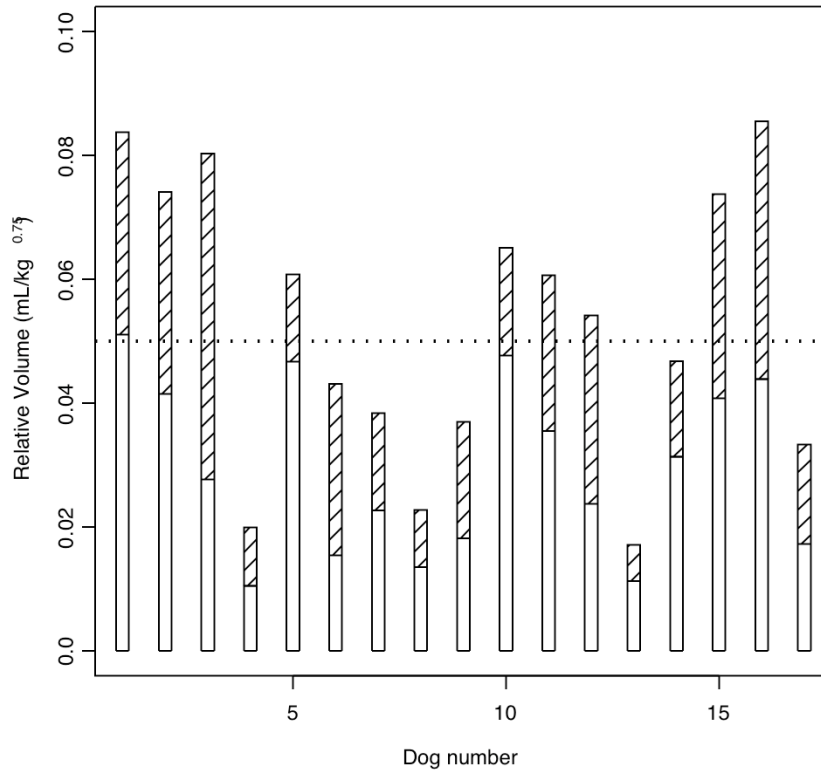


Fig. 5: Graphical representation of the relative thyroid gland volume and the relative thyroid lobe volumes at the time of first presentation in each dog. The height of each bar represents the relative thyroid gland volume, which is the sum of the right (shaded area) and left (blank area) relative thyroid lobe volumes. The horizontal dashed line represents the cut-off value of $0.05 \text{ mL/kg}^{0.75}$ for the relative thyroid gland volume.

The sensitivity for relative thyroid gland volume was 47.1% (95% CI [23.0-72.2]). When looking at the 5 parameters together, the sensitivity for B-mode ultrasonography in the detection of acquired hypothyroidism before treatment was 94.1% (95% CI [71.3%-99.9%]), as only one dog was normal for all assessed characteristics.

The highest correlation was seen between the shape and the capsule delineation of the thyroid lobes. A high correlation was also found between the relative volume and the shape of the lobe, where abnormally small lobes had a more rounded shape (Table 1).

	rvolume	homogen	echogen	capsule	shape
rvolume	1.000	-0.370	0.141	-0.221	-0.439
		0.031	0.426	0.209	0.010
homogen	-0.370	1.000	0.339	0.279	0.257
		0.031	0.050	0.111	0.142
echogen	0.141	0.339	1.000	0.436	0.237
		0.426	0.050	0.010	0.178
capsule	-0.221	0.279	0.436	1.000	0.699
		0.209	0.111	0.010	<0.0001
shape	-0.439	0.257	0.237	0.699	1.000
		0.010	0.178	<0.0001	

Table 1: Spearman rank correlation coefficients between 5 parameters (N=34) with P-value for coefficient being equal to zero given below the correlation coefficient. rvolume=relative thyroid lobe volume; homogen=homogeneity of the lobe; echogen=relative echogenicity of the lobe compared to the sternothyroid muscle; capsule=capsule delineation of the lobe; shape=shape of the lobe on transverse section

From the 10 dogs that had only one follow-up examination, one came at 29 days, five came between 51 and 65 days, one at 94 days, one at 193 days, one at 244 days, and one at 414 days after the initial ultrasound. The 3 dogs that underwent a second follow-up examination came between 27 and 41 days for their first follow-up and one at 288 days, one at 342 days and one at 358 days for their second follow-up. When looking at the effect over time, with before or after treatment as covariate, we found a significant difference in relative volume of the individual lobes at first presentation compared to a later presentation ($P=0.0368$). The relative lobe volume decreased significantly from an average of $0.02078 \text{ mL/kg}^{0.75}$ to an average of $0.01473 \text{ mL/kg}^{0.75}$ (Fig 6).

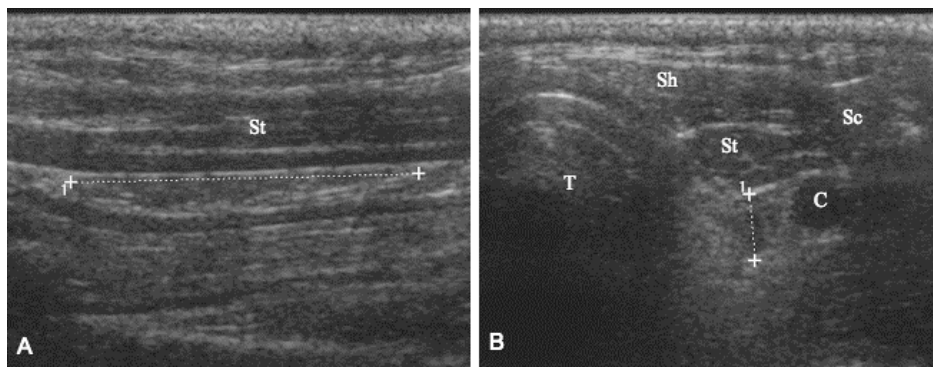


Fig. 6: Same dog as in figure 2, 288 days after treatment. Both lobes decreased further in size (relative thyroid gland volume of $0.039 \text{ mL/kg}^{0.75}$) and became more echoic. The heterogeneity of both lobes and the abnormal shape on transverse section remained. (C=common carotid artery; Sc=sternocephalic muscle; Sh=sternohyoid muscle; St=sternothyroid muscle; T=trachea)

When using time since start of the treatment as covariate, the relative individual lobe volume decreased significantly over time ($P=0.0349$) with a daily decrease of $0.00003 \text{ mL/kg}^{0.75}$. Finally, the relative thyroid gland volume at the last presentation was above $0.05 \text{ mL/kg}^{0.75}$ in only two dogs.

The echogenicity score at the first presentation was compared with the echogenicity score at the last presentation. The median difference in echogenicity score was equal to 0 and the mean difference was 0.38, but this decrease in score, or increase in echogenicity, over time was not significant ($P=0.28$). Neither the homogeneity, the shape nor the capsule delineation of the lobes were characterized by any significant change over time. In addition, when looking at the sum of the 4 subjective parameters scores (echogenicity, homogeneity, shape and capsule delineation), there was no significant difference between the score at first presentation and the last score measured ($P=0.63$). One dog developed a cystic lesion in one lobe, 2 months after treatment (Figure 7). For statistical analysis, this lobe was considered hypoechoic and heterogeneous.

Considering all parameters together, no single initially abnormal lobe at first presentation became normal at any time during the follow-up period and all thyroid glands were considered abnormal at the time of the last presentation. Therefore, the observed sensitivity at the last presentation was 100% (95% CI [75.3-100.0]) for all parameters combined.

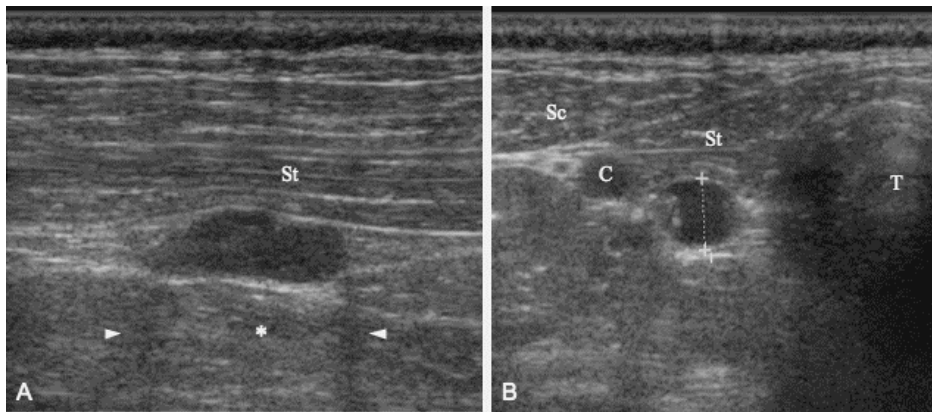


Fig. 7: Longitudinal (Fig. 6A) and transverse (Fig. 6B) ultrasound images of the right thyroid lobe of a hypothyroid dog 59 days after initial diagnosis. A 15x6x5 (LxWxH) mm, well-delineated, cystic lesion with dorsally located distal enhancement (*) and edge shadowing (arrowheads), is seen in this lobe. (C=common carotid artery; Sc=sternocephalic muscle; St=sternothyroid muscle; T=trachea)

DISCUSSION

The measurement of the length was the most difficult of the 3 measurements to obtain because of the difficulty in identifying the sharp caudal endpoint of the gland, as mentioned previously.²² Also, as the edge of the pathologic glands was ill-defined at some places, defining the shape and the capsule delineation of the gland was based on a more subjective interpretation than the determination of the relative echogenicity and homogeneity of the gland parenchyma.

The previously suggested lower limit of $0.05 \text{ mL/kg}^{0.75}$ for the relative volume of the thyroid gland in euthyroid dogs was successfully applied to the healthy control dogs, as the mean relative gland volume for these

dogs was 3 times higher than the suggested lower limit.²⁵ This means that the cut-off value could be applied by different observers, and that it was chosen low enough to keep different healthy dogs, other than those from the original study, above the lower limit. That only 8 of our 17 hypothyroid dogs had a relative thyroid volume below the limit of 0.05 mL/kg^{0.75} could mean that this value is too low for use by other examiners who might measure in a different way, as it was previously demonstrated that there is significant inter-observer variability in ultrasound measurement of the canine thyroid.²² This idea is reinforced by the fact that the volume measurements in our control dogs were well above the lower limit (3 times higher), suggesting the observer in this study systematically obtained larger measurements. The use of a higher cut-off value in our study would have resulted in a higher sensitivity for thyroid volume measurements. Our study however was limited to 18 dogs of 11 different breeds, making it irrelevant to suggest a new cut-off value.

The calculated overall sensitivity of 94.1% for detection of acquired hypothyroidism with B-mode ultrasound in our dogs, is somewhat lower than the recently published 98%.²⁵ This is mainly due to the difference in sensitivity for relative thyroid gland volume, being 47.1% in our study versus 81% in the other study.²⁵ As in our previous study, the larger inter-observer variability of ultrasound measurements between different observers is likely the reason for this difference.²² The observer of the current study might have taken systematically larger

measurements and used a different protocol with different measure points than the author of the suggested cut-off value.

Our obtained sensitivity of 76.5% for decreased echogenicity of the thyroid gland in hypothyroidism was comparable to previously reported values of 75% and 72%.^{24,25} Heterogeneous glands were seen in 64.7% of dogs compared to 45%, and a round to oval shape was seen in 64.7% versus 68% of the dogs in a previous study.²⁴ Finally, the capsule delineation was abnormal in 70.6% of our dogs and this was seen in only 27.2% of the dogs in a previous study.²⁴ A possible explanation for this last discrepancy may be the subjective nature of this parameter.

Results for the parameters other than the volume measurements of the left and the right thyroid lobes, were identical in 93% of the dogs. The echogenicity of both lobes was equal in 88% of our dogs. Others however described a similar echogenicity for both left and right lobes in 45% of hypothyroid dogs.²⁴ Similar findings comparing both thyroid lobes for parameters other than echogenicity are lacking in the other studies.

All dogs in our study were supplemented with levothyroxine shortly after the diagnosis of hypothyroidism. From these, 13 were followed over time. Ten had one revisit and 3 dogs underwent two subsequent sonographic assessments of their thyroid gland. The longest follow-up period was 414 days and the average follow-up period was 173 days. A significant continuous decrease in size of the thyroid lobes was seen during this period, with a decrease of 71% of the original value. The

only dog with normal parameters at first presentation was also considered abnormal at the time of the last follow-up because of a decrease of its relative thyroid volume below the cut-off value. A possible explanation for the further decrease in thyroid gland size observed in our dogs could be the negative feed back mechanism on the TSH secretion of the pituitary gland, being triggered by the supplementation of levothyroxine. Another reason could be the progression of lymphocytic thyroiditis into thyroid atrophy, supporting the hypothesis that idiopathic follicular atrophy may be the end-result of a lymphocytic thyroiditis. Although not statistically significant, an increase in relative echogenicity was also observed during the follow-up period. A possible cause for this phenomenon may be the gradual decrease of inflammatory reactions in these glands and the gradual replacement of destroyed gland parenchyma by fibrous connective tissue.^{1,3} However as our dogs were not sedated, cytologic or histologic samples confirming or negating the presence of fibrous connective tissue have not been obtained. The other parameters did not change significantly over time; so abnormal glands at first presentation remained abnormal during the follow-up period. This was an expected finding as supplementation of levothyroxine is symptomatic and not curative therapy for acquired hypothyroidism. The development of a cystic lesion in a lobe of one of the dogs has to our knowledge not been described in association with primary hypothyroidism. In contrast, cystic nodules are relatively common in people and are described in a

variety of thyroid diseases like Hashimoto's thyroiditis and multinodular goiter. They can represent colloid accumulation, necrosis, hemorrhage or neoplasia.²⁸

A limitation of our study is the lack of information on the correlation between ultrasound findings and cytology or histology. The reason for not having performed needle aspirates or biopsies is that the dogs used in this study were unsedated client owned dogs. Although needle aspirates of abdominal organs can safely be performed in many unsedated patients, it is our strong opinion that they cannot in the neck region. Because of the small size of the thyroid lobes, the slightest movement of the patient would result in perforation of vital neck organs. Another limitation was that no attempt was made to look at the differences in ultrasonographic features between TgAA positive and negative dogs, as TgAA levels were lacking in six dogs.

In conclusion, in our study the thyroid lobes in hypothyroid dogs were sonographically smaller, hypoechoic, heterogeneous, misshapen or ill-delineated in 94% of the dogs. An enhancement of some of the ultrasonographic characteristics was seen after treatment. Diagnostic ultrasound of the canine thyroid gland is relatively easy to perform, usually does not require sedation of the patient, gives a quick result compared to biochemical blood tests, and has been proven to be a sensitive test in the diagnosis of acquired canine hypothyroidism. It can therefore be considered as an effective additional test for the diagnosis of this disorder.

*: Logic 7, General Electric Medical Systems, Milwaukee, WI, USA.

†: Date Calculator, Leithauser Research, FL, USA.

http://leithauserresearch.com/date_calculator.html

REFERENCES

1. Gosselin SJ, Capen CC, Martin SL. Histologic and ultrastructural evaluation of thyroid lesions associated with hypothyroidism in dogs. *Vet Pathol* 1981;18:299-309.
2. Graham PA, Nachreiner RF, Refsal KR, *et al.* Lymphocytic thyroiditis. *Vet Clin North Am Small Anim Pract* 2001;31:915-933.
3. Scott-Moncrieff JC, Guptill-Yoran L. Endocrine disorders. Hypothyroidism. In: Ettinger SJ, Feldman EC (eds): *Textbook of Veterinary Internal Medicine*. St-Louis: Elsevier-Saunders, 2005;1535-1543.
4. Feldman EC, Nelson RW. Canine hypothyroidism. In: Feldman EC, Nelson RW (eds): *Canine and Feline Endocrinology and Reproduction*. St-Louis: Elsevier-Saunders, 2004;86-151.
5. S. Daminet. Evaluation of canine thyroid function in physiological and pathological conditions. Doctoral Thesis. Ghent University, Belgium, 2003.
6. Chastain CB, Young DW, Kemppainen RJ. Anti-triiodothyronine antibodies associated with hypothyroidism and lymphocytic thyroiditis in a dog. *J Am Vet Med Assoc* 1989;194:531-534.
7. Ferguson DC. Update on diagnosis of canine hypothyroidism. *Vet Clin North Am Small Anim Pract* 1994;24:515-39.

8. Herrtage MC. Diseases of the endocrine system. In: Dunn J (ed): Textbook of Small Animal Medicine. Philadelphia: W.B. Saunders, 1999;534-541.
9. Scarlett JM. Epidemiology of thyroid diseases of dogs and cats. Vet Clin North Am Small Anim Pract 1994;24:477-486.
10. Daminet S, Ferguson DC. Influence on drugs on thyroid function in dogs. J Vet Intern Med 2003;17:463-472.
11. Surks MI, Stievert R. Drugs and thyroid function. New Engl J Med 1995;333:1688-1694.
12. Davies PH, Franklyn JA. The effects of drugs on tests of thyroid function. Eur J Clin Pharmacol 1991;40:439-451.
13. Barraclough BM, Barraclough BH. Ultrasound of the thyroid and parathyroid glands. World J Surg 2000;24:158-165.
14. Raber W, Gessl A, Nowotny P, Vierhapper H. Thyroid ultrasound versus antithyroid peroxidase antibody determination: A cohort study of four hundred fifty-one subjects. Thyroid 2002;12:725-731.
15. Mazziotti G, Sorvillo F, Iorio S, *et al.* Gray-scale analysis allows a quantitative evaluation of thyroid echogenicity in the patients with Hashimoto's thyroiditis. Clin Endocrinol 2003;59:223-229.
16. Pedersen OM, Aardal NP, Larssen TB, *et al.* The value of ultrasonography in predicting autoimmune thyroid disease. Thyroid 2000;10:251-259.

17. Wisner ER, Mattoon JS, Nyland TG, Baker TW. Normal Ultrasonographic anatomy of the canine neck. *Vet Rad Ultrasound* 1991;32:185-190.
18. Wisner ER, Nyland TG, Mattoon JS. Ultrasonographic examination of cervical masses in the dog and cat. *Vet Rad Ultrasound* 1994;35:310-315.
19. Wisner ER, Mattoon JS, Nyland TG. The neck. In: Nyland TG, Mattoon JS (eds): *Small animal diagnostic ultrasound*. Philadelphia: W.B. Saunders, 2002;285-304.
20. Wisner ER, Nyland TG. Ultrasonography of the thyroid and parathyroid glands. *Vet Clin North Am Small Anim Pract* 1998;28:973-91.
21. Nautrup CP, Kästner W, Denkewitz B, Reese S. The neck. In: Cartee RE (ed): *An atlas and textbook of diagnostic ultrasonography of the dog and cat*. London: Manson Publishing, 2000;109-122.
22. Taeymans O, Duchateau L, Schreurs E, *et al.* Intra- and interobserver variability of Ultrasonographic measurements of the thyroid gland in healthy beagles. *Vet Rad Ultrasound* 2005;46:139-142.
23. Brömel C, Pollard RE, Kass PH, *et al.* Comparison of ultrasonographic characteristics of the thyroid gland in healthy small-, medium-, and large-breed dogs. *Am J Vet Res* 2006;67:70-77.

24. Brömel C, Pollard RE, Kass PH, *et al.* Ultrasonographic evaluation of the thyroid gland in healthy, hypothyroid, and euthyroid Golden Retrievers with nonthyroidal illness. *J Vet Intern Med* 2005;19:499-506.
25. Reese S, Breyer U, Deeg C, *et al.* Thyroid sonography as an effective tool to discriminate between euthyroid sick and hypothyroid dogs. *J Vet Intern Med* 2005;19:491-498.
26. Daminet S, Fifle L, Paradis M, Duchateau L, Moreau M. Use of recombinant human thyroid-stimulating hormone for thyrotropin stimulation test in healthy, hypothyroid and euthyroid sick dogs. *Can Vet J*. Submitted.
27. Sauvé F, Paradis M. Use of recombinant human thyroid-stimulating hormone for thyrotropin stimulation test in euthyroid dogs. *Can Vet J* 2000;41:215-219.
28. Tessler FN, Tublin ME. Thyroid sonography: current applications and future directions. *Am J Roentgenol* 1999;173:437-443.

**COMPUTED TOMOGRAPHIC FEATURES OF THE
NORMAL CANINE THYROID GLAND**

Olivier Taeymans¹, Tobias Schwarz², Luc Duchateau³, Virginie
Barberet¹, Ingrid Gielen¹, Mark Haskins⁴, Henri van Bree¹, Jimmy H.
Saunders¹

Department of Medical Imaging¹ and the Department of Physiology and
Biometrics³, Faculty of Veterinary Medicine, Ghent University, Salisburylaan
133, 9820 Merelbeke, Belgium, the Department of Surgical Sciences², School
of Veterinary Medicine, University of Wisconsin-Madison, 2015 Linden Drive,
Madison, WI 53706-1100, USA and the Department of Pathobiology⁴,
University of Pennsylvania School of Veterinary Medicine, 3800 Spruce Street,
Philadelphia, PA 19104-6051, USA.

Adapted from:

Computed Tomographic Features of the Normal Canine Thyroid Gland.
O. Taeymans, T. Schwarz, L. Duchateau, V. Barberet, I. Gielen, M.
Haskins, J.H. Saunders.
Vet Radiol Ultrasound, Accepted July 16, 2007.

SUMMARY

The CT features of the normal thyroid gland were compiled from images acquired in 25 client-owned dogs without thyroid gland disease. The mean pre- and post-contrast attenuation values were 107.5 HU and 169.0 HU, respectively. After injection of intravenous contrast medium (600 mg iodine / kg), the apparent thyroid gland volume (both lobes combined) increased from a mean value of 1148.0 mm³ to a mean value of 1188.9 mm³. All thyroid lobes were homogeneous on pre- and post-contrast images. In a craniocaudal direction, the gland spanned a region from the 1st to the 8th tracheal ring and the right lobe was often more cranial than the left. On transverse images the lobe shape was ovoid in 72%, and its location was dorsolateral to the trachea in 90% of dogs. Parathyroid glands could not be identified and an isthmus connecting both thyroid lobes was only seen in one dog. Considering the excellent visibility of the normal canine thyroid gland, CT can be beneficial in the differentiation of thyroidal versus non-thyroidal neck masses. CT also yields potential in the staging of thyroid carcinomas.

INTRODUCTION

The canine thyroid gland consists of two elongated lobes located on both dorsolateral aspects of the cranial portion of the trachea, medial to the common carotid arteries. Both lobes span a region from the cricoid cartilage to the 5th-8th tracheal rings and the right lobe is located more cranial than the left.¹⁻³ A thin isthmus, spanning the trachea ventrally and connecting the caudal aspects of both lobes, is inconsistently and infrequently present in dogs, being more often present in large breeds.^{1,2,4} On CT, both human and feline thyroid glands have been described as hyperattenuating structures relative to the surrounding soft tissues. The pre-contrast attenuation value ranges from approximately 70 to 120 HU in humans and has a mean of 123 HU in cats.⁵⁻¹⁰

Tumor staging is the major indication for CT of the thyroid gland in people. CT is able to define the local invasiveness of the tumor and can be used for detection of metastasis to lymph nodes and lungs.^{5,7,9,11-15} CT is also used to detect intrathoracic ectopic thyroid tissue and can provide diagnostic information regarding the different types of human thyroiditis, as CT attenuation values permit estimation of the functional status of the gland.^{5,7,8,10,11,13,14,16} Similar information regarding tumor staging and diagnosis of acquired hypothyroidism may be found in dogs and, thus, it is important to know the normal CT features of the thyroid gland in this species. The purpose of this study was to characterize the normal baseline CT appearance of the canine thyroid gland.

MATERIALS AND METHODS

The study was performed prospectively to obtain data on pre- and post-contrast features of the normal thyroid gland in dogs of different breeds and ages. It was conducted from January to June 2006. Twenty-five client-owned dogs undergoing a CT examination for orthopedic problems were evaluated. Inclusion criteria were: 1) free of concurrent systemic disease, 2) did not receive any drug for at least one week prior the CT examination and 3) normal TT4 and TSH serum concentrations. To measure the serum thyroid hormone levels, venous blood was collected via a transdermal puncture of the jugular vein prior to induction of anesthesia. The blood samples were centrifuged at 3500 rpm and plasma was kept in plastic tubes at -20°C as previously described.^{17,18} After completion of all CT scans, all blood samples were sent simultaneously to the same laboratory as to avoid daily fluctuations in laboratory results. The whole procedure was done with owner consent in accordance with university regulations for the use of client owned animals. Represented breeds were: Labrador Retriever (10), Bernese Mountain Dog (3), Golden Retriever (2), Chien Anglo-Français (2), Beagle (2), Bordeaux Dog (1), Foxhound (1), mongrel (1), Boerboel (1), German Shepherd (1), Nova Scotia Duck Tolling Retriever (1). Their mean body weight was 31.1 kg (range: 13 – 52 kg) and mean age was 39 months (range 5 – 121 months).

Data were obtained with a 3rd generation helical CT scanner*. Dogs were under general anesthesia using a mixture of oxygen and isoflurane

and were in dorsal recumbency with the front legs retracted caudally to avoid superimposition with the neck. A foam block was placed under the neck to obtain a perpendicular position of the thyroid gland relative to the X-axis of the gantry. Transverse contiguous slices of the thyroid gland were obtained, scanning an area from the caudal aspect of the cricoid cartilage to a distance of 8 cm more caudally. Technical settings were 120 kV, 160 mA, 1 s tube rotation time, 3 mm slice thickness, 3 mm slice interval, detail algorithm, 35 cm scan field of view, and a display field of view around 8 cm, depending on the size of the dog. For the post-contrast series, non-ionic iodinated contrast medium[‡] at a dosage of 600 mg iodine/kg bodyweight was injected manually into the cephalic vein. Scanning of the gland was performed within 1 minute after injection. Machine settings for the post-contrast CT series were identical to the pre-contrast series and the dogs were not moved between both scans. Images for both the pre- and post-contrast series were displayed on a dedicated workstation at the following window settings: WW = 220, WL = 120. ROI were manually drawn around each cross section of both thyroid lobes on both pre- and post-contrast series, this on every transverse CT slice including thyroid tissue. Images were magnified to allow proper ROI placement. The computer automatically calculated the lowest, highest, and mean HU values, the standard deviation of the mean, and the surface area of each ROI. As the thyroid glands could potentially be tilted in any of the three dimensions of the gantry, creating false width, height, or length measurements, the volume

of the lobes was calculated using the sum of areas method, (slice thickness) x (sum of the cross sectional areas), instead of the rotational ellipse method (max. height x max. width x max length x $\pi/6$), also known as the transverse ellipse method.¹⁹ The volume of the thyroid gland was given by the sum of the volume of both lobes. The relative gland volume was subsequently obtained by dividing the gland volume by $BW^{0.75}$ of the dog. The attenuation value of the gland was given by the mean of the mean attenuation value of each transverse section of both lobes. The first and last slice of each lobe were excluded from this calculation to avoid partial volume artifacts. A subjective visual assessment of the homogeneity of the lobes was made on both pre- and post-contrast series. Location relative to the trachea, visibility of the parathyroid glands and shape of the lobes were recorded on transverse sections. The craniocaudal location of the lobes in relation to the tracheal rings was noted on 3D MIP images using dedicated software[§]. The presence of an isthmus was searched for on both transverse sections and reformatted 3D images using a surface-rendering algorithm[§]. Post-contrast images were used to identify the vasculature of the gland.

To investigate how relative thyroid size and mean attenuation value related to age and weight, Spearman rank correlation coefficient was obtained, and it was tested whether it differed from zero. The effect of contrast (pre- vs. post-contrast) on absolute gland volume, relative gland volume and mean attenuation value was assessed by a mixed model with

dog as random effect. Left and right lobes were compared for both the absolute gland size and mean gland attenuation value by a mixed model with dog as random effect. Statistical analyses were performed at the 5% significance level using a commercial statistic software[‡] for all calculations.

RESULTS

The thyroid lobes could easily be identified on both pre- and post-contrast images in all dogs as a consequence of their high attenuation value relative to the surrounding soft tissues (Figures 1 & 2).

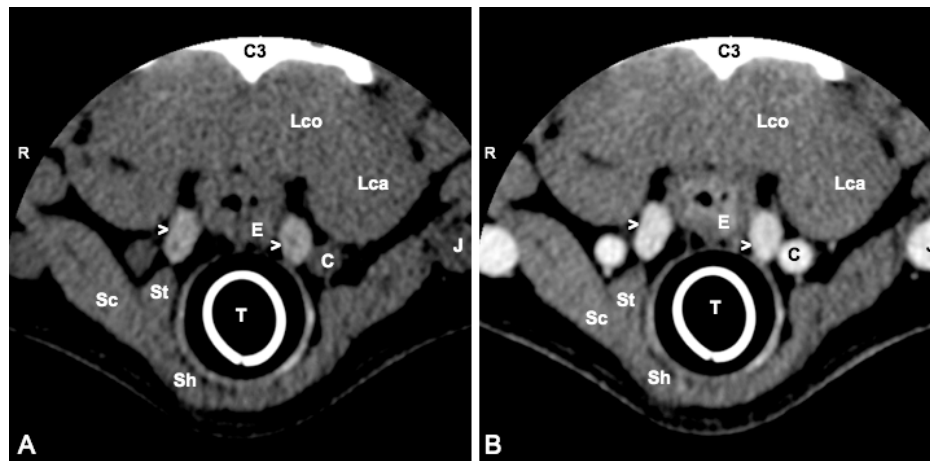


Fig. 1: Transverse pre- (A) and post-contrast (B) CT images of a normal adult dog neck. WL = 120; WW = 220. Slice location is at the mid-aspect of the thyroid gland, ventral to the third cervical vertebrae (C3). White arrowheads (>) indicate both thyroid lobes. Lco = longus colli muscle; Lca = longus capitis muscle; Sc = sternocephalic muscle; St = sternothyroid muscle; Sh = sternohyoid muscle; C = left common carotid artery; J = left external jugular vein; T = trachea with endotracheal tube.

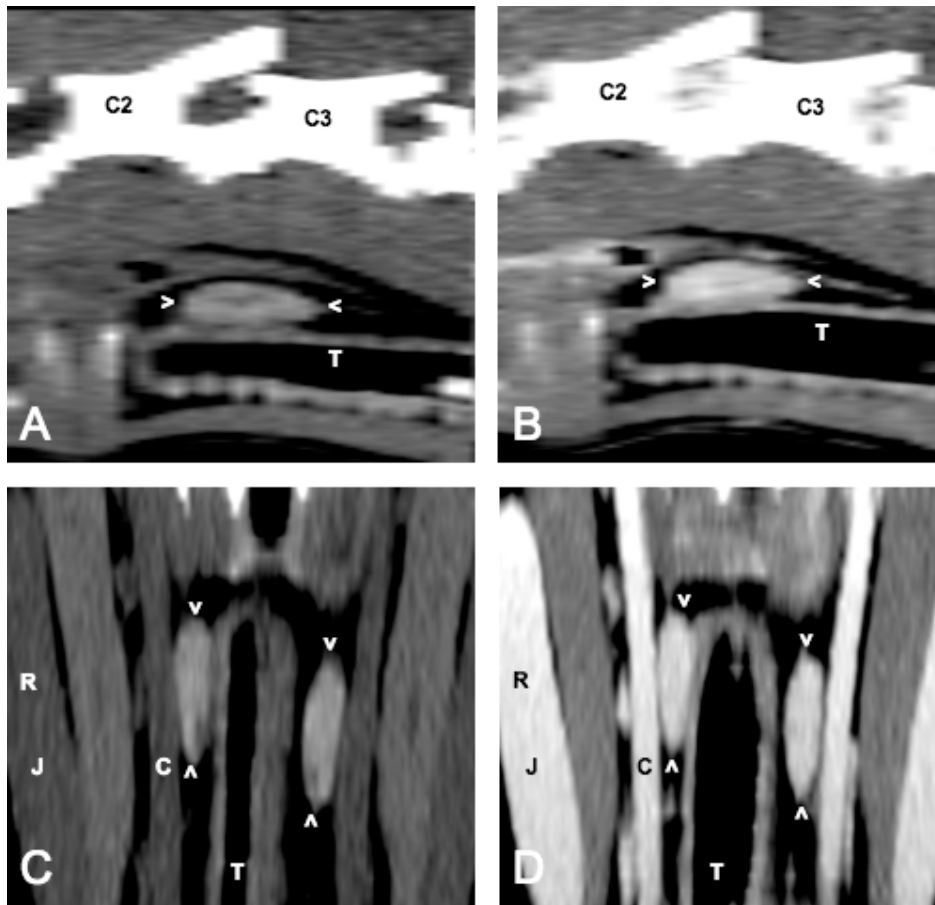


Fig. 2: Pre- (A) and post-contrast (B) sagittal reconstructed CT images of a normal adult dog neck. Slice location is at the level of the right thyroid lobe. Pre- (C) and post-contrast (D) dorsal reconstructed CT images of the same dog. Slice location is at the dorsal aspect of the trachea. WL = 120; WW = 220 for all images. White arrowheads (>) indicate both thyroid lobes. C2 = second cervical vertebra; C3 = third cervical vertebra; C = common carotid artery; J = external jugular vein; T = trachea.

Densitometric data and volume measurements of the thyroid gland for both groups are represented in Table 1.

Series	Gland volume (mm ³)	Rel. gland volume (mm ³ /kg ^{0.75})	Attenuation value (HU)
precontrast	1148.04 ± (957.02 – 1339.14)	87.83 ± (74.23 – 101.43)	107.50 ± (104.73 – 110.27)
postcontrast	1188.88 ± (986.32 – 1391.43)	91.01 ± (76.69 – 105.34)	169.02 ± (163.16 – 174.88)

Table 1: Mean ± (90% CI) gland volume, relative (rel.) gland volume and attenuation value of the thyroid glands.

The attenuation value ranges for both pre- and post-contrast series were: 87.4 – 137.0 HU and 124.8 – 230.4 HU, respectively. All thyroid lobes were homogeneous. Parathyroid glands could not be detected in any dog. On transverse sections, the most common location of the thyroid lobes was dorsolateral to the trachea in 45/50 lobes. Five lobes were located lateral and none were found ventrolateral to the trachea. An ovoid shape was assigned to 36/50 lobes, while 1/50 lobes had a triangular shape on transverse CT images. The remaining 13 lobes had a shape in between ovoid and triangular. Using 3D MIP reconstructed images, the craniocaudal location of both thyroid lobes was evident in 24/25 dogs. The right thyroid lobe was more cranial than the left in 14/24 dogs (1 ring more cranial in 13, and 2 rings more cranial in 1 dog), while the left was located one ring more cranial than the right in only 2 dogs. In 8/24 dogs, both lobes were located at the same craniocaudal level. The

average cranial and caudal location relative to the tracheal rings for both thyroid lobes are shown in Table 2. An isthmus spanning the ventral aspect of the trachea and connecting the caudal part of both lobes was seen in only one dog, a two-year-old Golden Retriever (Figure 3).

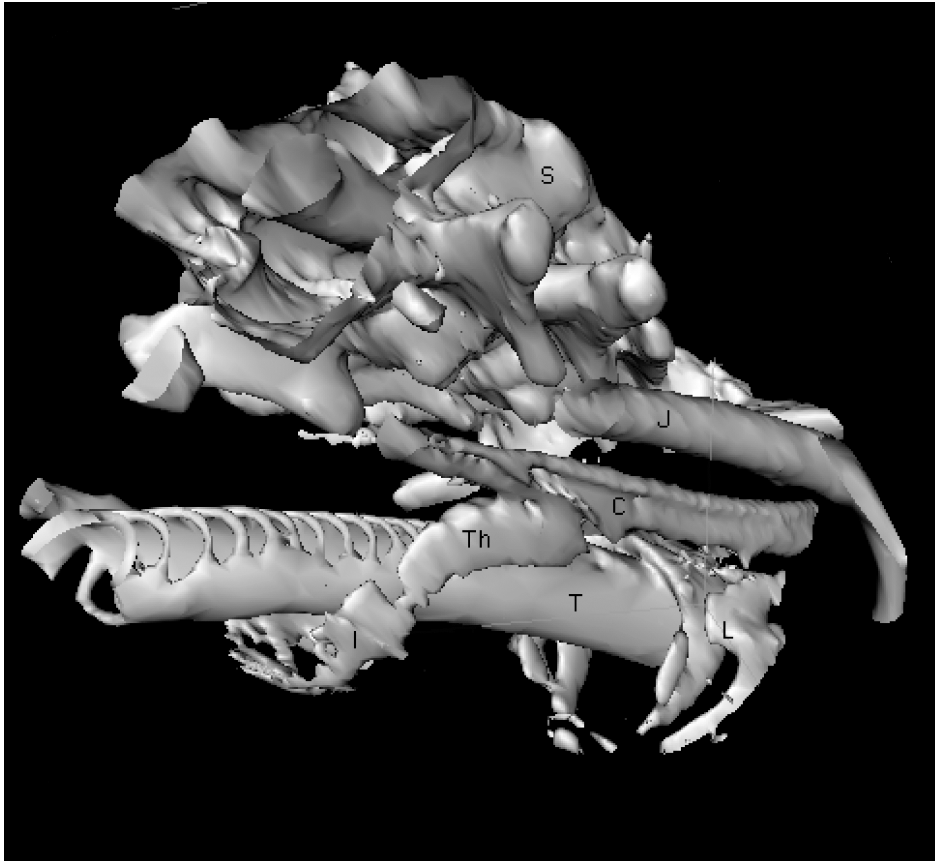


Fig. 3: 3D surface rendering reformatted CT image of the neck area. Note the isthmus connecting the caudal poles of both thyroid lobes, from a right ventrocaudal approach. I = isthmus; Th = right thyroid lobe; T = endotracheal tube; L = larynx; C = right common carotid artery; J = right external jugular vein; S = cervical spine.

	Right lobe	Left lobe
Cranial location	2.6 (1-5)	3.1 (1-4)
Caudal location	6.0 (4-8)	6.3 (4-8)

Table 2: Average (range) location of both thyroid lobes relative to tracheal rings.

After contrast medium injection, the cranial thyroid artery was seen in all dogs as a U-shaped structure originating from the ventral aspect of the common carotid artery cranial to the thyroid lobes, running in a caudomedial direction and joining the dorsal aspect of the cranial pole of the thyroid lobes (Figure 4).

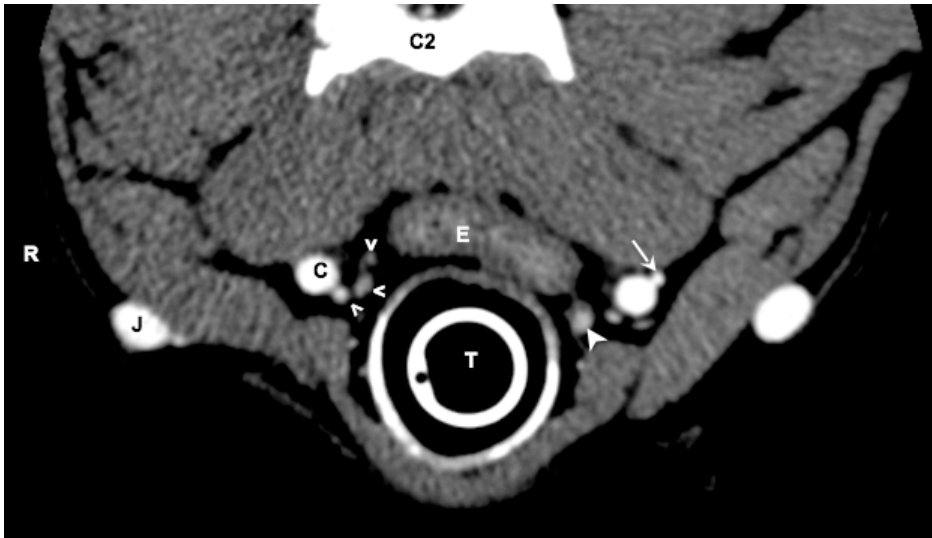


Fig. 4: Slice location is at the cranial aspect of the thyroid gland, ventral to the second cervical vertebra (C2). The right cranial thyroid artery (<) is seen exiting the ventral aspect of the right common carotid artery (C), making a U turn towards the location of the right thyroid lobe. The right thyroid lobe is not yet visible on this slice. A white arrowhead indicates the cranial aspect of the left thyroid lobe. A white arrow is pointing at the left internal jugular vein.

The caudal thyroid artery, which most commonly arises from the brachiocephalic artery and runs along the left lateral side of the trachea to join with the cranial thyroid artery, could not be identified in any dog.² The cranial thyroid vein, paralleling the course of the cranial thyroid artery, could be followed at the cranial aspect of only 17/50 lobes (Figure 5).

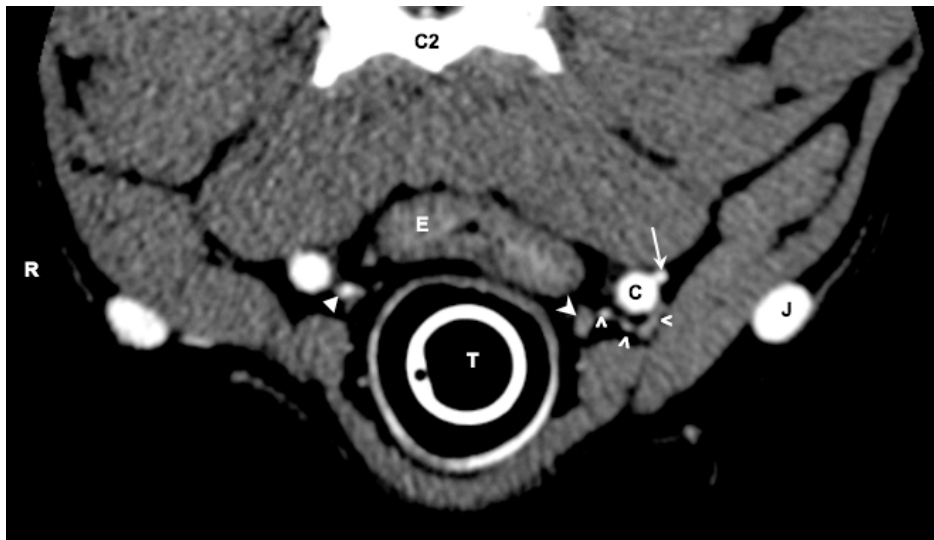


Fig. 5: Transverse post-contrast CT image of the same dog as in fig. 4. Slice location is 3 mm more cranial than in fig. 4. WL = 120; WW = 220. The dog's right (R) is to the viewer's left in the image. The left cranial thyroid vein (<) is seen entering the ventral aspect of the left internal jugular vein (arrow). The right thyroid lobe is not visible on this slice. A white stealth arrowhead indicates the cranial aspect of the left thyroid lobe. A white closed arrowhead is pointing at the right cranial thyroid artery. E = esophagus; T = trachea and endotracheal tube; J = left external jugular vein.

The caudal thyroid vein was frequently seen exiting the caudal pole of the thyroid lobe, running in a caudolateral direction to join the internal jugular vein (Figure 6). The internal jugular vein was in close proximity to the common carotid artery and had a diameter of approximately 20% of the common carotid artery.

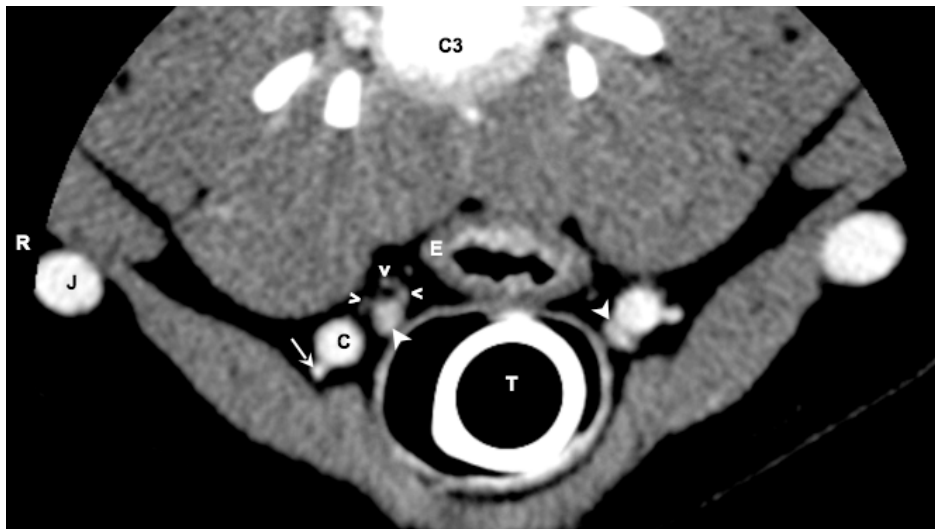


Fig. 6: Transverse post-contrast CT image of a normal adult dog neck. Slice location is at the caudal aspect of the thyroid gland, ventral to the third cervical vertebra (C3). WL = 120; WW = 220. The dog's right (R) is to the viewer's left in the image. The right caudal thyroid vein (<) is seen exiting the dorsal aspect of the right thyroid lobe. White arrowheads are indicating the caudal aspects of both thyroid lobes. A white arrow is pointing at the right internal jugular vein. E = esophagus; T = trachea and endotracheal tube; J = right external jugular vein.

The correlation between relative size and age was -0.27 and just failed to differ significantly from zero ($P=0.062$). This suggests that younger dogs may have a higher relative thyroid gland size. No correlation was observed between relative thyroid size and body weight ($P=0.62$), between mean attenuation value and age ($P=0.503$) and between mean attenuation value and body weight ($P=0.803$). When calculating the mean thyroid gland size before and after contrast medium injection, a significantly larger ($P=0.0037$) mean gland volume was obtained for the post-contrast images (1189 mm^3) compared to the pre-contrast series (1148 mm^3). No significant differences ($P=0.8002$) and ($P=0.3764$) were detected when comparing right and left thyroid lobes for size and attenuation value, respectively.

DISCUSSION

Pre-contrast cervical CT provides excellent visualization of the normal canine thyroid gland due to its higher attenuation compared to the surrounding soft tissues. The pre-contrast attenuation value of 107.5 HU is slightly lower than the reported value in cats (123.2 HU) and is within the reported range in people (70-120 HU).⁵⁻¹⁰ In people the thyroid attenuation value relates linearly to the iodine content of the thyroid follicles.^{5,7-9,20-22} An identical explanation can be assumed in dogs. The reference values reported here and elsewhere should however not be interpreted strictly, as alimentary iodine intake differences due to different food composition, tap water iodine concentration and

geographic differences alter the attenuation values significantly.^{8,23} No correlation was found between attenuation value and age, or between attenuation value and weight. The post-contrast thyroid attenuation value in our dogs (mean 169.0 HU) was almost identical to reported immediate post-contrast values in cats (168.5 HU).⁶ However these results should be interpreted cautiously since the time window for post-contrast image acquisition in our study was relatively wide (< 1 minute post start injection) albeit smaller than in the feline study. Dynamic contrast enhanced CT studies of the thyroid gland would be necessary to obtain reliable reference values. The significant increase in apparent thyroid size that we observed after contrast medium injection is likely related to the blooming artifact. The blooming artifact occurs at the margin of highly attenuating objects in a low attenuation environment, resulting in interface blurring, and is caused by averaging effects due to insufficient spatial resolution of the imaging system.²⁴⁻²⁶

The location and shape of the thyroid lobes reported here concur with published references, including the slightly more cranial position of the right lobe.^{1,2,4} These features are readily recognizable on CT images and help to identify the gland. As in cats, normal parathyroid glands were not observed.⁶ The variable location and number of the parathyroid glands, combined with technical factors like the presence of streaking artifacts, blooming artifacts and partial volume effects, hampered identification of these small structures. Only the cranial thyroid artery and the caudal thyroid vein were consistently identified and this is probably related to

the standard imaging protocol that was used. Angiographic CT protocols with exact vascular phase timing as used for other canine organs should allow identification of small vessels consistently.²⁷ Due to the tortuosity of the vessels, reformatted images in the two other planes were not useful and the limited size of the vessels hampered the use of 3D reconstructed images, as these were lost in the noise of structures with similar predefined pixel values.

Although scintigraphy provides functional information of the gland, CT provides important adjunctive anatomic information superior to that of nuclear imaging.^{5,7,28} Should both modalities be performed subsequently in a same patient, scintigraphy needs to be performed first as intravenous injection of iodinated contrast medium alters the uptake of radioactive iodine for a period of 6 to 8 weeks.^{5,8,14} In addition, since both iodinated contrast media and anesthetic drugs influence thyroid function in humans, it is important to collect blood for evaluation of thyroid hormone prior to administration of these drugs.^{8,29-31} In dogs, various anesthetic agents have an influence on thyroid function.³²⁻³⁵ Limited data are also available on the influence of intravenous iodinated contrast medium in dogs on thyroid function.³⁶ As a precaution we obtained all blood samples prior to induction of anesthesia and administration of iomeprol. Corticosteroids and non-steroidal anti-inflammatory drugs, as well as many non-thyroidal diseases like hyperadrenocorticism, diabetes mellitus, renal- or heart failure and liver disease are known to influence thyroid function in dogs.^{31-33,37-40} Dogs receiving any of these drugs or

having a systemic disease were therefore excluded from the study. However, our population was suffering from osteoarthritis, but it was recently proven that this disorder does not need to be considered a factor influencing thyroid function in dogs.⁴¹

Computed tomography of the thyroid gland yields interesting complementary information in different types of human thyroiditis and goiter.^{5,7-9,11,28} Diseased human thyroid tissues are isoattenuating or hypoattenuating to the adjacent musculature in pre-contrast CT images.^{7,8,20,21,42} An increase in follicular cells and interstitial tissue, besides a decrease of iodine concentration in the thyroid follicles, cause decreased attenuation values in diseased human thyroid tissue.²¹ Similar changes, together with a decrease in thyroid gland volume, may be seen in hypothyroid dogs and could be subject of future investigations. The detection of ectopic thyroid tissue and pharyngeal, cervical or mediastinal thyroglossal duct cysts are additional indications of CT in people and are of potential interest in dogs as well.^{5,7,8,13,14,28} One of the main indications for thyroid CT in people is the differentiation of thyroid masses from other neck masses and the evaluation of mediastinal or retrotracheal extension of thyroid masses, particularly in thyroid carcinoma, as the prognosis is related to local invasiveness and lymph node metastases.^{5,7-9,12-14,28,43} Invasiveness of the primary tumor, location of the tumor and presence of metastases equally influence treatment of dogs with thyroid carcinoma.⁴⁴ Canine thyroid tumors are very vascular and require careful surgical planning for which CT is an excellent

diagnostic tool.⁴⁵ Arterial invasion of thyroid carcinoma with rapid onset of cervical and mediastinal hemorrhage has been reported in the dog where the identification of the contrast enhancing thyroid mass and non-enhancing hemorrhage with CT was crucial in the further work up of the patient.⁴⁵

In conclusion we describe several imaging features of the normal canine thyroid gland that allow its identification on cervical CT scans. These landmarks can be used to determine thyroid involvement in masses of the neck, staging of thyroid carcinomas and have potential applications for other thyroidal diseases such as lymphocytic thyroiditis and idiopathic thyroid atrophy.

ACKNOWLEDGMENTS

The authors thank Annemie Van Caelenberg from the Department of Medical Imaging, Faculty of Veterinary Medicine, Ghent University, Belgium, for her kind assistance in the acquisition of the scans, and acknowledge the support of NIH grant RR02512 (MH).

* GE ProSpeed, General Electric Co., Milwaukee, WI, USA.

‡ Iomeron 300, iomeprol, Bracco Altana Pharma, Konstanz, Germany.

§ OsiriX v.2.6. Advanced open source PACS workstation. DICOM viewer.

¥ SAS v.9.1., SAS Institute Inc., Cary, NC, USA.

REFERENCES

1. König HE, Liebich H-G. Endocrine glands. Thyroid gland. In: König HE, Liebich H-G (eds). *Veterinary Anatomy of Domestic Mammals Textbook and Colour Atlas*. Stuttgart: Schattauer, 2004:539-41.
2. Hullinger R. The endocrine system. Thyroid gland. In: Evans HE, Christensen GC (eds). *Miller's anatomy of the dog*. 2nd ed. Philadelphia: W.B. Saunders Company, 1979:611-5.
3. Herrtage ME. Diseases of the endocrine system. In: Dunn J (ed). *Textbook of small animal medicine*. Philadelphia: W.B. Saunders, 1999:534-41.
4. Frewein J. Endokrine Drüsen. Schilddrüse, Glandula thyroidea. In: Frewein J, Vollmerhaus B (eds). *Anatomie von Hund und Katze*. Berlin: Blackwell Wissenschaftsverlag, 1994:442-3.
5. Loevner LA. Imaging of the thyroid gland. *Semin Ultrasound CT MR*. 1996;17(6):539-62.
6. Drost WT, Mattoon JS, Samii VF, Weisbrode SE, Hoshaw-Woodard SL. Computed tomographic densitometry of normal feline thyroid glands. *Vet Radiol Ultrasound*. 2004;45(2):112-6.
7. Silverman PM, Newman GE, Korobkin M, Workman JB, Moore AV, Coleman RE. Computed tomography in the evaluation of thyroid disease. *Am J Roentgenol*. 1984;142(5):897-902.

8. Arger PH, Jennings AS, Gordon LF, *et al.* Computed tomography findings in clinically normal and abnormal thyroid patients. *J Comput Tomogr.* 1985;9(2):111-7.
9. Reede DL, Bergeron RT, McCauley DI. CT of the thyroid and of other thoracic inlet disorders. *J Otolaryngol.* 1982;11(5):349-57.
10. Kaneko T, Matsumoto M, Fukui K, Hori T, Katayama K. Clinical evaluation of thyroid CT values in various thyroid conditions. *J Comput Tomogr.* 1979;3(1):1-4.
11. Radecki PD, Arger PH, Arenson RL, *et al.* Thyroid imaging: comparison of high-resolution real-time ultrasound and computed tomography. *Radiology.* 1984;153(1):145-7.
12. Weber AL, Randolph G, Aksoy FG. The thyroid and parathyroid glands. CT and MR imaging and correlation with pathology and clinical findings. *Radiol Clin North Am.* 2000;38(5):1105-29.
13. Hopkins CR, Reading CC. Thyroid and parathyroid imaging. *Semin Ultrasound CT MR.* 1995;16(4):279-95.
14. Hermans J. Les techniques d'imagerie thyroïdienne. *Ann Endocrinol (Paris).* 1995;56(5):495-506.
15. Reading CC, Gorman CA. Thyroid imaging techniques. *Clin Lab Med.* 1993;13(3):711-24.
16. Iida Y, Konishi J, Harioka T, Misaki T, Endo K, Torizuka K. Thyroid CT number and its relationship to iodine concentration. *Radiology.* 1983;147(3):793-5.

17. Behrend EN, Kemppainen RJ, Young DW. Effect of storage conditions on cortisol, total thyroxine, and free thyroxine concentrations in serum and plasma of dogs. *J Am Vet Med Assoc.* 1998;212(10):1564-8.
18. Paradis M, Laperriere E, Lariviere N. Effects of administration of a low dose of frozen thyrotropin on serum total thyroxine concentrations in clinically normal dogs. *Can Vet J.* 1994;35(6):367-70.
19. Drost WT, Mattoon JS, Weisbrode SE. Use of helical computed tomography for measurement of thyroid glands in clinically normal cats. *Am J Vet Res.* 2006;67(3):467-71.
20. Imanishi Y, Ehara N, Mori J, *et al.* Measurement of thyroid iodine by CT. *J Comput Assist Tomogr.* 1991;15(2):287-90.
21. Imanishi Y, Ehara N, Shinagawa T, *et al.* Correlation of CT values, iodine concentration, and histological changes in the thyroid. *J Comput Assist Tomogr.* 2000;24(2):322-6.
22. Nagataki S, Shizume K, Nakao K. Effect of chronic graded doses of iodide on thyroid hormone synthesis. *Endocrinology.* 1966 Oct;79(4):667-74.
23. Joseph K, Berg-Schlosser F, Herbert K. Computertomografische Bestimmung der intrathyreoidalen Jodkonzentration im Strumaendemiegebiet. *Rofo.* 1986;144(4):417-21.

-
24. Choi HS, Choi BW, Choe KO, *et al.* Pitfalls, artifacts, and remedies in multi-detector row CT coronary angiography. *Radiographics*. 2004;24(3):787-800.
 25. Hoffmann MH, Shi H, Manzke R, *et al.* Noninvasive coronary angiography with 16-detector row CT: effect of heart rate. *Radiology*. 2005;234(1):86-97.
 26. Muhlenbruch G, Mahnken AH, Das M, *et al.* Evaluation of aortocoronary bypass stents with cardiac MDCT compared with conventional catheter angiography. *Am J Roentgenol*. 2007;188(2):361-9.
 27. Cáceres AV, Zwingenberger AL, Hardam E, Lucena JM, Schwarz T. Helical computed tomographic angiography of the normal canine pancreas. *Vet Radiol Ultrasound*. 2006;47(3):270-8.
 28. Vette JK. Computed tomography of the thyroid gland. *Acta Endocrinol Suppl*. 1985;268:1-82.
 29. Nygaard B, Nygaard T, Jensen LI, *et al.* Iohexol: effects on uptake of radioactive iodine in the thyroid and on thyroid function. *Acad Radiol*. 1998;5(6):409-14.
 30. Surks MI, Sievert R. Drugs and thyroid function. *N Engl J Med*. 1995;333(25):1688-94.
 31. Wenzel KW. Disturbances of thyroid function tests by drugs. *Acta Med Austriaca*. 1996;23(1-2):57-60.
 32. Daminet S, Ferguson DC. Influence of drugs on thyroid function in dogs. *J Vet Intern Med*. 2003;17(4):463-72.

33. Daminet S, Paradis M, Refsal KR, Price C. Short-term influence of prednisone and phenobarbital on thyroid function in euthyroid dogs. *Can Vet J.* 1999;40(6):411-5.
34. Gieger TL, Hosgood G, Taboada J, Wolfsheimer KJ, Mueller PB. Thyroid function and serum hepatic enzyme activity in dogs after phenobarbital administration. *J Vet Intern Med.* 2000;14(3):277-81.
35. Muller PB, Wolfsheimer KJ, Taboada J, Hosgood G, Partington BP, Gaschen FP. Effects of long-term phenobarbital treatment on the thyroid and adrenal axis and adrenal function tests in dogs. *J Vet Intern Med.* 2000;14(2):157-64.
36. Laurberg P, Boye N. Inhibitory effect of various radiographic contrast agents on secretion of thyroxine by the dog thyroid and on peripheral and thyroidal deiodination of thyroxine to triiodothyronine. *J Endocrinol.* 1987;112(3):387-90.
37. Davies PH, Franklyn JA. The effects of drugs on tests of thyroid function. *Eur J Clin Pharmacol.* 1991;40(5):439-51.
38. Kaptein EM, Moore GE, Ferguson DC, Hoenig M. Effects of prednisone on thyroxine and 3,5,3'-triiodothyronine metabolism in normal dogs. *Endocrinol.* 1992;130(3):1669-79.
39. Kantrowitz LB, Peterson ME, Melian C, Nichols R. Serum total thyroxine, total triiodothyronine, free thyroxine, and thyrotropin concentrations in dogs with nonthyroidal disease. *J Am Vet Med Assoc.* 2001;219(6):765-9.

40. Peterson ME, Ferguson DC, Kintzer PP, Drucker WD. Effects of spontaneous hyperadrenocorticism on serum thyroid hormone concentrations in the dog. *Am J Vet Res.* 1984;45(10):2034-8.
41. Paradis M, Sauve F, Charest J, Refsal KR, Moreau M, Dupuis J. Effects of moderate to severe osteoarthritis on canine thyroid function. *Can Vet J.* 2003;44(5):407-12.
42. Sekiya T, Tada S, Kawakami K, Kino M, Fukuda K, Watanabe H. Clinical application of computed tomography to thyroid disease. *Comput Tomogr.* 1979;3(3):185-93.
43. Wippold II FJ. Neck. In: Lee JKT, Sagel SS, Stanley RJ, Heiken JP (eds). *Computed body tomography with MRI correlation.* 4th ed. Volume 1. Philadelphia: Lippincott William & Wilkins, 1999:145-224.
44. Turrel JM, McEntee MC, Burke BP, Page RL. Sodium iodide I - 131 treatment of dogs with nonresectable thyroid tumors: 39 cases (1990-2003). *J Am Vet Med Assoc.* 2006;229(4):542-8.
45. Slensky KA, Volk SW, Schwarz T, Duda L, Mauldin EA, Silverstein D. Acute severe hemorrhage secondary to arterial invasion in a dog with thyroid carcinoma. *J Am Vet Med Assoc.* 2003;223(5):649-53, 36.

**HIGH-FIELD MRI OF THE NORMAL CANINE
THYROID GLAND**

Olivier Taeymans¹, Ruth Dennis², Jimmy H. Saunders¹

Department of Medical Imaging¹, Faculty of Veterinary Medicine, Ghent University, Salisburylaan 133, 9820 Merelbeke, Belgium and the Centre for Small Animal Studies², Animal Health Trust, Newmarket, Suffolk, United Kingdom.

Adapted from:

MR Imaging of the Normal Canine Thyroid Gland. O. Taeymans, R. Dennis, J.H. Saunders.

Vet Radiol Ultrasound, Accepted October 30, 2007.

SUMMARY

The MRI features of the normal canine thyroid gland were retrospectively compiled from images acquired in 44 dogs of different breeds presented for a variety of diseases unrelated to the thyroid gland. The appearance of the thyroid gland on different sequences, including pre- and post-contrast T1W, T2W, 2D GE, 3D T2* GE and PD weighted images, were described in different image planes. The characteristic shape, location and intensity of thyroid lobes compared to surrounding structures made them easily detectable in all dogs. By far the most common location of the thyroid lobes was dorsolateral to the trachea with the maximal cross-sectional area of the lobes located ventral to C2/3 or C3 in more than 85% of the cases. The majority of the lobes were ovoid on transverse images. An isthmus was seen in 1 large breed dog and parathyroid glands could not be seen. The mean maximal thyroid lobe diameter measured on transverse images was 8.1 mm, being twice the mean average diameter of the common carotid artery. Considering the excellent conspicuity and characteristic appearance of the canine thyroid gland, MRI can be beneficial in the diagnosis of diffuse thyroid diseases, in differentiating thyroidal versus non-thyroidal neck masses and, in staging and treatment planning of thyroid tumors in this species.

INTRODUCTION

The canine thyroid gland consists of two elongated lobes located on both dorsolateral aspects of the cranial portion of the trachea, medial to the common carotid arteries. Both lobes span a region from the cricoid cartilage to the 5th-8th tracheal rings and the right lobe is located more cranial than the left.¹⁻³ A thin isthmus, spanning the trachea ventrally and connecting the caudal aspects of both lobes, is inconsistently and infrequently present in dogs, being more often present in large breeds.^{1,2,4} For the diagnosis of thyroid masses in people and dogs, US and/or radionuclide scintigraphy, both combined with percutaneous needle biopsy are usually performed.⁵⁻¹⁷ Invasion of surrounding tissues (strap muscles, carotid vein and artery, internal jugular vein, recurrent laryngeal nerve, esophagus and trachea) by thyroid masses may significantly affect the outcome of surgical resection and the long-term survival of those patients.¹⁸⁻²¹ Scintigraphy however lacks spatial resolution to assess local invasiveness of the mass.^{6,22-24} Opposed to that, US has an excellent spatial resolution, making it very suitable for evaluating the integrity of tumor margin.^{6,14,15,25} Limitations of US include limited lateral approach of the soft tissues dorsal to the trachea, limited field of view, limited access to intrathoracic structures, and difficulty in confirming the thyroid origin of large neck masses that distort the anatomy.^{6,23,26,27} Cross-sectional imaging modalities, such as CT and MRI, overcome these limitations by having a large field of view and by eliminating areas of limited accessibility,

therefore having great potentials as supplementary preoperative diagnostic tools.^{5,6,8,9,11,24,26} Before using MRI for assessing thyroid disease, it is important to know the normal features of the thyroid gland with this imaging modality. The purposes of this retrospective study were to 1) determine the signal characteristics of the normal thyroid gland on commonly used sequences; 2) evaluate the signal intensity of thyroid tissue relative to adjacent tissues; 3) describe the shape, location, and homogeneity of the thyroid lobes.

MATERIAL AND METHODS

For this retrospective study, the clinical database of the Animal Health Trust, Newmarket, United Kingdom, was searched for cervical MRI scans performed in client-owned dogs presented for a variety of diseases. Dogs with cervical masses were excluded from the search. One hundred and two cervical MRI studies performed between November 2000 and July 2007 that included thyroid tissue on at least one image plane on at least one sequence were reviewed. Inclusion criteria were: 1) complete patient signalment (breed, gender, age, body weight, and clinical history), 2) normal serum thyroid hormone levels, 3) known final diagnosis, 4) diagnostic quality images and 5) inclusion of the thyroid gland on at least two different image planes on at least one image sequence. Forty-four dogs from 24 different breeds were

identified. Most common breeds were: Cavalier King Charles Spaniel (6), Springer Spaniel (5), cross breed (4), Rottweiler (3), Labrador Retriever (3), Staffordshire Bull Terrier (3), Bull Terrier (2) and German Shepherd (2). Only one subject was included from the remaining represented breeds. There were 29 males (18 intact, 11 neutered), and 15 females (7 intact, 8 neutered). The mean age was: 6 years 1 month (9 months – 17 years 2 months) and mean body weight was: 15.9 kg (4.6 – 63.0 kg).

All scans were performed using a 1.5T MRI scanner*, using different types of receiver coils (quadrature head, extremity, torso phased array and spine coils), depending on the dog's size. Dogs were under general anesthesia using a mixture of isoflurane and oxygen, and positioned in dorsal recumbency. A variety of sequences, slice orientation, slice thickness, interslice gap and image matrix size were used. Performed sequences were: TS FSE T1 and SAG FSE T1, TS FSE T1+C and SAG FSE T1+C using 0.1 mmol/kg of gadobenate dimeglumine†, TS FSE T2, SAG FSE T2 and DORS FSE T2), TS 2D GE and SAG 2D GE, 3D T2* GE, and TS PD weighted images (Table 1). The ranges of used relaxation time (TR), time to echo (TE), flip angle (FA), slice thickness (ST), slice interspace (SI) and image matrix size used for the different sequences are shown in Table 2.

Table 1: Used sequences in each dog.

Dog	TS FSE T1	TS FSE T1+C	TS FSE T2	TS GE	DORS FSE T1	DORS FSE T1+C	DORS FSE T2	SAG FSE T1	SAG FSE T1+C	SAG FSE T2	SAG GE	3D GE T2*	TS PD
1	x		x	x				x		x	x		
2			x							x			
3	x	x	x										
4	x		x	x			x			x			
5			x				x	x	x	x			
6	x		x					x	x	x	x		
7				x								x	
8	x		x	x									
9		x	x					x	x	x	x		
10	x	x	x	x									
11	x		x					x	x	x			
12		x	x										
13	x		x	x			x			x	x		
14	x	x	x			x							
15	x	x	x			x		x	x	x			
16	x	x	x	x	x		x			x			
17	x	x	x	x			x			x			
18	x	x	x	x						x			
19	x	x	x				x	x		x			
20	x	x	x	x						x	x		
21	x	x	x							x	x		
22	x		x					x	x	x	x		
23		x	x					x	x	x			
24	x	x	x	x						x	x		
25	x		x				x	x		x	x		
26	x	x	x					x	x	x	x		
27	x	x	x	x				x	x	x			
28	x		x	x			x			x			
29			x									x	
30												x	
31			x	x						x	x	x	
32										x		x	
33												x	
34										x		x	
35			x	x						x			
36	x	x	x				x			x		x	
37													x
38													x
39													x
40													x
41													x
42													x
43													x
44													x

Sequence	TR	TE	FA	ST	SI	Matrix
TS FSE T1 (+C)	320-620	7.9-14.7	90	2.5-5.0	0.0-1.5	256x256 / 512x512
SAG FSE T1 (+C)	460-620	9.5-22.0	90	2.0-3.5	0.1-0.5	256x256 / 512x512
DORS FSE T1 (+C)	600-620	12.5-17.0	90	3.0-4.0	0.3-1.5	256x256 / 512x512
TS FSE T2	2800-6000	79.9-105.2	90	2.0-5.0	0.0-1.5	256x256 / 512x512
SAG FSE T2	2740-5420	81.9-105.8	90	2.0-3.0	0.1-0.5	256x256 / 512x512
DORS FSE T2	2800-5420	82.3-90.2	90	3.0-4.0	0.1-0.5	256x256 / 512x512
TS GE	160-660	14.0-15.0	20	2.5-5.0	0.0-0.5	256x256
SAG GE	200-660	15.0-20.0	20	2.0-3.0	0.1-0.5	256x256 / 512x512
3D T2* GE	7.7-15.6	3.3-4.4	30	3.0	-1.5	512x512
TS PD	2500-4000	11.9-35.9	90	2.5-4.0	0.1-0.5	256x256

Table 2: Parameters used for the different sequences. TR = repetition time, TE = echo time, FA = flip angle, ST = slice thickness, SI = slice interspace.

All images including thyroid tissue were analyzed in DICOM format, using dedicated software[§]. Using a combination of different sequences the following parameters were recorded: location of the thyroid lobes relative to the trachea (dorsal, ventral, lateral, ventrolateral or dorsolateral), location of the maximum cross-sectional area of the lobes relative to the vertebrae, shape of the thyroid lobes in cross-section (ovoid, triangular, or in between both), visibility of parathyroid glands and presence of an isthmus connecting the caudal aspect of both thyroid lobes. Relative thyroid tissue intensity compared to surrounding structures and homogeneity of the lobes were recorded for all sequences. When considered inhomogeneous, it was noted whether this resulted from the presence of hypointense zones, hyperintense zones or a combination of both. For pre- and post-contrast T1W, T2W and PD-weighted images relative intensity of the lobes was recorded as

isointense to surrounding muscles, in between muscle and fat, isointense to fat or hyperintense to fat. For gradient echo sequences, intensity was recorded as isointense to surrounding muscles, in between muscle and CSF, isointense to CSF or hyperintense to CSF.

Maximum thyroid lobe diameter, measured at the level of maximum thyroid lobe cross-sectional area, and diameter of the adjacent common carotid artery, measured at the same image level, were both obtained on transverse images. A ratio of maximum lobe diameter over common carotid artery diameter was then obtained for each lobe. Correlation between dogs' weight and diameter of common carotid artery, and between dogs' weight and thyroid lobe diameter were searched for using Pearson rank correlation test. Mean and 95% CI of the mean for ratio of largest thyroid lobe diameter over common carotid artery diameter was calculated for the population and normal distribution of this ratio was tested using Shapiro-Wilk test of normality.

RESULTS

All thyroid lobes could easily be detected on all available sequences in each dog. The location of the thyroid lobes was dorsal to the trachea in 4 (4.5%), lateral in 14 (15.9%) and dorsolateral in 70 (79.5%) of 88 lobes. The location of the maximum cross-sectional area of the lobes was at the level of the second cervical vertebra (C2) in 4 (4.5%), the intervertebral disc space between C2 and C3 (C2/3) in 30 (34.1%), C3 in 48 (54.5%), C3/4 in 5 (5.7%) and C4 in 1 (1.1%) lobes. The cross-sectional shape of

the lobes was ovoid in 49 (55.7%), triangular in 5 (5.7%) and having a shape between both in 34 (38.6%) lobes. An isthmus, connecting the caudal aspect of both lobes ventral to the trachea, was seen in only one dog. It was only visible on transverse image planes, but was visible on all image weightings. The best visibility of the isthmus was obtained on subtraction images (post-contrast T1W – pre-contrast T1W images) (Figure 1).



Fig. 1: Transverse subtraction (post-contrast T1W minus pre-contrast T1W) image obtained at the caudal part of the thyroid gland. Two open white arrowheads indicate the presence of an isthmus, spanning the ventral aspect of the trachea and connecting the caudoventral aspect of both thyroid lobes. C3=third cervical vertebra; E=esophagus; T=trachea, J=external jugular vein.

Parathyroid glands could not be detected in any sequence in any dog. The homogeneity of the lobes on pre-contrast T1-weighted images was assessed on 45 lobes in 23 dogs. Of these, 14 (31.1%) had a homogeneous parenchyma, and 31 (68.9%) had a heterogeneous parenchyma. The inhomogeneity resulted from hypointense areas in 20 (64.5%), hyperintense areas in 2 (6.5%), and from a combination of hypointense and hyperintense areas in 9 (29.0%) lobes. A difference in homogeneity between both left and right lobes was seen in 4 of 22 thyroid glands. On post-contrast T1-weighted images, 34 lobes in 18 dogs were evaluated. Of these, 28 (82.4%) were homogeneous, and 6 (17.6%) were inhomogeneous. The inhomogeneity resulted from hypointense areas in 4 (66.7%), and hyperintense areas in 2 (33.3%) lobes. None of these contained a combination of both hypointense and hyperintense areas. A difference in homogeneity between both lobes was only seen in 1 thyroid gland. Sixty-two lobes were assessed on T2-weighted images. Of these, 3 (4.8%) were homogeneous, and 59 (95.2%) were inhomogeneous. The inhomogeneity resulted from hypointense areas in 13 (22.0%), hyperintense areas in 14 (23.7%), and from a combination of hypointense and hyperintense areas in 32 (54.2%). A difference in homogeneity between both lobes was seen in 1 thyroid gland. Thirty-seven lobes in 19 dogs were assessed on transverse and sagittal 2D T2* GE sequences. Of these, 24 (64.9%) were homogeneous, and 13 (35.1%) inhomogeneous. The inhomogeneity resulted from hypointense areas in 11 (84.6%), hyperintense areas in

none, and a combination of hypointense and hyperintense areas in 2 (15.4%) lobes. A difference in homogeneity between both lobes was seen in 1 thyroid gland. On 3D T2* GE sequences, 16 lobes were evaluated. Two (12.5%) lobes were homogeneous, and 14 (87.5%) were inhomogeneous. The inhomogeneity resulted from hypointense areas in 12 (85.7%), hyperintense areas in 1 (7.1%), and a combination of hypointense and hyperintense areas in 1 (7.1%) lobes. A difference in homogeneity between both lobes was seen in 2 thyroid glands. Sixteen lobes were evaluated on PD-weighted sequences. Ten (62.5%) lobes were homogeneous, and 6 (37.5%) were inhomogeneous. The inhomogeneity resulted from hypointense areas in none, hyperintense areas in 2 (33.3%) and a combination of hypointense and hyperintense areas in 4 (66.7%) lobes. A difference in homogeneity between both lobes was not found in any thyroid gland. The homogeneity of thyroid gland parenchyma on the different sequences is graphically represented in (Figure 2).

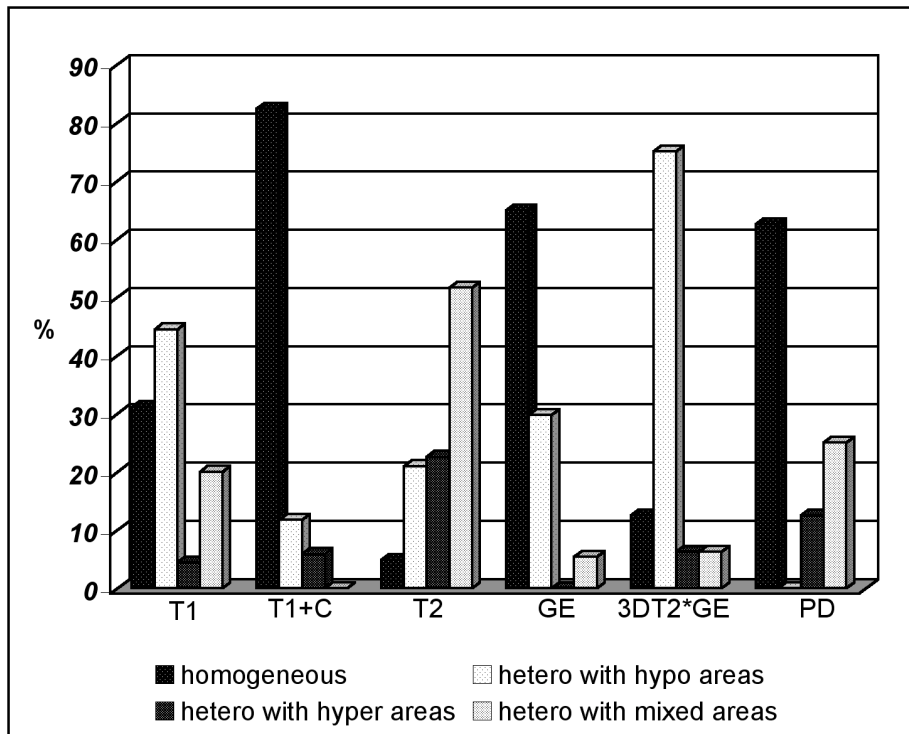


Fig. 2: Column chart representing different patterns of homogeneity in the different sequences used. T1=pre-contrast T1-weighted images; T1+C=post-contrast T1-weighted images; T2=T2-weighted images, GE=2D T2* gradient echo; 3DT2*GE=three-dimensional T2* gradient echo; PD=proton density weighted images.

The intensity of the lobes on pre-contrast T1-weighted images was evaluated on 47 lobes in 24 dogs. Of these, 24 (51.1%) were isointense to the surrounding muscles, and 23 (48.9%) had an intensity between muscle and fat (Figure 3A). No lobe was iso- or hyperintense to fat. On post-contrast T1-weighted images, 36 lobes were assessed in 19 dogs.

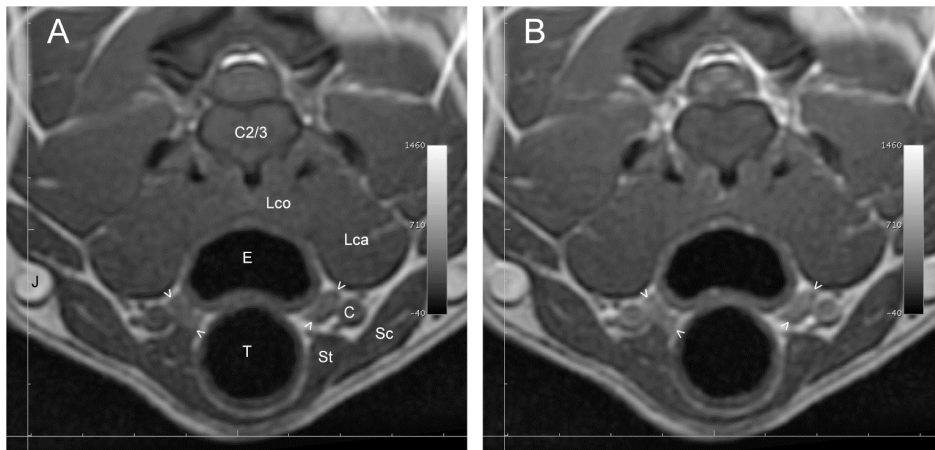


Fig. 3: Pre (A)- and post (B)- contrast transverse T1-weighted images obtained at the maximum cross-sectional diameter of the thyroid lobes. White arrowheads indicate both thyroid lobes. C2/3=intervertebral disc space between the second and third cervical vertebrae; E=esophagus; T=trachea; Lco=musculus longus colli; Lca=musculus longus capitis; St=musculus sternothyroideus; Sc=musculus sternocephalicus; C=common carotid artery; J=external jugular vein.

None were isointense to muscles, 25 (69.4%) had an intensity between muscle and fat, 9 (25.0%) were isointense to fat, and 2 (5.6%) were hyperintense to fat (Figure 3B). The intensity of the lobes on T2-weighted images was evaluated on 62 lobes. None were isointense to muscles, 60 (96.8%) had an intensity between muscle and fat, 2 (3.2%) lobes were isointense to fat, and none were hyperintense to fat (Fig. 4).

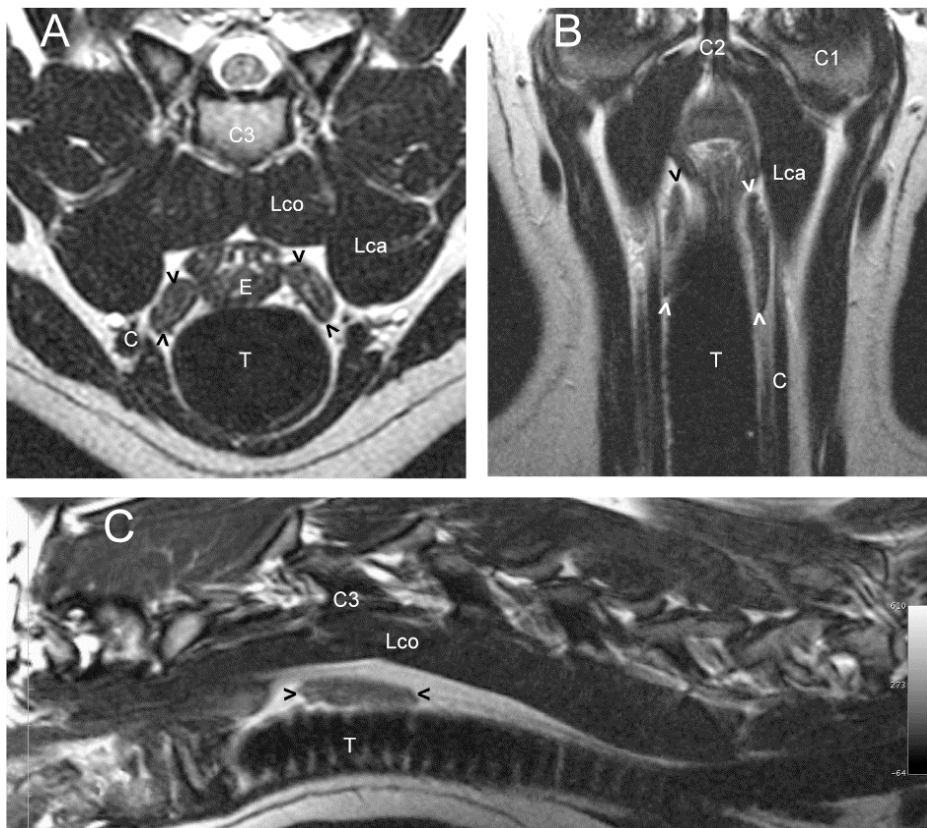


Fig. 4: Transverse (A), dorsal (B) and sagittal (C) T2-weighted images showing the thyroid gland (arrowheads). Right side is left on the transverse and dorsal images and cranial is left on the sagittal image. C1=transverse process of the atlas; C2=dens axis; C3=vertebral body of the third cervical vertebra; E=esophagus; T=trachea; Lco=musculus longus colli; Lca=musculus longus capitis; C=common carotid artery.

The intensity of the lobes on transverse and sagittal 2D T2* GE sequences was evaluated on 38 lobes in 20 dogs. Two (5.3%) lobes were isointense to muscle, 10 (26.3%) lobes had an intensity between muscle

and CSF, 22 (57.9%) were isointense to CSF and 4 (10.5%) were hyperintense to CSF (Figure 5A). The intensity of the lobes on 3D T2* GE sequences was assessed on 16 lobes. All of them had an intensity equal to that of CSF (Figure 5B).

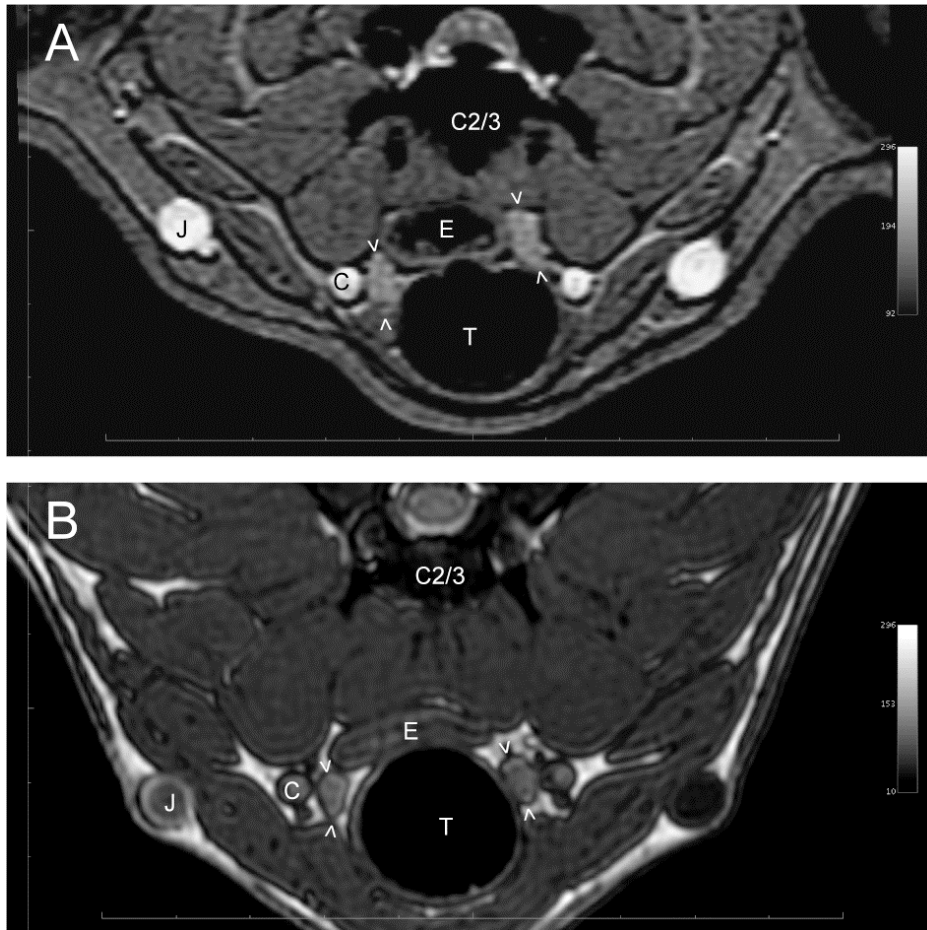


Fig. 5: Transverse GE (A) and 3D T2* GE (B) images showing both thyroid lobes at their maximum cross-sectional diameter (arrowheads).

The intensity of the lobes on PD-weighted images was assessed on 16 lobes. None were isointense to muscles, 14 (87.5%) had an intensity between muscle and fat, 2 (12.5%) were isointense to fat and none were hyperintense to fat (Figure 6).

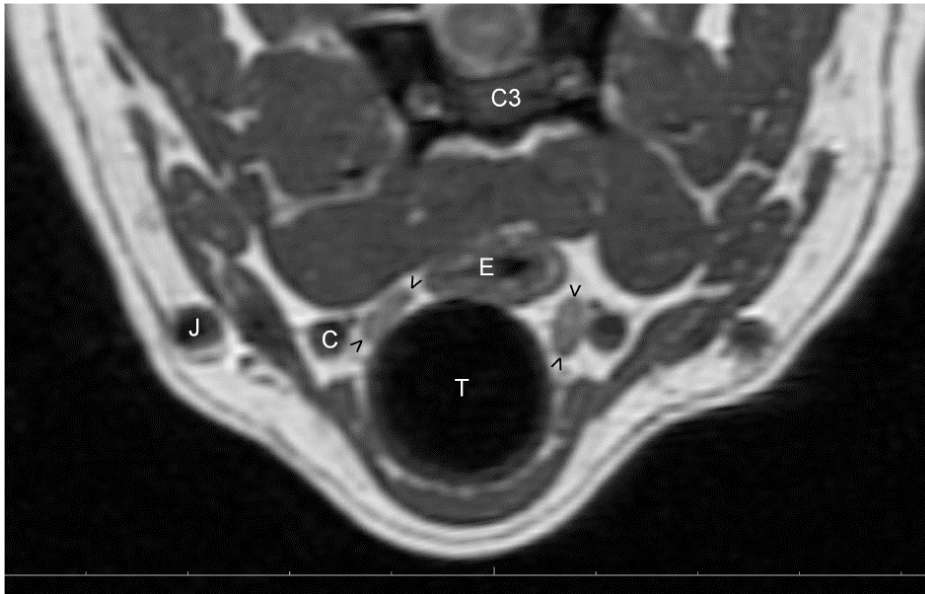


Fig. 6: Transverse proton density weighted image obtained at the maximum cross-sectional diameter of the thyroid lobes (arrowheads). C3=third cervical vertebra; E=esophagus; T=trachea; C=common carotid artery; J=external jugular vein.

The relative intensity of thyroid gland parenchyma on different sequences is graphically represented in (Figure 7).

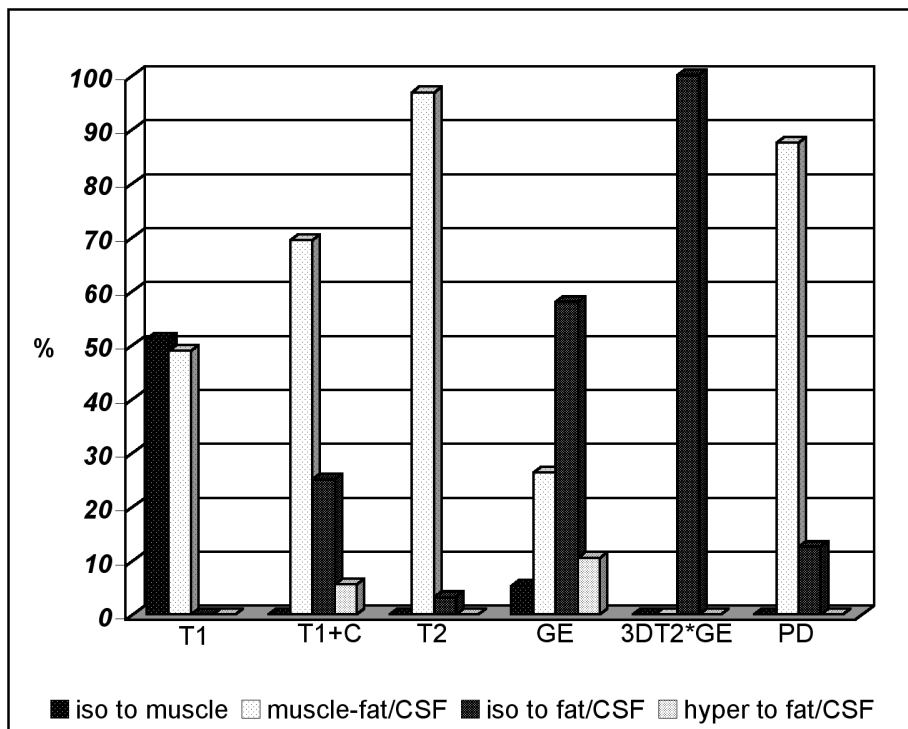


Fig. 7: Column chart representing relative thyroid tissue intensity on the different sequences used. T1=pre-contrast T1-weighted images; T1+C=post-contrast T1-weighted images; T2=T2-weighted images, GE=2D T2* gradient echo; 3DT2*GE=three-dimensional T2* gradient echo; PD=proton density weighted images.

On transverse sections, the mean common carotid diameter was 4.0 mm (95% CI [3.8 – 4.2]), the mean maximal thyroid lobe diameter was 8.1 mm (95% CI [7.6 – 8.5]) and the mean ratio of maximal thyroid diameter over common carotid diameter was 2.04 (95% CI [1.96 – 2.13]). There was a strong correlation between body weight and

common carotid size ($r_s=0.814$) and a moderate correlation between body weight and thyroid size ($r_s=0.690$). As expected, no correlation was found between body weight and ratio of thyroid lobe size over common carotid size. This ratio was also normally distributed, as the null hypothesis of normality was not rejected ($P=0.071$).

DISCUSSION

The characteristic shape, location and different intensity of thyroid lobes compared to surrounding structures made them easily detectable in all dogs. By far the most common location of the thyroid lobes was dorsolateral to the trachea, having a maximal cross-sectional area located ventral to C2/3 or C3 in 85% of the cases, and with the majority of the lobes being ovoid shaped on transverse section. Similar observations regarding the location and shape of the lobes were made in a previous study describing the CT appearance of the normal thyroid gland in a different population of dogs.²⁸ An isthmus was seen in 1 out of 44 dogs in this study, and in 1 out of 25 dogs in the CT study, both being present in large breed dogs.²⁸ The uncommon presence of an isthmus, which is predominantly seen in large breed dogs agrees with the literature.⁴ Similar to CT, normal parathyroid glands could not be seen on MRI and results from the limited spatial resolution of this technique.^{6,28-30}

On pre-contrast T1W images, the relative intensity of the gland was isointense to muscle or slightly higher. The parenchyma was considered inhomogeneous with hypointense areas in the majority of the cases.

After gadolinium administration, the intensity of the gland diffusely increased to an intensity in between muscle and fat or equal to fat. Additionally, the parenchyma became homogeneous in more than 80% of the subjects. On T2W images, the gland nearly always had a heterogeneous parenchyma with a relatively higher intensity compared to pre-contrast T1W images, having an intensity in between muscle and fat. The most common pattern of heterogeneity was due to a mixture of hypo- and hyperintense areas in this sequence. On 2D T2* GE images, the intensity was generally high, often being equal or higher than CSF. The parenchyma appeared homogeneous in 65% and heterogeneous in 35%. When heterogeneous, it was most often due to focal hypointense areas. On 3D T2* GE, a sequence with different TR, TE, FA and with higher spatial resolution than previous sequence, the parenchyma was much more frequently heterogeneous with presence of hypointense areas. The intensity of the gland was always isointense to CSF in this sequence. Finally, on PD-weighted images, the intensity of thyroid tissue was at least always higher than surrounding muscles, sometimes being isointense to fat. Contrary to T2W images, thyroid parenchyma was most often homogeneous in this sequence. In all sequences, a difference in homogeneity in between both left and right lobes was only rarely seen, while a difference in intensity was never observed. The thyroid lobes were on average almost exactly twice the size of the common carotid artery. This ratio is an easy method for estimating the thyroid gland size as it is easy to measure, easy to remember and most

importantly, is not dependent on the dog's body weight, avoiding the necessity of using reference tables for thyroid size in different breeds.

The limitation of our study is its retrospective nature, resulting in different parameter settings used for different sequences, making exact descriptions for specific sequences impossible, but rather gives a summary of MRI features on commonly used image weightings.

Due to the excellent visibility, characteristic signal intensity and homogeneity of normal thyroid tissue, MRI can be used in the diagnosis of both diffuse and focal thyroid disease. Various reports in human medicine have attested to the usefulness of MR imaging in evaluating congenital thyroid disorders and diffuse diseases of the thyroid such as adenomatous multinodular goiter, amyloidosis, hemochromatosis, Hashimoto thyroiditis, Riedel's thyroiditis, granulomatous thyroiditis, infectious thyroiditis, and lymphoma.^{5,6,11,23,24,26,27} Although an overlap in intensity and homogeneity changes was described in the different types of diffuse thyroid disease in people, similar indications may be found in dogs helping in the diagnosis of lymphocytic thyroiditis and thyroid atrophy. More important, we expect in analogy to human literature this modality to have great benefits in thyroid tumor treatment planning in dogs. Indications for cross-sectional imaging are the assessment of local tumor invasion, detecting regional lymphadenopathy, differentiating thyroid neoplasia from other large neck masses and evaluating the intrathoracic extent of such masses.^{5,19,23,27} At this stage however, it seems unlikely that MRI will

accurately permit definition of the histological type of tumor.^{6,7,23,29} Advantages of MRI over CT are the excellent contrast resolution resulting in better tissue characterization and better anatomical detail, the absence of streak artifacts caused by x-ray beam hardening, the absence of need to administer contrast medium to delineate blood vessels, the absence of ionizing radiation and the direct multiplanar imaging capabilities.^{6,7,27,29,30} Another advantage is that gadolinium, contrary to iodinated contrast media, does not interfere with thyroid function and subsequent nuclear imaging.^{6,10,11,24} Finally, accuracy in tumor invasion detection in trachea, esophagus, blood vessels, muscle and nerves, detection of cervical lymphadenopathy and detection of recurrent thyroid carcinoma after treatment is thought to be higher with MRI.^{6,8,23,26,31,32} This technique therefore potentially combines the advantages of CT and US.^{7,23,29}

* GE Signa 1.5 Tesla Echospeed; General Electric Medical Systems, Milwaukee, WI, USA.

† Multihance, Bracco, Milan, Italy.

§ OsiriX v.2.7.5. Advanced open source PACS workstation. DICOM viewer.

REFERENCES

1. König HE, Liebich H-G. Endocrine glands. Thyroid gland. In: König HE, Liebich H-G (eds). *Veterinary Anatomy of Domestic Mammals Textbook and Colour Atlas*. Stuttgart: Shattauer, 2004:539-41.
2. Hullinger R. The endocrine system. Thyroid gland. In: Evans HE, Christensen GC (eds). *Miller's anatomy of the dog*. 2nd ed. Philadelphia: W.B. Saunders Company, 1979:611-5.
3. Herrtage MC. Diseases of the endocrine system. In: Dunn J (ed). *Textbook of Small Animal Medicine*. Philadelphia: W.B. Saunders, 1999:534-41.
4. Frewein J. Endokrine Drüsen. Schilddrüse, Glandula thyroidea. In: Frewein J, Vollmerhaus B (eds). *Anatomie von Hund und Katze*. Berlin: Blackwell Wissenschafts, 1994:442-3.
5. Noma S, Nishimura K, Togashi K, *et al.* Thyroid gland: MR imaging. *Radiology*. 1987;164:495-499.
6. Gotway MB, Higgins CB. MR imaging of the thyroid and parathyroid glands. *MRI Clin North Am*. 2000;8:163-182.
7. Stark DD, Moss AA, Gamsu G, Clark OH, Gooding GA, Webb WR. Magnetic resonance imaging of the neck. Part II: Pathologic findings. *Radiology*. 1984;150:455-461.
8. Cavalieri RR, Blum M. Thyroid imaging. In: Degroot LJ, Jameson JL (eds). *Endocrinology*. 4 ed. Philadelphia: W.B. Saunders Company, 2001:1399-1408.

-
9. Hopkins CR, Reading CC. Thyroid and parathyroid imaging. *Semin Ultrasound CT MR*. 1995;16:279-295.
 10. Hermans J. Les techniques d'imagerie thyroïdienne. *Annal Endocrinol (Paris)*. 1995;56:495-506.
 11. Weber AL, Randolph G, Aksoy FG. The thyroid and parathyroid glands. CT and MR imaging and correlation with pathology and clinical findings. *Radiol Clin North Am*. 2000;38:1105-1129.
 12. Brawner WR. Thyroid and Parathyroid Imaging. In: Berry CR, Daniel GB (eds). *Handbook of Veterinary Nuclear Medicine*. North Carolina, NC: North Carolina State University, 1996:71-79.
 13. Daniel GB, Brawner WR. Thyroid scintigraphy. In: Daniel GB, Berry CR (eds). *Textbook of veterinary nuclear medicine*. North Carolina, NC: American College of Veterinary Radiology, 2006:181-198.
 14. Wisner ER, Nyland TG. Ultrasonography of the thyroid and parathyroid glands. *Vet Clin North Am*. 1998;28:973-991.
 15. Wisner ER, Nyland TG, Mattoon JS. Ultrasonographic examination of cervical masses in the dog and cat. *Vet Rad Ultrasound*. 1994;35:310-315.
 16. Kintzer PP, Peterson ME. Thyroid scintigraphy in small animals. *Semin Vet Med Surg (Small Anim)*. 1991;6:131-139.
 17. Marks SL, Koblik PD, Hornof WJ, Feldman EC. ^{99m}Tc-pertechnetate imaging of thyroid tumors in dogs: 29 cases (1980-1992). *J Am Vet Med Assoc*. 1994;204:756-760.

18. Yousem DM, Hatabu H, Hurst RW, *et al.* Carotid artery invasion by head and neck masses: prediction with MR imaging. *Radiology.* 1995;195:715-720.
19. Wang JC, Takashima S, Takayama F, *et al.* Tracheal invasion by thyroid carcinoma: prediction using MR imaging. *Am J Roentgenol.* 2001;177:929-936.
20. Turrel JM, McEntee MC, Burke BP, Page RL. Sodium iodide I - 131 treatment of dogs with nonresectable thyroid tumors: 39 cases (1990-2003). *J Am Vet Med Assoc.* 2006;229:542-548.
21. Takashima S, Takayama F, Wang J, Kobayashi S, Kadoya M. Using MR imaging to predict invasion of the recurrent laryngeal nerve by thyroid carcinoma. *Am J Roentgenol.* 2003;180:837-842.
22. Higgins CB, Auffermann W. MR imaging of thyroid and parathyroid glands: a review of current status. *Am J Roentgenol.* 1988;151:1095-1106.
23. Geftter WB, Spritzer CE, Eisenberg B, *et al.* Thyroid imaging with high-field-strength surface-coil MR. *Radiology.* 1987;164:483-490.
24. Loevner LA. Imaging of the thyroid gland. *Semin Ultrasound CT MR.* 1996;17:539-562.
25. Simeone JF, Daniels GH, Mueller PR, *et al.* High-resolution real-time sonography of the thyroid. *Radiology.* 1982;145:431-435.

26. Higgins CB, McNamara MT, Fisher MR, Clark OH. MR imaging of the thyroid. *Am J Roentgenol*. 1986;147:1255-1261.
27. Taeymans O, Schwarz T, Duchateau L, *et al*. Computed tomographic features of the normal canine thyroid gland. *Vet Rad Ultrasound*. Accepted for publication, August 2007.
28. Frewein J. Endokrine Drüsen. Schilddrüse, Glandula thyroidea. In: Frewein J, Vollmerhaus B (eds). *Anatomie von Hund und Katze*. Berlin: Blackwell Wissenschafts, 1994:442-443.
29. Stark DD, Clark OH, Moss AA. Magnetic resonance imaging of the thyroid, thymus, and parathyroid glands. *Surgery*. 1984;96:1083-1091.
30. Stark DD, Moss AA, Gamsu G, Clark OH, Gooding GA, Webb WR. Magnetic resonance imaging of the neck. Part I: Normal anatomy. *Radiology*. 1984;150:447-454.
31. Glazer HS, Niemeyer JH, Balfe DM, *et al*. Neck neoplasms: MR imaging. Part I. Initial evaluation. *Radiology*. 1986;160:343-348.
32. Mancuso AA, Dillon WP. The neck. *Radiol Clin North Am*. 1989;27:407-434.

GENERAL DISCUSSION

Acquired primary hypothyroidism and neoplasia are the two most common thyroid pathologies in the adult dog.¹⁻⁴ Acquired primary hypothyroidism has a prevalence of 0.2-0.8% in the canine population and is the consequence of an immune-mediated lymphocytic thyroiditis or an idiopathic follicular atrophy. Both conditions result in a decreased secretion and a subsequent shrinking of the gland.¹⁻⁶ Hypothyroidism is the most common endocrine disorder in the dog, but is at the same time the most over-diagnosed one.⁷⁻¹¹ The frequent false-positive diagnoses result from the non-specific presenting clinical signs (e.g. obesity, alopecia, lethargy), the suboptimal accuracy of available biochemical tests, and the fact that many factors may lower the serum thyroid hormone concentrations. These last mentioned complicating factors may be physiologic influences (breed, age, daily fluctuations,...), pharmaceuticals (corticoids, NSAID's, anesthetics,...), and systemic diseases (Cushing's disease, chronic renal failure, diabetes mellitus,...).^{1,3,8-10,12-15} The fact that acquired hypothyroidism is a relatively common disorder and not always straightforward to diagnose, led to the necessity for additional diagnostic tests increasing the accuracy in this disorder.

Scintigraphy is capable of evaluating the function, but not the morphology of the gland as a consequence of its extremely poor inherent spatial resolution.¹⁶⁻¹⁹

Tumor treatment planning is therefore made impossible using this technique, and its usefulness in the diagnosis of acquired hypothyroidism is still under investigation by other research teams.²⁰⁻²⁴ It has therefore been decided that nuclear medicine of the canine thyroid gland would fall beyond the scope of this work and that we would focus on the “non-functional” or “morphological” imaging modalities, including RX, US, CT, and MRI.

The first hypothesis of our study was that grayscale ultrasound measurements, using electronic calipers, would accurately pick up the shrinking of the gland and would therefore result in a quick and efficient complementary diagnostic tool in the diagnosis of hypothyroidism. Before being able of using US measurements as a diagnostic tool, we needed to test the precision or repeatability of such measurements. This was obtained by calculating the intra- and interobserver variability of US measurements on healthy thyroid glands.

From this first study (Chapter 2) it appeared that US measurements performed by different observers had a low repeatability, or in other words, that the measurements showed a large variability. However, the variability decreased significantly when a single observer performed the measurements. It was also shown that the lowest variability was obtained when measuring the maximal height of the gland, or when calculating the volume of the gland by using a formula for a rotational ellipse (height x width x length x 0,479).

On the contrary, maximal width and maximal length measurements resulted in the largest variability.²⁵ The reason for the large variability of length measurements was 1) thyroid lobes anatomically have a pointed caudal end, thereby rendering the most caudal point of the gland difficult to identify on longitudinal images and 2) thyroid lobes have a curving shape in a dorsal plane, making it unlikely to include the entire lobe on thin ultrasound images when scanning them in a sagittal plane. The reason that width measurements also resulted in a large variation was less clear. The fact that one observer used a different scanning protocol was hypothesized to be the reason for this finding. This observer measured height and width of the gland on the same transverse images, while the two others did not identify the maximal height and maximal width at the same craniocaudal level in the gland. We therefore presumed that the first observer did not always correctly identify the maximal width of the gland. A first conclusion from this study was that performing thyroid gland measurements should be based on a well-defined protocol. The second conclusion was that as a result of the high inter-observer variability, and because we are probably looking for small size differences between healthy and hypothyroid thyroid glands, we could question the value of performing such measurements in an attempt to differentiate both groups. For confirming this, similar studies should be performed on hypothyroid dogs to determine if the inter-observer variability would be higher than the difference observed between hypothyroid versus normal dogs.

A last conclusion was that when measurements are to be performed (e.g. in follow-up studies), they should be done by a single observer that should measure the maximal height or calculate the volume of the gland for estimating the size of the gland.

Because results from the first study demonstrated that US measurements alone would be insufficient to diagnose hypothyroidism with grayscale US, we looked for additional US features in hypothyroid dogs in the subsequent study (Chapter 3).

The formulated hypothesis was that several other US characteristics would be recognizable in hypothyroid dogs. Recorded parameters beside thyroid gland size were lobe shape, thyroid capsule demarcation, relative echogenicity of the gland parenchyma compared to the surrounding musculature, and homogeneity of the gland parenchyma.

The highest sensitivity was obtained for relative echogenicity. It was seen that 77% of the diseased thyroid lobes were hypoechoic compared to surrounding muscles, instead of being hyperechoic as previously described.²⁶ An abnormal capsule demarcation, represented by an undulating thyroid capsule, was seen in 71%, and an abnormal lobe shape and abnormal parenchyma homogeneity were both seen in 65% of the lobes. As expected from the previous study, the lowest sensitivity was obtained for thyroid size (47%). Combining the five parameters in the same dog, grayscale US was able to detect 94% of abnormal thyroid glands.

Because of this excellent test result, we suggested that US could be used as an easy and quick additional test in the diagnosis of acquired primary hypothyroidism.²⁷⁻²⁹

During the follow-up period, after initiation of treatment against acquired hypothyroidism, a significant continuous decrease of the thyroid volume was noted. A slight, but not significant, increase in echogenicity of the gland was also noted. A possible explanation for the further decrease in thyroid gland size observed in our dogs could be the negative feedback mechanism on the TSH secretion of the pituitary gland, being triggered by the supplementation of levothyroxine. Another reason could be the progression of lymphocytic thyroiditis into thyroid atrophy, supporting a hypothesis that idiopathic follicular atrophy may be the end-result of a lymphocytic thyroiditis. The possible cause for the slight increase in echogenicity of the gland may be the gradual decrease of inflammatory reactions in these glands and the gradual replacement of destroyed gland parenchyma by fibrous connective tissue.

In a future study we would need to define the accuracy of grayscale ultrasound in a blinded study, using both healthy and hypothyroid dogs. It would further be interesting to investigate whether the two different causes of acquired primary hypothyroidism, lymphocytic thyroiditis and idiopathic thyroid gland atrophy, would result in different US features. For doing so, thyroid gland biopsies should be obtained under accurate US guidance during the same US investigation.

Unfortunately this was not performed in the current study, as our dogs were simultaneously involved in another study, making the use of anesthetic drugs needed to safely perform biopsies impossible.

The other important but less frequent thyroid gland pathology in the adult dog is neoplasia. Thyroid neoplasia account for 1-4% of all canine neoplasia and for 10-15% of all head and neck neoplasms in the dog.⁴ In contrast to most feline thyroid tumors, neoplasia in dogs are carcinomas in up to 90% of all clinically detectable masses. These carcinomas are large, rapidly growing, locally invasive and usually non-secreting tumors.^{2,4,30,31} Only 10-20% secrete excessive thyroid hormones, resulting in clinical signs of hyperthyroidism. On the other hand, when almost the entire gland is destroyed by a bilateral carcinoma, signs of hypothyroidism can be seen. This has been reported to be present in up to 30% of thyroid neoplasia.^{2,4}

Confirmation of thyroid carcinoma is usually obtained by performing an US examination, combined with cytology/histopathology from FNAs or tissue core biopsies under accurate US guidance.^{26,31-34} Because of its superficial location, high frequency transducers can be used to examine the morphology of the thyroid gland. This results in high spatial-resolution images, making US a very well suited imaging modality for this purpose. Other advantages of US are its widespread availability, the relative low cost compared to other imaging modalities, the absence of ionizing radiation, and a short examination time.^{19,30,32-39}

On US, thyroid carcinomas appear as large, hypoechoic, non-homogeneous masses, sometimes containing multiple cysts, and with variable delineation. Particularly in poorly delineated neoplasia, invasion of surrounding structures such as the esophagus, fascial sheaths and the cervical vasculature can be detected with US. This information is helpful in determining whether surgical treatment is a plausible therapeutic option.^{26,31}

Another hypothesis in this thesis was that CEUS, by looking at the vascularization and perfusion of thyroid neoplasia, could add substantial information to grayscale US in grading the malignancy of these tumors.^{30,40-44} We however, in several unpublished attempts, failed to accurately demonstrate the vascularization and perfusion of the gland in healthy experimental dogs. This failure resulted from massive contrast enhancement of the adjacent common carotid artery, obscuring much lower signal intensities from the thyroid gland parenchyma. Further attempts, using different imaging protocols (e.g. lower contrast dosages, lower beam intensity), will hopefully lead to successful description of the normal vascularization and perfusion of the gland, both potentially useful in the diagnosis of thyroid neoplasia and acquired primary hypothyroidism.

The prognosis of thyroid carcinoma, besides the presence of distant metastasis, has been reported to be dependent on the location, local invasiveness and size of the mass.⁴⁵⁻⁴⁸ Limitations of US in this regard however are 1) the low confidence in identifying thyroidal origin of large neck masses distorting the anatomy of the neck, 2) the limited field of view related to the small size of US probes and 3) the inability of US beams to penetrate soft tissue - gas interfaces, thereby making it impossible to detect tumor invasion in the thoracic cavity and limiting the assessment of soft tissues dorsal to the trachea to a lateral approach of the neck.^{16,18,36,49}

A next hypothesis therefore was that cross-sectional imaging modalities, like CT and MRI, would overcome the aforementioned limitations of US.^{16,19,32,38-40,50,51} However, before being able to use these imaging modalities in staging and planning the treatment of thyroid neoplasia and also potentially use them as an additional diagnostic test in acquired hypothyroidism, normal CT and MRI characteristics need to be described first. The formulated hypothesis for the subsequent study (Chapter 4) was that canine thyroid tissue would easily be recognizable and would have a characteristic appearance on CT.

Even in the absence of intravenous contrast medium injection, normal thyroid lobes demonstrated a high HU value compared to surrounding tissues, confirming the hypothesis that thyroid tissue is readily distinguishable on CT.⁵²

The natural high iodine concentration present in thyroid follicles is the reason for the high HU values, as iodine is an effective X-ray absorber as a consequence of its atomic number of 53.^{19,53-58}

The mean pre-contrast attenuation value of 107 HU for normal canine thyroid tissue reported here, should however not be interpreted strictly, as geographic differences and alimentary iodine intake differences due to different food compositions and tap water iodine concentrations have been reported to alter the HU values significantly in people.^{54,59} After intravenous contrast injection, thyroid attenuation values increased homogeneously to a mean value of 169 HU. It was also noted that measured volume of the gland significantly increased after contrast medium injection. This apparent increase in size is likely related to false size measurements related to blooming artifacts, rather than true volume augmentations. This artifact, appearing at the edges of highly attenuating structures on post-contrast CT images, is for instance known to falsely increase size measurements of vascular stents in human angiographic studies.⁶⁰⁻⁶² The size, location, shape and vascularization of the thyroid gland were also described in this study. Although not statistically significant, younger dogs had relatively larger glands than older dogs, potentially underlying the importance of the thyroid gland during growth. Normal parathyroid glands could not be detected, which is related to the relatively low spatial resolution of CT compared to US.^{52,63,64}

In conclusion, this study demonstrated several imaging features of the normal canine thyroid gland allowing its identification on cervical CT scans. These characteristic features could be used to determine a thyroïdal origin of large neck masses, staging and planning the treatment of thyroid carcinomas and have potential applications in acquired primary hypothyroidism. The last mentioned relates, besides a measurable shrinking of the gland, to decreased number of thyroid follicles, subsequent lowered iodine concentrations, and resulting decreased HU values.^{19,35,53-55,65}

The same hypothesis as for the previous study was formulated for the MRI study (Chapter 5). The appearance of the thyroid gland on different MRI sequences was described using different image planes. The characteristic shape, location and intensity of thyroid lobes compared to surrounding structures made the thyroid gland readily discernible in all dogs.⁶⁶ The maximal thyroid lobe diameter measured on transverse section was on average twice the average diameter of the common carotid artery. This newly introduced measurement could facilitate the size evaluation of thyroid glands, obviating the need of using time consuming formulas in the correction of thyroid volume for body weight (since reference values for thyroid size in different dog breeds are not available in the literature).^{27,29,52}

Considering the excellent conspicuity and characteristic appearance of the canine thyroid gland, we concluded that MRI could be beneficial in the diagnosis of diffuse thyroid diseases like acquired hypothyroidism, in differentiating thyroidal versus non-thyroidal neck masses and, in staging and surgery planning of thyroid neoplasia in this species.^{16,18,19,36,38,40,46,47,49-51,67-71}

REFERENCES:

1. Scott-Moncrieff JC, Guptill-Yoran L. Endocrine disorders. Hypothyroidism. In: Ettinger SJ, Feldman EC (eds). Textbook of veterinary internal medicine. 6th ed. St. Louis, MO: Elsevier-Saunders, 2005:1535-43.
2. Feldman EC, Nelson RW. Canine thyroid tumors and hyperthyroidism. In: Feldman EC, Nelson RW (eds). Canine and feline endocrinology and reproduction. St-Louis, MO: Elsevier-Saunders, 2004:219-50.
3. Feldman EC, Nelson RW. Canine Hypothyroidism. In: Feldman EC, Nelson RW (eds). Canine and Feline Endocrinology and Reproduction. St-Louis, MO: Elsevier-Saunders, 2004:86-151.
4. Mooney CT. Thyroid Neoplasia and Hyperthyroidism in Dogs. In: Ettinger SJ, Feldman EC (eds). Textbook of Veterinary Internal Medicine. 6 ed. St-Louis, MO: Elsevier Inc., 2005:1558-60.
5. Panciera DL. Hypothyroidism in dogs: 66 cases (1987-1992). J Am Vet Med Assoc. 1994 Mar 1;204(5):761-7.
6. Dixon RM, Reid SW, Mooney CT. Epidemiological, clinical, haematological and biochemical characteristics of canine hypothyroidism. Vet Rec. 1999 Oct 23;145(17):481-7.

7. Chastain CB, Young DW, Kemppainen RJ. Anti-triiodothyronine antibodies associated with hypothyroidism and lymphocytic thyroiditis in a dog. *J Am Vet Med Assoc.* 1989 Feb 15;194(4):531-4.
8. Daminet S, Ferguson DC. Influence of drugs on thyroid function in dogs. *J Vet Intern Med.* 2003 Jul-Aug;17(4):463-72.
9. Ferguson DC. Testing for hypothyroidism in dogs. *Vet Clin North Am.* 2007 Jul;37(4):647-69, v.
10. Ferguson DC. Update on diagnosis of canine hypothyroidism. *Vet Clin North Am.* 1994 May;24(3):515-39.
11. Herrtage MC. Diseases of the endocrine system. In: Dunn J (ed). *Textbook of Small Animal Medicine.* Philadelphia: W.B. Saunders, 1999:534-41.
12. Daminet S, Paradis M, Refsal KR, Price C. Short-term influence of prednisone and phenobarbital on thyroid function in euthyroid dogs. *Can Vet J.* 1999 Jun;40(6):411-5.
13. Kaptein EM, Moore GE, Ferguson DC, Hoenig M. Effects of prednisone on thyroxine and 3,5,3'-triiodothyronine metabolism in normal dogs. *Endocrinol.* 1992 Mar;130(3):1669-79.
14. Paradis M, Sauve F, Charest J, Refsal KR, Moreau M, Dupuis J. Effects of moderate to severe osteoarthritis on canine thyroid function. *Can Vet J.* 2003 May;44(5):407-12.

15. Kantrowitz LB, Peterson ME, Melian C, Nichols R. Serum total thyroxine, total triiodothyronine, free thyroxine, and thyrotropin concentrations in dogs with nonthyroidal disease. *J Am Vet Med Assoc.* 2001 Sep 15;219(6):765-9.
16. Gotway MB, Higgins CB. MR imaging of the thyroid and parathyroid glands. *Magn Reson Imaging Clin N Am.* 2000 Feb;8(1):163-82.
17. Higgins CB, Auffermann W. MR imaging of thyroid and parathyroid glands: a review of current status. *AJR Am J Roentgenol.* 1988 Dec;151(6):1095-106.
18. Geftter WB, Spritzer CE, Eisenberg B, *et al.* Thyroid imaging with high-field-strength surface-coil MR. *Radiology.* 1987 Aug;164(2):483-90.
19. Loevner LA. Imaging of the thyroid gland. *Semin Ultrasound CT MR.* 1996 Dec;17(6):539-62.
20. Kintzer PP, Peterson ME. Thyroid scintigraphy in small animals. *Semin Vet Med Surg (Small Anim).* 1991 May;6(2):131-9.
21. Kintzer PP, Peterson ME. Nuclear medicine of the thyroid gland. Scintigraphy and radioiodine therapy. *Vet Clin North Am.* 1994 May;24(3):587-605.

22. Daniel GB, Brawner WR. Thyroid scintigraphy. In: Daniel GB, Berry CR (eds). Textbook of veterinary nuclear medicine. North Carolina, NC: American College of Veterinary Radiology, 2006:181-98.
23. Balogh L, Thuroczy J, Biksi I, *et al.* Thyroid volumetric measurement and quantitative thyroid scintigraphy in dogs. *Acta Vet Hung.* 1998;46(2):145-56.
24. Diaz Espineira MM, Mol JA, Peeters ME, *et al.* Assessment of thyroid function in dogs with low plasma thyroxine concentration. *J Vet Intern Med.* 2007 Jan-Feb;21(1):25-32.
25. Taeymans O, Duchateau L, Schreurs E, Kramer M, Daminet S, Saunders JH. Intra- and interobserver variability of ultrasonographic measurements of the thyroid gland in healthy Beagles. *Vet Radiol Ultrasound.* 2005 Mar-Apr;46(2):139-42.
26. Wisner ER, Nyland TG. Ultrasonography of the thyroid and parathyroid glands. *Vet Clin North Am.* 1998 Jul;28(4):973-91.
27. Reese S, Breyer U, Deeg C, Kraft W, Kaspers B. Thyroid sonography as an effective tool to discriminate between euthyroid sick and hypothyroid dogs. *J Vet Intern Med.* 2005 Jul-Aug;19(4):491-8.

28. Bromel C, Pollard RE, Kass PH, Samii VF, Davidson AP, Nelson RW. Ultrasonographic evaluation of the thyroid gland in healthy, hypothyroid, and euthyroid Golden Retrievers with nonthyroidal illness. *J Vet Intern Med.* 2005 Jul-Aug;19(4):499-506.
29. Taeymans O, Daminet S, Duchateau L, Saunders JH. Pre- and post-treatment ultrasonography in hypothyroid dogs. *Vet Radiol Ultrasound.* 2007 May-Jun;48(3):262-9.
30. Taeymans O, Peremans K, Saunders JH. Thyroid imaging in the dog: current status and future directions. *J Vet Intern Med.* 2007 Jul-Aug;21(4):673-84.
31. Wisner ER, Nyland TG, Mattoon JS. Ultrasonographic examination of cervical masses in the dog and cat. *Vet Rad Ultrasound.* 1994;35:310-5.
32. Hopkins CR, Reading CC. Thyroid and parathyroid imaging. *Semin Ultrasound CT MR.* 1995 Aug;16(4):279-95.
33. Hermans J. Les techniques d'imagerie thyroïdienne. *Ann Endocrinol (Paris).* 1995;56(5):495-506.
34. Reading CC, Gorman CA. Thyroid imaging techniques. *Clin Lab Med.* 1993 Sep;13(3):711-24.
35. Radecki PD, Arger PH, Arenson RL, *et al.* Thyroid imaging: comparison of high-resolution real-time ultrasound and computed tomography. *Radiology.* 1984 Oct;153(1):145-7.

36. Yousem DM, Scheff AM. Thyroid and parathyroid gland pathology. Role of imaging. *Otolaryngol Clin North Am.* 1995 Jun;28(3):621-49.
37. Brawner WR. Thyroid and Parathyroid Imaging. In: Berry CR, Daniel GB (eds). *Handbook of Veterinary Nuclear Medicine.* North Carolina, NC: North Carolina State University, 1996:71-9.
38. Cavalieri RR, Blum M. Thyroid imaging. In: Degroot LJ, Jameson JL (eds). *Endocrinology.* 4 ed. Philadelphia: W.B. Saunders Company, 2001:1399-408.
39. Simeone JF, Daniels GH, Mueller PR, *et al.* High-resolution real-time sonography of the thyroid. *Radiology.* 1982 Nov;145(2):431-5.
40. Argalia G, De Bernardis S, Mariani D, *et al.* Ultrasonographic contrast agent: evaluation of time-intensity curves in the characterisation of solitary thyroid nodules. *Radiol med.* 2002 Apr;103(4):407-13.
41. Calliada F, Pallavicini D, Pasamonti M, *et al.* Topical role and future perspectives of sonographic contrast agents in the differential diagnosis of solid thyroid lesions. *Rays.* 2000 Apr-Jun;25(2):191-7.
42. O'Brien RT, Iani M, Matheson J, Delaney F, Young K. Contrast harmonic ultrasound of spontaneous liver nodules in 32 dogs. *Vet Radiol Ultrasound.* 2004 Nov-Dec;45(6):547-53.

43. Solbiati L, Osti V, Cova L, Tonolini M. Ultrasound of thyroid, parathyroid glands and neck lymph nodes. *Eur Radiol*. 2001;11(12):2411-24.
44. Spiezia S, Farina R, Cerbone G, *et al*. Analysis of color Doppler signal intensity variation after levovist injection: a new approach to the diagnosis of thyroid nodules. *J Ultrasound Med*. 2001 Mar;20(3):223-31; quiz 33.
45. Turrel JM, McEntee MC, Burke BP, Page RL. Sodium iodide I 131 treatment of dogs with nonresectable thyroid tumors: 39 cases (1990-2003). *J Am Vet Med Assoc*. 2006 Aug 15;229(4):542-8.
46. Takashima S, Takayama F, Wang J, Kobayashi S, Kadoya M. Using MR imaging to predict invasion of the recurrent laryngeal nerve by thyroid carcinoma. *AJR Am J Roentgenol*. 2003 Mar;180(3):837-42.
47. Wang JC, Takashima S, Takayama F, *et al*. Tracheal invasion by thyroid carcinoma: prediction using MR imaging. *AJR Am J Roentgenol*. 2001 Oct;177(4):929-36.
48. Yousem DM, Hatabu H, Hurst RW, *et al*. Carotid artery invasion by head and neck masses: prediction with MR imaging. *Radiology*. 1995 Jun;195(3):715-20.

49. Higgins CB, McNamara MT, Fisher MR, Clark OH. MR imaging of the thyroid. *Am J Roentgenol.* 1986 Dec;147(6):1255-61.
50. Noma S, Nishimura K, Togashi K, *et al.* Thyroid gland: MR imaging. *Radiology.* 1987 Aug;164(2):495-9.
51. Weber AL, Randolph G, Aksoy FG. The thyroid and parathyroid glands. CT and MR imaging and correlation with pathology and clinical findings. *Radiol Clin North Am.* 2000 Sep;38(5):1105-29.
52. Taeymans O, Schwarz T, Duchateau L, *et al.* Computed tomographic features of the normal canine thyroid gland. *Vet Rad Ultrasound.* Accepted for publication, 16 July 2007.
53. Silverman PM, Newman GE, Korobkin M, Workman JB, Moore AV, Coleman RE. Computed tomography in the evaluation of thyroid disease. *Am J Roentgenol.* 1984 May;142(5):897-902.
54. Arger PH, Jennings AS, Gordon LF, *et al.* Computed tomography findings in clinically normal and abnormal thyroid patients. *J Comput Tomogr.* 1985 Apr;9(2):111-7.
55. Reede DL, Bergeron RT, McCauley DI. CT of the thyroid and of other thoracic inlet disorders. *J Otolaryngol.* 1982 Oct;11(5):349-57.
56. Imanishi Y, Ehara N, Mori J, *et al.* Measurement of thyroid iodine by CT. *J Comput Assist Tomogr.* 1991 Mar-Apr;15(2):287-90.

57. Imanishi Y, Ehara N, Shinagawa T, *et al.* Correlation of CT values, iodine concentration, and histological changes in the thyroid. *J Comput Assist Tomogr.* 2000 Mar-Apr;24(2):322-6.
58. Nagataki S, Shizume K, Nakao K. Effect of chronic graded doses of iodide on thyroid hormone synthesis. *Endocrinol.* 1966 Oct;79(4):667-74.
59. Joseph K, Berg-Schlosser F, Herbert K. [Computed tomographic determination of thyroid iodine concentration in an endemic goiter area]. *Rofo.* 1986 Apr;144(4):417-21.
60. Choi HS, Choi BW, Choe KO, *et al.* Pitfalls, artifacts, and remedies in multi-detector row CT coronary angiography. *Radiographics.* 2004 May-Jun;24(3):787-800.
61. Hoffmann MH, Shi H, Manzke R, *et al.* Noninvasive coronary angiography with 16-detector row CT: effect of heart rate. *Radiology.* 2005 Jan;234(1):86-97.
62. Muhlenbruch G, Mahnken AH, Das M, *et al.* Evaluation of aortocoronary bypass stents with cardiac MDCT compared with conventional catheter angiography. *Am J Roentgenol.* 2007 Feb;188(2):361-9.
63. Drost WT, Mattoon JS, Samii VF, Weisbrode SE, Hoshaw-Woodard SL. Computed tomographic densitometry of normal feline thyroid glands. *Vet Radiol Ultrasound.* 2004 Mar-Apr;45(2):112-6.

64. Drost WT, Mattoon JS, Weisbrode SE. Use of helical computed tomography for measurement of thyroid glands in clinically normal cats. *Am J Vet Res.* 2006 Mar;67(3):467-71.
65. Vette JK. Computed tomography of the thyroid gland. *Acta Endocrinol Suppl (Copenh).* 1985;268:1-82.
66. Taeymans O, Dennis R, Saunders JH. High-field MRI of the normal canine thyroid gland. *Vet Radiol Ultrasound.* Accepted, October 2007.
67. Stark DD, Moss AA, Gamsu G, Clark OH, Gooding GA, Webb WR. Magnetic resonance imaging of the neck. Part II: Pathologic findings. *Radiology.* 1984 Feb;150(2):455-61.
68. Stark DD, Clark OH, Moss AA. Magnetic resonance imaging of the thyroid, thymus, and parathyroid glands. *Surgery.* 1984 Dec;96(6):1083-91.
69. Stark DD, Moss AA, Gamsu G, Clark OH, Gooding GA, Webb WR. Magnetic resonance imaging of the neck. Part I: Normal anatomy. *Radiology.* 1984 Feb;150(2):447-54.
70. Glazer HS, Niemeyer JH, Balfe DM, *et al.* Neck neoplasms: MR imaging. Part I. Initial evaluation. *Radiology.* 1986 Aug;160(2):343-8.
71. Mancuso AA, Dillon WP. The neck. *Radiol Clin North Am.* 1989 Mar;27(2):407-34.

SUMMARY

For the diagnosis of thyroid abnormalities in people, all currently available medical imaging modalities are used, each of them having advantages and disadvantages. Reports on the use of medical imaging in canine thyroid pathology are sparse. Those available relate to the use of US and planar scintigraphy in cases of thyroid carcinomas. The increased availability of other imaging modalities in veterinary medicine, like CT and MRI, makes them potentially useful as complementary tests in the sometimes-difficult diagnosis and treatment planning of thyroid pathology in the dog.

The first chapter gives a review of the current literature regarding thyroid imaging in the dog. It describes the advantages and disadvantages of RX, US and scintigraphy in the two most frequent thyroid pathologies of the dog: acquired hypothyroidism and thyroid neoplasia. US and scintigraphy remain the two most indicated imaging modalities for these thyroid abnormalities. However, as in human medicine, CT and MRI also have potential indications.

The second chapter complements the literature on the normal US anatomy of the thyroid gland. The repeatability of US measurements was evaluated by calculating the variability of four different parameters (maximal length, maximal width, maximal height and volume) within observer, between observer and between dogs.

The height and the volume had the lowest intra- and inter-observer variability, while measurements of the length had the biggest intra- and inter-observer variability. The intra-observer variability was smaller than the inter-observer variability. These conclusions were important to conduct the study from the third chapter.

The third chapter described the US features of the thyroid gland in a population of dogs suffering from acquired hypothyroidism. A combination of the following features could be observed: hypoechoic gland parenchyma, inhomogeneous gland parenchyma, irregular glandular capsule demarcation, rounded lobe shape on transverse section and decreased thyroid gland size. Subsequently, the sensitivity of US was described for this population. Combining the five aforementioned US features resulted in a sensitivity of 94% for the detection of acquired hypothyroidism. Finally the evolution of those US features after initiation of treatment was described. A continuous decrease of thyroid gland volume was seen after treatment; while other investigated parameters did not change significantly during the follow-up period. It was concluded from this study that US is a sensitive and quick test for the diagnosis of acquired hypothyroidism in dogs.

The fourth chapter described the CT features of the normal canine thyroid gland. The mean pre- and post-contrast attenuation values were very high for soft tissues being 107.5 HU and 169.0 HU, respectively. After injection of IV contrast medium, the thyroid gland volume increased in size. All thyroid lobes were homogeneous on pre- and post-contrast images. In a craniocaudal direction, the gland spanned a region from the 1st to the 8th tracheal ring and the right lobe was more cranially positioned than the left in 58% of the cases. On transverse images the lobe was ovoid in 72%, and its location was dorsolateral to the trachea in 90%. Parathyroid glands could not be identified, and an isthmus was only seen in 1 out of 25 dogs. Considering the excellent visibility and characteristic appearance of the normal canine thyroid gland, we concluded that CT could be beneficial in the differentiation of thyroidal versus non-thyroidal neck masses. CT also yields potential in the staging of thyroid carcinomas.

Finally, the fifth chapter described the normal MRI features of the thyroid gland on a population of forty-four dogs. The appearance of the gland was described on commonly used MRI sequences. The characteristic shape, location and intensity of thyroid lobes compared to surrounding structures made the thyroid gland easily detectable in all dogs.

SUMMARY

The far most common location of the thyroid lobes was dorsolateral to the trachea in 80% of the dogs, with the maximal cross-sectional area of the lobes located ventral to C2/3 or C3 in more than 85% of the cases. Fifty-six percent of the lobes had an ovoid shape on transverse section. An isthmus was seen in 1 large breed dog and parathyroid glands could not be seen. The maximal thyroid lobe diameter measured on transverse section was on average twice the average diameter of the common carotid artery. Considering the excellent conspicuity and characteristic appearance of the canine thyroid gland, it was concluded that MRI could be beneficial in the diagnosis of diffuse thyroid diseases, in differentiating thyroidal versus non-thyroidal neck masses and, in staging and surgery planning of thyroid neoplasia.

Alle huidig beschikbare beeldvormingstechnieken worden tegenwoordig aangewend bij de diagnosestelling van schildklierandoeningen bij de mens. Elke beeldvormingsmodaliteit heeft hierbij zijn voor- en nadelen. In de diergeneeskunde daarentegen, is het aantal publicaties over het gebruik van medische beeldvorming van schildklierandoeningen bij de hond beperkt. Beschikbare studies rapporteren het gebruik van echografie en planaire scintigrafie in gevallen van schildklier carcinomen. De toegenomen beschikbaarheid van andere beeldvormingstechnieken in de diergeneeskunde, zoals bijvoorbeeld CT en MRI, maakt deze potentieel waardevol als bijkomstige testen in de soms moeilijke diagnose en het opstellen van een geschikt behandelingsprotocol voor schildklierandoeningen.

Het eerste hoofdstuk is een literatuurstudie over bestaande medische beeldvorming van de schildklier bij de hond. Hierbij worden de voor- en nadelen van RX, echografie en scintigrafie besproken in het licht van de twee meest voorkomende schildklierandoeningen, namelijk verworven hypothyroidie en schildkliertumoren. Echografie en scintigrafie blijven hiervoor de twee meest aangewezen beeldvormingstechnieken. Maar, in analogie met de mens, hebben CT en MRI evenzeer potentiële toepassingen.

Het tweede hoofdstuk is een aanvulling op de huidige literatuur over echografie van de normale schildklier. De herhaalbaarheid van echografische metingen werd hierbij nagegaan door de variatie van drie verschillende parameters (maximale lengte, maximale breedte, maximale hoogte en volume) na te gaan binnen dezelfde onderzoeker, tussen verschillende onderzoekers en tussen verschillende honden. De hoogte- en volumemetingen hadden de kleinste variatie binnen dezelfde onderzoekers en tussen verschillende onderzoekers. De variatie binnen de verschillende onderzoekers was kleiner dan tussen de onderzoekers. Deze bevindingen waren belangrijk voor de uitvoering van de studie uit volgend hoofdstuk.

Het derde hoofdstuk beschrijft de echografische veranderingen van de schildklier in een populatie van honden met verworven hypothyroidie. De volgende kenmerken werden waargenomen: hypoechogeen parenchym, heterogeen parenchym, onregelmatige aflijning van het kapsel, ronde vorm van de schildklierlob op dwarsdoorsnede en verkleinde schildklier grootte. Vervolgens werd de sensitiviteit van echografie berekend voor deze populatie. Door de vijf voorgenoemde parameters te combineren, bereikten we met echografie een sensitiviteit van 94% in de detectie van verworven hypothyroidie. Tot slot werd, na het opstarten van de behandeling, de evolutie van deze kenmerken in de tijd beschreven. Een continue afname in volume van de schildklier werd opgemerkt na het opstarten van de behandeling.

De andere beoordeelde parameters bleven ongewijzigd tijdens de opvolgingsperiode. We besloten dat echografie een gevoelige en snelle test was voor het opsporen van verworven hypothyroidie bij de hond.

Het vierde hoofdstuk handelt over de CT kenmerken van de normale schildklier bij de hond. De gemiddelde pre- en post-contrast attenuatie waarden waren respectievelijk 107,5 en 169,0 HU, hetgeen zeer hoog is voor weke delen. Na injectie van intraveneus contrast nam het schildklier volume eveneens toe. Alle schildklierlobben zagen er homogeen uit op zowel pre- als post-contrast beelden. In een craniocaudale richting besloeg de schildklier een regio van de 1^{ste} tot en met de 8^{ste} trachearing, waarbij de rechter lob meer craniaal lag dan de linker lob in 58% van de gevallen. Op dwarse doorsneden waren de schildklierlobben ovaalvormig in 72%, en waren ze dorsolateraal van de trachea gelegen in 90% van de gevallen. Bijschildklieren werden niet gezien en een isthmus werd slechts bij 1 op de 25 honden aangetroffen. Gezien de uitstekende zichtbaarheid en kenmerkende eigenschappen van de normale schildklier bij de hond besloten we dat het gebruik van CT voordelig zou kunnen zijn om het onderscheid te maken tussen nekmassa's afkomstig van schildklierweefsel en nekmassa's van andere oorsprong. CT heeft eveneens een potentiële rol bij het stageren van schildkliercarcinomen.

Tot slot werden de normale MRI kenmerken van de schildklier op een populatie van 44 honden in het vijfde hoofdstuk beschreven. Het uitzicht van de klier werd hierbij beschreven gebruik makende van frequent gebruikte sequenties. De kenmerkende vorm, ligging en intensiteit vergeleken met de omliggende structuren maakten de schildklier duidelijk herkenbaar bij alle honden. Veruit de meest frequente ligging van de schildklierlobben was dorsolateraal van de trachea in 80% van de honden. De maximale diameter van de lobben was ventraal van C2/3 of C3 in 85% van de gevallen gelegen. Zesenvijftig procent van de lobben had een ovale vorm op dwarse doorsnede. Een isthmus werd bij slechts één hond van een groot rastype aangetroffen en bijschildklieren werden niet gezien. De diameter van de schildklierlobben op dwarsdoorsnede was gemiddeld gelijk aan twee maal de diameter van de a. carotis communis. Gezien de uitstekende zichtbaarheid en kenmerkende eigenschappen van de schildklier op MRI werd er besloten dat MRI kon bijdragen tot de diagnose van diffuse schildklieraandoeningen, bij het onderscheiden van nekmassa's van schildklieroorsprong en andere nekmassa's, en bij de stagering en pre-operatieve planning van schildkliertumoren.

Het is ongetwijfeld dankzij Prof. Dr. J. Saunders dat dit proefschrift tot stand is gekomen. Hij kwam, met zijn bijzonder goede kennis van de literatuur en scherpe zin voor onderzoek, tot het besluit dat er op het gebied van de beeldvorming van de schildklier nog een grote nood aan klinisch bruikbare studies bestaat. Als supervisor van mijn specialistenopleiding gaf hij mij de opdracht om tijdens mijn Residency hieromtrent een eerste artikel te schrijven. Na het behalen van mijn diploma van radioloog stimuleerde hij mij dan ook om de draad van dit onderzoek op te pikken. Omdat de structuur van dit werk reeds van in het begin duidelijk omljnd was, aarzelde ik niet lang om mij op dit werk te storten. Ik zou Jimmy van harte willen bedanken voor de fantastische opleiding gedurende mijn Residency, voor de begeleiding van dit werk en voor de hechte vriendschap die er na al die jaren uit onze samenwerking voortvloeide. Jimmy, bedankt om mij steeds tot het uiterste te drijven. Bedankt voor jouw tijd, jouw advies, de ontelbare toffe momenten die we samen op de werkvloer mochten beleven en vooral voor het vertrouwen dat je in mij hebt gesteld !

Prof. Dr. H. van Bree wil ik bedanken voor de kansen die hij mij gaf. Vooreerst de kans om meteen na mijn Internship een Residency te mogen starten en vervolgens voor zijn volledige steun bij het opstarten van dit project. Hij heeft van in het begin in mijn capaciteiten geloofd en heeft mij altijd de nodige tips, steun en vrijheid gegeven.

Em. Prof. Verschooten wil ik in het bijzonder bedanken. De passie voor het prachtig vak radiologie heb ik aan hem te danken. Zijn ongelooflijk boeiende lessen in eerste proef en de radiologie rondes op zaterdag ochtend, liggen hierbij aan de oorsprong. Van toen af wist ik dat ik mij in de medische beeldvorming zou specialiseren. Ik zou hem dan ook nogmaals willen bedanken voor mij die kans gegeven te hebben, en voor de onnoemelijke uren en energie die hij in mijn opleiding gestoken heeft. Ik beschouw het bovendien als een ware eer om zijn laatste pupil te zijn geweest. Zijn onuitputtelijk enthousiasme voor het vak zullen mij altijd blijven en zullen voor de rest van mijn carrière als voorbeeld dienen.

Prof. Dr. B. Van Ryssen wil ik bedanken omdat zij mij op de dienst binnenhaalde. Dankzij haar kreeg ik de kans mijn studies verder te zetten. Had zij mij haar steun niet verleend, was ik waarschijnlijk nooit aan een specialisatie in Gent kunnen beginnen.

Prof. Dr. L. Duchateau wens ik in het bijzonder te bedanken voor zijn intense medewerking bij dit werk. Zijn constructieve opmerkingen, zijn onwaarschijnlijk inzicht en zijn talrijke statistische analyses hebben enorm bijgedragen tot de fundamenten van dit werk.

Dit werk is natuurlijk ook mede dankzij Prof. Dr. S. Daminet tot stand gekomen. Haar voorafgaande onderzoeken lagen aan de basis van dit project en haar kennis over de schildklier was onontbeerlijk tijdens het verloop ervan.

Ook wens ik alle leden van de begeleidingscommissie te bedanken. Jullie inbreng heeft mij enorm geholpen dit werk tot een mooi samenhangend geheel te bundelen.

Ik zou tevens alle mensen van de vakgroep willen bedanken voor de toffe werksfeer die er op onze dienst heerst. Het is met veel vreugde dat ik op de afgelopen 7 jaar terug zal blikken en misschien krijg ik ooit de eer om terug met jullie te mogen werken.

Onze residents wens ik allen enorm veel moed bij de voortzetting van hun opleiding. Ik twijfel er niet aan dat jullie het tot een goed einde zullen brengen en het was een waar genoegen om jullie te mogen opleiden. "May the force be with you" !

Aan mijn vrienden, familie en overleden grootmoeders: bedankt voor jullie luisterend oor, voor de toffe momenten van ontspanning en het begrip dat jullie opbrachten voor mijn talrijke afwezigheden.

Mijn ouders in het bijzonder kan ik niet genoeg bedanken. Ondanks de vele moeilijke situaties hebben jullie mij altijd de beste kansen gegeven. Altijd zijn jullie in mij blijven geloven, ook op momenten waar ik er zelf niet meer in geloofde. Bedankt voor jullie begrip en toeverlaat !

Ook mijn schoonouders wil ik speciaal in de verf zetten. Zonder jullie zouden we er niet geraakt zijn. Altijd stonden jullie klaar voor ons. Nooit was het teveel gevraagd om een handje bij te steken, vooral als ik weer eens afwezig was of ik het weer veel te druk had !

Dank u !

DANKWOORD

Tot slot zou ik mijn fantastische vrouw Inge willen bedanken. Zonder jou had ik het heel eenvoudig nooit gered. Altijd stond je vol liefde klaar om mij te helpen of te troosten. Van in het begin stond alles in het teken van mijn carrière; eerst mijn specialisatie, dan mijn doctoraat en nu het vertrek naar het buitenland. Maar nooit heb ik je horen klagen, of nooit was het je te veel gevraagd. Je bent het mooiste wat mij kon overkomen en met de geboorte van onze zoon Matthieu heb je me bovendien het mooiste geschonken dat er bestaat !

CURRICULUM VITAE

Olivier Taeymans werd op 26 september 1975 te Antwerpen geboren. In 1997 behaalde hij het diploma van kandidaat-dierenarts met onderscheiding aan het RUCA en in 2000 studeerde hij met onderscheiding af als dierenarts aan de UGent.

Onmiddellijk daarna volgde hij een Rotating Internship in small animal medicine aan de UGent, gevolgd door een vier jaar durende Residency in de medische beeldvorming, eveneens aan de UGent. In 2003 won hij de Resident Award van de European College of Veterinary Diagnostic Imaging en in 2005 behaalde hij zijn board examen van diezelfde College en verkreeg daarbij het statuut van Europees specialist.

Olivier Taeymans is auteur of medeauteur van 12 publicaties in internationale tijdschriften en 4 in nationale tijdschriften. Hij is tevens auteur van een hoofdstuk in een radiologie boek. Hij heeft 21 abstracts op internationale congressen gepubliceerd, heeft talrijke postuniversitaire bijscholingen voor practici gegeven en werd reeds verscheidene malen als gastspreker op internationale congressen en buitenlandse universiteiten uitgenodigd.

Vanaf 1 februari 2008 zal hij als Assistant Professor of Radiology werkzaam zijn aan de Tufts University te Boston in de Verenigde Staten.

PUBLICATIONS

J.H. Saunders, **O. Taeymans**, F.R. Snaps, A. François, R.F. Dondelinger. Renal embolization with sterile absolute ethanol for treatment of unilateral ectopic ureter in three female dogs.
Vlaams Dier Tijd 2001;70:147-153.

O. Taeymans, J.H. Saunders, H. van Bree. Radiology Corner: Myelography of the dog.
Vet Radiol & Ultrasound 2002;42:550-551.

J.H. Saunders, C. Clercx, J.L. Zonderland, **O. Taeymans**. Nasal aspergillosis associated to an intra-nasal tooth in a 10-month-old German Shepherd dog.
Vlaams Dier Tijd 2003;72:396-398.

F. Verschooten, P. Deprez, H. Nollet, G. Van Loon, L. Lefère, A. Van Zeveren, L. Devriese, K. Van Schandevijl, F. Vandenberghe, C. Delesalle, D. De Clercq, P. Vervaet, J.H. Saunders, B. Vandevelde, **O. Taeymans**, M. Hoegaerts, F. Pille, F. Gasthuys, K. Peremans. De hengstenkeuring van het Belgisch Trekpaard: een bilan!
Vlaams Dier Tijd 2003;72:224-232.

J.H. Saunders, M. Heimann, **O. Taeymans**, F.R. Snaps. Aneurismal bone cyst in the pelvis of a cat.
Vlaams Dier Tijd 2003;72:424-428.

K. Vermeersch, L. Van Ham, J. Caemaert, M. Tshamala, **O. Taeymans**, S. Bhatti, I. Polis. Suboccipital craniectomy, dorsal laminectomy of C1, durotomy and dural graft placement as a treatment for Syringohydromyelia with cerebellar tonsil herniation in Cavalier King Charles Spaniels.
Vet Surgery 2004;33:355-360.

K. Görtz, B. Van Ryssen, **O. Taeymans**, M. Van Heerden, I. Gielen, M. Risselada. Traumatic fracture of the medial coronoid process in a dog. Radiographic, computed tomographic, arthroscopic and histological findings.

Vet Comp Orthop Traumatol 2004;3:159-162.

M. Risselada, M. Kramer, H. de Rooster, **O. Taeymans**, P. Verleyen, H. van Bree. Ultrasonographic and Radiographic Assessment of Uncomplicated Secondary Fracture Healing of Long Bones in Dogs and Cats.

Vet Surgery 2005;34:99-107.

O. Taeymans, L. Duchateau, E. Schreurs, M. Kramer, S. Daminet, J.H. Saunders. Intra- and inter-observer variability of ultrasonographic measurements of the thyroid gland in healthy Beagles.

Vet Radiol & Ultrasound 2005;46:139-142.

P.M. Martin, B. Van Ryssen, I. Gielen, **O. Taeymans**, H. van Bree. Diagnostic findings in a lame-free dog with complete rupture of the biceps brachii tendon – a case report in a unilaterally affected working Labrador Retriever.

Vet Comp Orthop Traumatol 2007;20:73-77.

M. Risselada, H. de Rooster, **O. Taeymans**. Penetrating injuries in dogs and cats.

Submitted JSAP, January 2006.

O. Taeymans, S. Daminet, L. Duchateau, J.H. Saunders. Pre- and post-treatment ultrasonography in hypothyroid dogs.

Vet Radiol Ultrasound 2007;48:262-269.

O. Taeymans, K. Peremans, J.H. Saunders. Thyroid Imaging in the Dog: Current status and future directions.

J Vet Intern Med 2007;21:673-684.

O. Taeymans, T. Schwarz, L. Duchateau, V. Barberet, I. Gielen, M. Haskins, J.H. Saunders. Computed Tomographic Features of the Normal Canine Thyroid Gland.

Accepted, Vet Radiol Ultrasound, July 16, 2007.

V. Barberet, E. Schreurs, N. Rademacher, D. Nitzl, **O. Taeymans**, L. Duchateau, J.H. Saunders. Quantification of the effect of various patient and image factors on ultrasonographic detection of select canine abdominal organs.

Accepted, Vet Radiol Ultrasound, November 14, 2007.

O. Taeymans, R. Dennis, J.H. Saunders. MR Imaging Features of the Normal Canine Thyroid Gland.

Accepted, Vet Radiol Ultrasound, October 30, 2007.

CHAPTER IN BOOKS

O. Taeymans and H. Rudolf. Basics of thoracic Radiography. In: *BSAVA Manual of Canine and Feline Thoracic Imaging*. Eds: T. Schwarz and V. Johnson. BSAVA Publications, Gloucester, United Kingdom. 2007.

ABSTRACTS

F. Verschooten, M. Pannekoek, T. De Clercq, J.H. Saunders, B. Vandeveldel, **O. Taeymans**, K. Peremans. Osteochondral fragments at the distal border of the navicular bone: radiographical and clinical significance. Proceedings 9th Annual Conference EAVDI, July 24-27, 2002, Archena, Spain. Abstract in *Vet Radiol Ultrasound* 2003;44:250.

O. Taeymans, J.H. Saunders, H. van Bree. Intramedullary spinal cord swelling in dogs. Proceedings EAVDI (British and Irish division) October 11-12, 2002, Cambridge, United Kingdom. Abstract in the *EAVDI Yearbook 2003*.

CURRICULUM VITAE

O. Taeymans, J.H. Saunders. Etude myélographique chez 7 chiens présentant un gonflement intramédullaire. Proceedings AFVAC-CNVSPA, November 21-23, 2003. Nantes, France.

J.H. Saunders, **O. Taeymans**. Comparaison entre la radiographie, la TDM, l'IRM et la rhinoscopie chez 15 chiens avec une aspergillose nasale. Proceedings AFVAC-CNVSPA, November 21-23, 2003. Nantes, France.

K. Vermeersch, L. Van Ham, J. Caemaert, M. Tshamala, **O. Taeymans**, S. Bhatti, I. Polis. Suboccipital craniectomy and dorsal laminectomy of C1 as treatment option for Chiari type I malformations in Cavalier King Charles Spaniels. Proceedings 16th Annual Symposium "Neurosurgery", September 26-27, 2003. Prague, Czech Republic.

M. Risselada, H. van Bree, M. Kramer, **O. Taeymans**, K. Chiers, P. Verleyen. The use of ultrasonography in the diagnosis and prognosis of femoral diaphysis non-unions in two dogs. Abstract 13th Annual ACVS Veterinary Symposium (31st Annual Surgical Forum, 38th Annual Scientific Meeting), Washington D.C., October 9-12, 2003. Abstract in *Vet Surgery* 2003;32(6):601.

O. Taeymans, J.H. Saunders, L. Duchateau, E. Schreurs, M. Kramer, S. Daminet. Intra- and inter-observer variability of ultrasound measurements of the thyroid gland in healthy beagles. Proceedings EAVDI (British & Irish division), October 10-11, 2003, Cambridge, United Kingdom. Abstract in the *EAVDI Yearbook 2004*.

O. Taeymans, J.H. Saunders, L. Duchateau, E. Schreurs, M. Kramer, S. Daminet. An evaluation of the Intra- and inter-observer variability of measurements of the thyroid gland in beagle dogs. Proceedings ACVR congress 2004, Montreal, Canada. Abstract in *Vet Radiol Ultrasound* 2004;45:488.

CURRICULUM VITAE

O. Taeymans, J.H. Saunders. Limited CT scanning for diagnosis of chronic nasal disease in dogs. Proceedings 11th Annual EAVDI congress, September 8-11, 2004, Ghent, Belgium. Abstract in *Vet Radiol Ultrasound* 2004;45:602.

O. Taeymans, J.H. Saunders, S. Daminet. Ultrasonographic features of the thyroid gland in 8 hypothyroid dogs. Proceedings 11th Annual EAVDI congress, September 8-11, 2004, Ghent, Belgium. Abstract in *Vet Radiol. Ultrasound* 2004;45:612.

O. Taeymans, J.H. Saunders, S. Daminet. Ultrasonographic features of the thyroid gland in 16 hypothyroid dogs. Proceedings 12th Annual EAVDI congress, October 5-8, 2005, Naples, Italy. Abstract in *Vet Radiol Ultrasound* 2006;47:425.

O. Taeymans. The diagnosis and follow-up of thyroid diseases in dogs and cats. 4th International Workshop of Ultrasonography. March 17-20, 2006, Vienna, Austria.

E. Schreurs, N. Rademacher, D. Nitzl, **O. Taeymans**, L. Duchateau, J.H. Saunders. Ultrasonographic examination of small parts in the abdomen of dogs: risk factors and frequency of imaging. Proceedings IVRA/ACVR conference, August 7-11, 2006, Vancouver, Canada. Abstract in *Vet Radiol Ultrasound* 2007;48:167.

J.H. Saunders, M. Hoegaerts, K. Vanderperren, T. De Clercq, **O. Taeymans**. Ultrasound findings in 55 horses suspected of tarsal joint pathology. Proceedings IVRA/ACVR conference, August 7-11, 2006, Vancouver, Canada. Abstract in *Vet Radiol Ultrasound* 2007;48:169.

O. Taeymans, L. Duchateau, S. Daminet, J.H. Saunders. Pre- and post-treatment ultrasonography in hypothyroid dogs. British Medical Ultrasound Society (BMUS). 38th Annual Scientific Meeting & Exhibition. 12-14 December, 2006, Manchester, United Kingdom. Abstract in *Ultrasound* 2006;14:251-272.

CURRICULUM VITAE

M. Hoegaerts, **O. Taeymans**. How to approach the equine pelvis on ultrasound? De Voorjaarsdagen, April 28-29, 2007, Rotterdam, The Netherlands.

O. Taeymans, T. Schwarz, L. Duchateau, V. Barberet, I. Gielen, M. Haskins, J.H. Saunders. Computed Tomographic Features of the Normal Canine Thyroid Gland. Proceedings 13th Annual EAVDI meeting, August 29 – September 1, 2007, Thessaloniki, Greece.

E. Van der Vekens, **O. Taeymans**, K. Peremans, I. Van Hoek, S. Daminet, J.H. Saunders. Ultrasonographic changes of the thyroid gland in hyperthyroid cats 6 months after ¹³¹I radioactive Iodine therapy. Proceedings 13th Annual EAVDI meeting, August 29 – September 1, 2007, Thessaloniki, Greece.

O. Taeymans, L. Duchateau, S. Daminet, J.H. Saunders, V. Barberet. Pre- and post-treatment ultrasonography in hypothyroid dogs. Proceedings Annual AFVAC meeting, December 7-9, 2007, Paris, France.

V. Barberet, **O. Taeymans**. La place de l'imagerie médicale chez les chiens hypothyroïdiens. Proceedings AFVAC-CNVSPA, December 7-9, 2007. Paris, France.

INVITED SPEAKER

Pennsylvania State University, Philadelphia, USA. Ultrasonography of the Thyroid Gland. February 4, 2004.

Pennsylvania State University, Philadelphia, USA. Spinal cord swelling on myelography in dogs. February 11, 2004.

CURRICULUM VITAE

University of Rabat, Morocco, December 3-4, 2004.

- Une introduction à l'échographie. **O. Taeymans**, J.H. Saunders.
- Echographie tendineuse équine. J.H. Saunders, M. Hoegaerts, **O. Taeymans**.
- Echographie du boulet équin. J.H. Saunders, **O. Taeymans**, T. Liuti.
- Practical sessions on ultrasonography of equine tendons and articulations.

4th International Workshop of Ultrasonography. The diagnosis and follow-up of thyroid diseases in dogs and cats. March 17-20, 2006, Vienna, Austria.

5th International Workshop of Ultrasonography. Practical sessions, demonstration of "shunt protocol" and general abdominal ultrasound and participation in the discussion panel. September 30-October 1, 2006, Ghent, Belgium.

Cummings School of Veterinary Medicine, Tufts University, North Grafton, MA, USA. Cross-sectional Imaging of the Canine Thyroid Gland. June 5, 2007.

European Association of Veterinary Diagnostic Imaging (British and Irish division) Autumn meeting. Wellcome Trust Conference Centre, Cambridge, UK. Cross-sectional Imaging of the Canine Thyroid Gland. November 9-10, 2007.

SCIENTIFIC AWARDS

"ECVDI Resident Award". Intra- and interobserver variability of ultrasonographic measurements of the thyroid gland in healthy Beagles. October 11, 2003, Cambridge, United Kingdom.

